INVESTIGATION OF CHANNEL ESTIMATION METHODS FOR MASSIVE MIMO SYSTEM WITH PILOT DECONTAMINATION IN RICIAN FADING

MSc THESIS

MOATA HAILE

MARCH 2025

HARAMAYA UNIVERSITY, HARAMAYA

Investigation of Channel Estimation Methods for Massive MIMO System with pilot decontamination in Rician fading

A Thesis Submitted to the School of Electrical and Computer Engineering

Postgraduate Graduate program

HARAMAYA UNIVERSITY

In Partial Fulfilment of the Requirements for the Degree of

MASTER OF COMMUNICATION SYSTEM ENGINEERING

Moata Haile

March, 2025

Haramaya University, Haramaya

Post Graduate Program

I hereby certify that I have read and evaluated this thesis entitled Investigation of channel estimation methods for massive MIMO system with pilot decontamination in Rician fading prepared under my guidance by Moata Haile. I recommend that it be submitted as fulfilling the thesis requirement.

Ritesh Pratap Singh (PhD)	______	______
Major Advisor	Signature	Date
Mr. Eyob Mersha	______	______
Co-Advisor	Signature	Date

As a member of the Board of Examiners MSc Thesis Open Defense Examination, I certify that I have read and evaluated the thesis prepared by Moata Haile and examined the candidate. I recommend that the thesis be accepted as fulfilling the thesis requirements for the degree of Master of Science in Communication Systems Engineering.

______	______	______
Chairperson	Signature	Date
______	______	______
Internal Examiner	Signature	Date
______	______	______
External Examiner	Signature	Date

STATEMENT OF THE AUTHOR

By my signature below, I declare and affirm that this thesis is my work. I have followed all ethical and technical principles of scholarship in the preparation, data collection, data analysis, and compilation of this thesis. Any scholarly matter that is included in the thesis has been given recognition through citation.

This thesis is submitted in partial fulfillment of the requirements for a Master of Science degree at Haramaya University. The thesis is deposited in the Haramaya University library and is made available to borrowers under the rules of the library. I solemnly declare that this thesis has not been submitted to any other institution anywhere for the award of any academic degree, diploma, or certificate.

Brief quotations from this thesis may be made without special permission, provided that accurate and complete acknowledgment of the source is made. Requests for permission for extended quotations from or reproduction of this thesis in whole or in part may be granted by the Head of the School or Department when in his or her judgment the proposed use of material is in the interest of scholarship. In all other instances, however, permission must be obtained from the author of the thesis.

Name: Moata Haile
Date: December 30, 2024
School: Electrical and Computer Engineering
Signature:

AUTOBIOGRAPHY

The author was born on March 13, 1997, in the East Welega zone of Oromia regional state, Gudeya Bila. He joined Gudeya Bila Primary School in 2003 and followed his grades 1 to 8 from 2003 to 2011. After completing his study there, he joined Gudeya Bila secondary school where he followed his grades of 9 to 10. Then he joined Gudeya Bila Preparatory School to attend grades 11 to 12. After that, he joined Haramaya University, School of Electrical and Computer Engineering (Communication System Engineering focus), where he scored an outstanding point. After completing his studies at this university, he was recruited as an Assistant Lecturer at Haramaya University where he has been working until today.

ACKNOWLEDGMENT

I would like to express my deepest reverence for my Almighty God for His good providence. Generally, I can say Thanks be unto God for his unspeakable gift.

I would like to extend my deep appreciation to my thesis advisor, Dr. Ritesh Pratap Singh, and my co-advisor, Mr. Eyob Mersha, for their valuable comments, encouragement, dedication, unstoppable guidance, and mentorship. I would like to acknowledge Haramaya University for its financial support, which made this thesis possible. I would like to extend my sincere gratitude to the Dean of the School of Electrical and Computer Engineering, Mr. Wehib Abubeker for providing me with a good environment

Finally, I want to extend my deep respect for my family members, especially my father Mr. Haile Birdida and My mother Mrs. Aschalu Mokonnen for their financial support, and continuous advice, without them it hardly be possible to complete this thesis work. My special thanks go to Ms. Derartu Temesgen (Kennaa koo) for her unwavering encouragement in all aspects; with you, I can reach this new horizon of success.

LIST OF ACRONYMS

BS	Base station
CDF	Cumulative distribution function
CSI	Channel state information
DFT	Discrete fourier transform
EW-MMSE	Element-wise minimum mean squared error
FDD	Frequency division duplex
iid	independent and identically distributed
LFSR	Linear feedback shift register
LS	Least square
LTE	Long term evolution
MATLAB	MATtrix LABoratry
MIMO	Multiple input multiple output
MMSE	Minimum mean squared error
MR	Maximum ratio
MRC	Maximum ratio combining
MRT	Maximum ratio transmission
MU-MIMO	Multi user-multiple input multiple output
OFDM	Orthogonal frequency division multiplexing
PN	Pseudonoise
RF	Radio frequency
Rx	Reciever
RZF	Regularized zero-forcing
SE	Spectral effeciency
SIC	sequential interference cancellation
SINR	signal to interference and noise ratio
SNR	signal to noise ratio
TDD	Time division duplex
Tx	Transmiter

ULA	Uniform linear array
Wi-Fi	Wireless fidelity
WiMAX	Worldwide interoperability for microwave access
ZF	Zero-forcing

ABSTRACT

Massive multiple input multiple output (MIMO) systems are essential to meet the growing need for enhanced capacity and faster data rates in modern wireless communication networks, particularly in the fifth generation (5G). These systems serve many users at once on the same frequency band by using a lot of antennas at the base station (BS). The computational complexity of many antenna numbers and pilot contamination are the main obstacles to estimating the channel of the massive MIMO system. To overcome pilot contamination challenges, this thesis aims to investigate pilot-based channel estimate methods with pilot decontamination in Rician fading. In this thesis, soft pilot reuse is combined with the weighted graph coloring pilot decontamination mechanism to overcome the impact of pilot contamination in Rician fading scenarios, which is the main weakness in massive MIMO systems. In both Rayleigh and Rician fading, the accuracy of the channel estimate is increased by mitigating the effects of pilot contamination. MATLAB simulations are used to examine how well the minimum mean squared error (MMSE), element-wise minimum mean squared error (EW-MMSE), and least squares (LS) techniques work with the Rayleigh and Rician fading channels model. The simulation result shows that the better method for channel estimation in both uplink and downlink situations is MMSE with Rician fading. In the uplink system, spectral efficiency (SE) of the channel estimate is increased from 20.9 b/s/Hz/cell to 24.7 b/s/Hz/cell with pilot decontamination at BS antenna M = 90. For downlink, it increased from 21.8 b/s/Hz/cell to 27.5 b/s/Hz/cell. In Rayleigh fading, for the uplink system, SE increased from 14.0 b/s/Hz/cell to 16.5 b/s/Hz/cell at M = 90 with pilot decontamination, whereas in the downlink it improved from 14.2 b/s/Hz/cell to 17.5 b/s/Hz/cell. The results show that the addition of decontamination techniques increases the accuracy of channel estimates, hence improving system performance for massive MIMO networks. So, MMSE are useful for utilizing channel characteristics, while the proposed method (soft pilot reuse combined with weighted graph coloring) is a reliable way to reduce the impact of pilot contamination on Rayleigh and Rician fading.

Keywords: Channel estimation, Massive MIMO, Pilot decontamination, Rayleigh fading, Rician fading, Spectral efficiency

List of Figures

List of Tables

Contents

1. INTRODUCTION

1.1 Background of the study

Over the past 20 years, a lot of study has been done on the potential of Multiple input multiple output (MIMO) technology to greatly boost the performance and dependability of wireless systems. As a result, it has been incorporated into a number of wireless standards. However, in recent years, attention has turned to Multi user-multiple input multiple output (MU-MIMO), in which a base station (BS) with several antennas can serve a group of users simultaneously with a single antenna, allowing each user to share the multiplexing gain (Chataut & Akl, 2020; Heath Jr & Lozano, 2018).

Moreover, the performance of the MU-MIMO system (Heath Jr & Lozano, 2018) is generally less vulnerable to propagation conditions due to the diversity of users than in the point-to-point MIMO situation. Consequently, MU-MIMO has emerged as a key element of communications standards such as 802.11 Wireless fidelity (Wi-Fi), 802.16 Worldwide interoperability for microwave access (WiMAX), and Long term evolution (LTE), and it is being progressively accepted globally. In most MIMO systems, the BS often employs less than ten antennas; hence, even if the Spectral effeciency (SE) improvement is important it is still rather small. However, Massive MIMO (Björnson et al., 2017; Marzetta, 2010) is a significant technique in wireless communication systems due to improving 5G networks capacity, reliability, and SE. It significantly increases SE by enabling simultaneous data transmission to various users in the same frequency band by providing BS with many antennas. So, in order to improve SE and throughput, massive MIMO will use additional antennas to help concentrate radiation into a smaller area of space (Chataut & Akl, 2020). A well-known method of enhancing throughput is by improving the cellular network SE. Increasing more antennas to the BS and/or user equipment is one method of boosting SE. Throughput can be calculated using (Borges et al., 2021)

$$\text{Throughput (b/s)} = \text{Bandwidth (Hz)} \times \text{SE (b/s/Hz)} \tag{1.1}$$

The primary possible technologies to satisfy the performance needs of emerging wireless systems are massive MIMO, hybrid beamforming, and communication at larger frequency bands (Masood, 2022; Masood et al., 2023). Nevertheless, bands with greater frequencies are more susceptible to blocking and absorption and produce larger path losses. In order to minimize potential losses, massive MIMO can be used to benefit from beamforming benefits due to the increased number of antennas. Additional benefits of massive MIMO include the

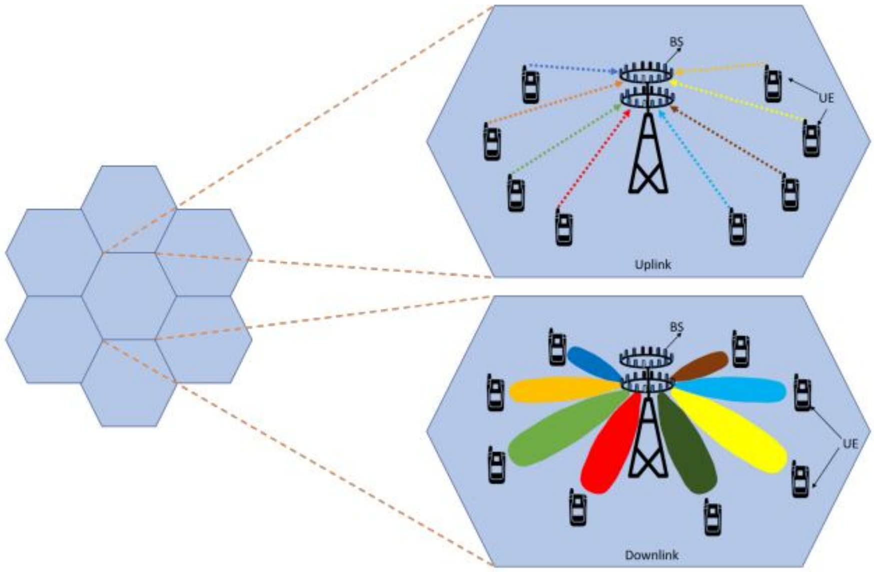

Figure 1.1: Massive MIMO downlink and uplink framework (Chataut & Akl, 2020)

simple nature of antenna array deployment with large antenna elements and the compact antenna size at larger frequencies. Because every antenna has a unique Radio frequency (RF) chain (Masood, 2022), a completely digital massive MIMO system requires more energy. Figure 1.1 illustrates a massive MIMO uplink and downlink framework.

A vital component of communication systems, particularly in wireless communication, is the process by which the transmitter and receiver estimate the channel parameters. Estimating the channel parameters enables the adjustment of impairments like distortion, delay, and attenuation to ensure reliable and efficient data transfer(Goldsmith et al., 2003a; Rappaport et al., 2013). For channel estimation, a variety of techniques are used, such as pilot-based estimation, training sequence-based estimation, and blind estimating techniques, each of which is appropriate for a particular communication scenario and set of criteria (Goldsmith et al., 2003a). This thesis mainly focuses on pilot-based massive MIMO channel estimation in Rician fading scenarios with pilot decontamination. A variety of challenges arise when estimating channels in communication systems because wireless channels are essentially not precise and dynamic. The difficulties include interference and noise, multipath propagation, computational complexity, time-varying nature, frequency selectivity, and pilot overhead.

The most common algorithm that uses channel estimates in massive MIMO includes Element-wise minimum mean squared error (EW-MMSE) estimation, Minimum mean squared error (MMSE) estimation, and Least square (LS) estimation. Consider the single-cell network depicted in Figure 1.2. The system consists of the transmitter, channel, and receivers (user equipment) (Busari et al., 2017). Achieving better efficiency in large-scale antenna systems requires precise CSI at the transmitter for downlink precoding tasks.

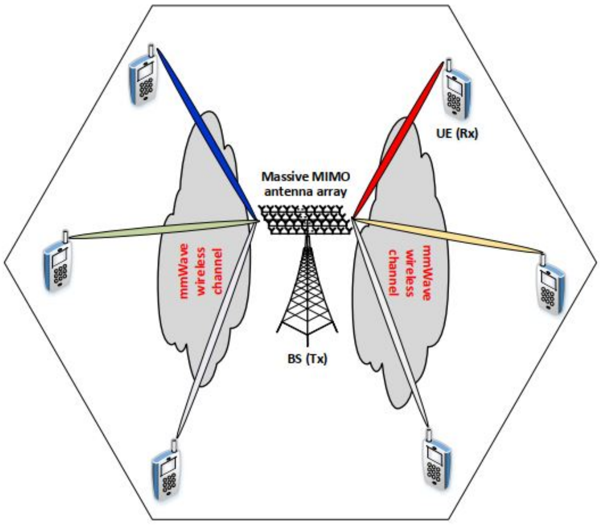

Figure 1.2: mmwave massive MIMO single cell system (Busari et al., 2017)

Channel estimation is done by uplink pilots, followed by downlink precoding and transmission. The uplink and downlink functions in TDD systems utilize identical frequency bands. Because TDD assumes that the downlink channel matrix is a conjugate of the uplink channel matrix, it obtains CSI by training pilots in uplink transmission (Heath Jr & Lozano, 2018; Larsson et al., 2014a; Marzetta & Hochwald, 2006; Naqvi et al., 2017). The arrangement of uplink pilots orthogonally between terminals is preferable. The maximum number of identical orthogonal pilot signals that each user within each cell can receive calculated by

$$\tau_{p_{max}} = \frac{T_{coh}}{dS} \tag{1.2}$$

Where the maximum number of pilots is τ_p, T_{coh} is the interval of coherence, and dS is the delay spread of the channel. Due to the restricted number of orthogonal pilot sequences, users in neighboring cells use pilots that are no more orthogonal to those inside the cell. Orthogonal pilot patterns cannot be assigned to each user in each cell due to the channel coherence interval restriction in the multicell systems. Reuse of orthogonal pilot sequences from one cell to another is necessary. The channel estimated in that cell would be distorted as a result of pilots provided by users in other cells. This result is called pilot contamination, and it lowers the performance of the system. Pilot contamination presents a challenge, as it limits the maximum achievable throughput. Although orthogonal pilot transfer reduces the number of users that can be scheduled in a cell during a coherent interval, it is a useful technique for preventing intracellular pilot contamination (Fernandes et al., 2013; Jose et al., 2011; Marzetta, 2010). Pilot decontamination is the technique that is used to minimize the effects of this issues in massive MIMO channel estimation.

In massive MIMO, pilot decontamination is crucial for increasing channel estimate accuracy, particularly when several users share similar pilot signals across cells, which can cause interference and decreased CSI. This problem more affects TDD systems because channel estimates are based on uplink and downlink reciprocity (Salh et al., 2020). The pilot decontamination techniques that this thesis mainly focuses on are soft pilot reuse and graph coloring-based pilot assignment.

1.2 Statement of the Problem

There are a plethora of benefits with massive MIMO wireless communication systems. One of the most key functions of massive MIMO is providing high data rates while supporting enormous users and antennas at once. Channel estimation is the technique of predicting the characteristics of the communication channel between the transmitter and receiver. The channel estimation technique is used to approximate the real channel properties at the receiver of a massive MIMO system. In massive MIMO systems, the growing number of antennas in the BS causes higher computational complexity for channel estimation. Traditional methods struggle to manage the increased antennas and unknown parameters efficiently, causing a rise in computational burden. The accuracy of channel estimates may be impacted by pilot contamination in situations when pilot signals are repeated by several users or cells. By adding interference and inaccurately calculating the channel status information, this phenomenon might affect the system performance (Benzaghta & Rabie, 2021). The efficiency of massive MIMO systems is directly determined by the quality of the channel estimation. Massive MIMO relies on CSI for signal identification and decoding. The combined effect of fading, scattering, and other factors is represented by the communication link status information, which is conveyed from the transmitter to the receiver. If the CSI is good, the performance of massive MIMO rises linearly with the number of transmitting or receiving antennas (Chataut & Akl, 2020). Reduced SE, poor overall communication quality, and poor system performance might result from inaccurate CSI estimates (Benzaghta & Rabie, 2021). The goal of this thesis is to investigate channel estimation for massive MIMO in Rician fading with pilot decontamination techniques that can improve the performance of the system. By overcoming this issue, the thesis will make Massive MIMO more robust and scalable, meeting the increasing requirements of data rates in the current wireless communication networks.

1.3 Significance of the Research

Massive MIMO technology is crucial to improving the ability, coverage, and user satisfaction of 5G networks, as it improves mobile broadband performance. 5G provides faster connection speeds for uses such as streaming high-definition video and virtual reality. Through the deployment of many antennas at the BS, it also increases the signal strength and dependability for users at the network edge. This can improve coverage, which is especially crucial in the indoor and rural areas where signal strength is usually lower. Furthermore, it minimizes system interference for other users by enabling reliable signal direction toward targeted users. The system's overall efficiency is enhanced by this spatial resolution. Channel estimation is therefore essential for wireless communication to benefit from massive MIMO.

1.4 Objectives of the Research

1.4.1 General objectives

The general objective of this research is to investigate massive MIMO channel estimation in Rician fading scenarios with the combination of soft pilot reuse and weighted graph coloring pilot decontamination.

1.4.2 Specific objectives

The specific objectives of this research are:

1. To examine conventional channel estimate methods for massive MIMO systems and conduct an evaluation study of massive MIMO wireless systems.
2. To investigate the mathematical basis of channel estimation techniques within the framework of a massive MIMO cellular network.
3. To study and analyze pilot decontamination methods in massive MIMO channel estimation.
4. To analyze various channel estimation techniques for multiuser scenarios of a massive MIMO system using simulation tools for both Rician and Rayleigh fading.
5. To assess the performance of channel estimation algorithms in massive MIMO systems with soft pilot reuse and weighted graph coloring under Rician and Rayleigh fading using metrics such as Cumulative distribution function (CDF), and SE.

1.5 Scope of the Research

Massive MIMO is an essential technique for modern wireless communication systems because it enables greater capacity and faster data rates, particularly when 5G networks are developed. Issues like pilot contamination, which have significant impacts on the scalability and performance of massive MIMO systems, are the focus of this thesis. It focuses on TDD-based systems and utilizes channel reciprocity to improve system efficiency. The simulations are carried out using MATLAB in order to assess SE in uplink and downlink under pilot decontamination situations and fading channels like Rayleigh and Rician fading channels.

This thesis mainly focuses on reducing the constraints caused by pilot contamination and increasing the accuracy of channel estimation in order to further the development of massive MIMO systems. The thesis scope is limited to theoretical models and simulation tools, with the knowledge that real-world applications may be used for different factors.

1.6 Executive summary

The remaining chapters of this thesis are arranged as follows:
The **second chapter** includes fundamental ideas such as the properties of massive MIMO systems, difficulties in channel estimation, and widely applied strategies, including pilot-based, semi-blind, and blind estimation approaches. Additionally, it discusses pilot contamination and how to mitigate its effects. It critically evaluates comparable studies to find gaps in the literature and support the need to look into better approaches.

In the **third chapter**, pilot-based channel estimation techniques and decontamination tactics such as weighted graphed coloring pilot decontamination, random pilot, and soft pilot reuse are covered in detail. The modeling environment and experimental setup are described, along with important assessment metrics including SINR and SE.

In the **fourth chapter**, the results of the simulations and discussion of the finding are presented, comparing several methods for channel estimation under various scenarios, including those with and without pilot decontamination. The analysis focuses on the performance gains made possible by the suggested techniques.

In the **fifth chapter**, the research findings are finally summarized, with a focus on the importance of efficient pilot decontamination for enhancing channel estimation in massive MIMO systems. Future research recommendations center on improving estimating methods even further and tackling scalability and practical implementation issues.

2. LITERATURE REVIEW

2.1 Introduction

A multi-user MIMO system functioning in Time division duplex (TDD) Lu et al., 2014 was extended establishing massive MIMO. Multi-user MIMO systems use a multi-antenna base station (BS) to serve many users simultaneously (Gesbert et al., 2008). When utilized effectively, many antennas at the BS provide array gain. As a result, the Base station (BS) increases the received signal power by directing beamforming toward the intended receiver. Another advantage of having several antennas is spatial multiplexing, which allows various signals to be transmitted simultaneously with varying directional beamforming to serve numerous users at the same time and frequency. The number of integrated users may cause the SE per cell increase proportionately through spatial multiplexing (Caire & Shamai, 2003). Nevertheless, the system can only multiplex a small number of users at once in a typical multi-user MIMO because of the restricted number of antennas at the BSs.

Massive MIMO (Van Chien & Björnson, 2017) is a MU-MIMO system with many users and BS antennas. In a massive MIMO system, hundreds or thousands of BS antennas share a single frequency resource to service tens or hundreds of users at once. Increasing the number of antennas is the key to enhancing the capacity of massive MIMO systems. This functionality enables the 5G network requirements. Proper channel estimation is one of the factors that allow massive MIMO to perform more efficiently. CSI is necessary for the BS to recognize user-provided information in the uplink and precode the information in the downlink. The uplink study is used to obtain this CSI. every user is given an orthogonal pilot pattern, which they then transmit to the BS. The BS uses the pilot signals it receives to estimate the channels, and it knows the pilot sequences of each user transmits (Van Chien & Björnson, 2017).

Massive MIMO describes a system comprised of BSs that can support tens of users simultaneously with hundreds of antennas. All users are served over the same time-frequency block by the BSs through the use of spatial multiplexing. Every antenna at a BS has its own RF chain. Therefore, there are benefits to fully digital beamforming within the system. Two advantages of massive MIMO systems are: 1) when compared to conventional MIMO systems, massive MIMO BSs first improve the SE per cell by enabling the spatial multiplexing of more users (Marzetta et al., 2016). Additionally, several antennas on the massive MIMO BSs increase array gain, and their enhanced directivity reduces inter-user interference, increasing SE per user. Thus, massive MIMO dramatically raises the SE for the per-cell cellular network. 2) In massive MIMO, the user channels are nearly orthogonal due to the numerous antennas at the BSs. This property of massive MIMO is a favorable propagation. Favorable propagation allows for the implementation of relatively straight-forward processing methods that treat interference as noise. Channel hardening is the process by which the effects of small-scale fading of wireless propagation channels are averaged out in massive MIMO BSs due to the large number of antennas (Marzetta et al., 2016; Ngo et al., 2014; Wu et al., 2017). It might be said that the channels become more deterministic with channel hardening. Consequently, it is achievable to carry out resource allocation, power control, and other processes over large-scale fading without requiring small-scale fading for either the allocation or control method. Resource allocation over the large-scale fading reduces the complexity of the system signal processing (Björnson et al., 2014; Hoydis et al., 2013).

2.2 Basic Scenarios of Massive MIMO

Consider the fundamental situations of massive MIMO and apply the following operational assumptions to a spatially multiplexing M antenna BS that serves K single-antenna users. Figure 2.1 illustrates how the matrix transposition connects the downlink and uplink channel matrices when channel reciprocity is assumed (X. Gao et al., 2012). When K single-antenna

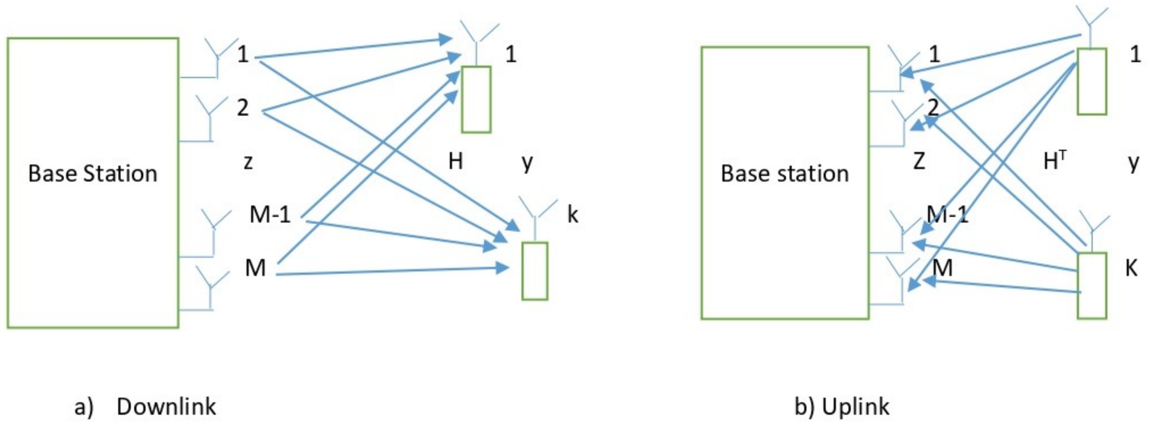

Figure 2.1: Model of MU-MIMO setup (X. Gao et al., 2012)

users in the spatial domain are multiplexed by an M-antenna BS. The channel matrix for $H \in C^{M \times N}$ is given as;

$$H = \begin{bmatrix} h_{11} & h_{12} & h_{13} \cdots & h_{1N} \\ h_{21} & h_{22} & h_{23} \cdots & h_{2N} \\ \vdots & \vdots & \ddots & \vdots \\ h_{M1} & h_{N2} & h_{N3} \cdots & h_{MN} \end{bmatrix}, \quad H \in C^{M \times N}.$$

The framework for every time-frequency resource downlink transmission is given by

$$y = \sqrt{p_{dl}} H_z + n \tag{2.1}$$

where n is the white noise Gaussian vector with iid random signals, z is the transmit signal vectors over M antennas, y is the received signal vector at K users, and H is the channel array propagation. Assuming $\Sigma||z||^2 = 1$, the total power transferred in the downlink is p_{dl}. The signals for the Uplink channel matrix H^T are modeled considering reciprocity become

$$z = \sqrt{p_{ul}} H^T y + n \tag{2.2}$$

In massive MIMO, the total transmit power from all users is p_{ul}. Depending on the power scaling method, $p_{ul} = pK$ or $p_{ul} = pK/M$.ăTo achieve good spatial separation of user signals, massive MIMO typically assumes that $M \gg K$ (Björnson et al., 2016). As seen in

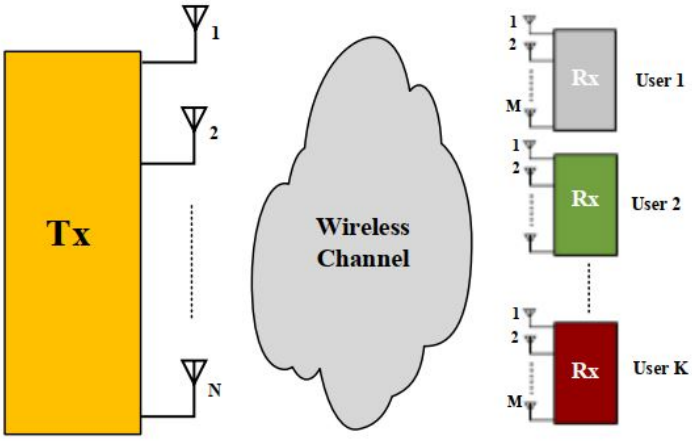

Figure 2.2: A single transmitter with K users and N transmit antennas (Busari et al., 2017)

Figure 2.2, every user in the configuration has a Reciever (Rx) with *M* receive antennas, one Transmiter (Tx) with *N* transmit antennas, and *K* users (Busari et al., 2017).

As the number of antennas increases to the level where $N \gg M$ and $N \rightarrow \infty$, the massive

MIMO channel rate is

$$C \approx M\log_2(1+\rho) \tag{2.3}$$

But, when $M \gg N$ and $M \rightarrow \infty$, the channel rate approximates to;

$$C \approx N\log_2\left(1+\frac{\rho M}{N}\right) \tag{2.4}$$

where C is the massive MIMO system capacity, expressed in bits per second per Hz, M is the number of antennas at the BS, and ρ is SNR. Massive MIMO uses spatial multiplexing, requires CSI for both uplink and downlink, and relies on phase coherent broadcasts from all antennas at the BS. It is a technology that makes networks both fixed and mobile more secure, reliable, robust, and efficient in terms of energy and spectrum (Busari et al., 2017). During the training stage, channels will be generated at the BS and users with perfect CSI and all K users sharing the same time-frequency resource. Figure 2.3 illustrates how the M-antenna BS supports K single-antenna users in the same time-frequency resource in multi-user MIMO systems.

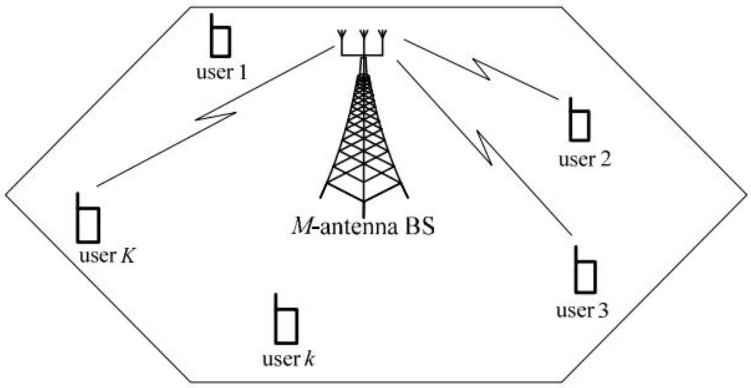

Figure 2.3: Multiuser MIMO Systems with *M* antenna BS and *K* single-antenna users (Ngo, 2015a)

2.3 Major Characteristics of massive MIMO

Some of massive MIMO properties will be discussed in this section. Specifically, the duplexing protocol, channel hardening, SE, and favorable propagation.

2.3.1 High Spectral Efficiency (SE)

The term SE describes the bit-per-second (bps) data transmission capacity over a specified bandwidth (Hz) in given channel conditions. Serving numerous users concurrently on the same time-frequency resource allows massive MIMO systems to achieve a significant increase in SE (Larsson et al., 2014a). This is accomplished through spatial multiplexing, in which numerous data streams are sent at the same frequency but separated spatially. The SE can be defined as (Saatlou et al., 2019)

$$SE = \frac{T - \tau_u - \tau_d}{T} \sum_{u=1}^{U} R_u \tag{2.5}$$

where T represents the length of the coherence interval used in downlink transmission and R_u is the lower bound of achievable downlink rate for the u_{th} user and defined as;

$$R_u = E\left[\log_2\left(1 + \frac{p_d|\hat{a}_{uu}|^2}{p_d \sum_{i=1}^{U} E\{|\epsilon_{ui}|^2\} + p_d \sum_{i\neq u}^{U} |\hat{a}_{ui}|^2 + 1}\right)\right] \tag{2.6}$$

From Maximum ratio transmission precoding

$$\begin{cases} \hat{a}_{ui} = \frac{\sqrt{\tau_d p_p}}{\tau_d p_p + U} \tilde{y}_{p,ui} & i \neq u \\ \hat{a}_{uu} = \frac{\sqrt{\tau_d p_p}}{\tau_d p_p + U} \tilde{y}_{p,uu} + \frac{U}{\tau_d p_p + U} \sqrt{\frac{\tau_u p_u M}{K(\tau_u p_u + 1)}} & i = k \\ E\{|\epsilon_{ui}|^2\} = \frac{1}{\tau_d p_p + U} & i \,\forall\, u \end{cases} \tag{2.7}$$

2.3.2 Favorable Propagation

Favorable propagation occurs when the transmission channels of two cell users are orthogonal to one another. Favorable propagation allows the BS to cancel out co-channel interference between users, reducing the need for complicated interference suppression algorithms. Consequently, it raises SE for each user. Consider a BS with *M* antennas, a single cell with two users, and a single antenna. The channel responses of both users across a narrow band channel are represented by the vectors $g_1 \sim CN(0, I_M)$ and $g_2 \sim CN(0, I_M)$. This channel model is described as independent and identically distributed (iid) Rayleigh fading. These vectors have zero mean and a correlation matrix I_M, and they are circularly symmetric complex Gaussian distributed (Vieira et al., 2014).

$$g_1^H g_2 = 0 \tag{2.8}$$

without losing any received signals, the BS is able to differentiate the signals it receives from each user. The transmitted signal, shown by the received signal from users x_1 and x_2, can be expressed as follows

$$y = g_1 x_1 + g_2 x_2 \tag{2.9}$$

When the BS has perfect knowledge of both channel vectors, it can minimize user interference by taking the inner product of the received signal y and the desired user channel. Furthermore, the effect of noise is neglected for reasons of simplicity. Regarding user 1, the inner product is

$$g_1^H y = ||g_1||x_1 + g_1^H g_2 x_2 = ||g_1||^2 x_1 \tag{2.10}$$

Due to the orthogonality of the vectors in (2.10), the component $g_1^H g_2 x_2$ is zero, giving the user the desired signal. This is characterized as advantageous propagation since it is the greatest possible scenario for the BS; nevertheless, if the channel vectors are set at random, this is unlikely to occur in practice. Conversely, it demonstrates that in the case of Rayleigh fading channels, the approximate advantageous propagation can happen asymptotically in massive MIMO BSs (Marzetta et al., 2016). As the product of two normalized vectors, its inner product must satisfy (Ngo et al., 2014):

$$\frac{g_1^H g_2}{M} \rightarrow 0 \tag{2.11}$$

Convergence occurs when $M \rightarrow \infty$. These two channel vectors are asymptotically orthogonal as the number of antennas M increases.

2.3.3 Channel Hardening

Channel hardening is the process of a channel become less vulnerable to small-scale fading effects by getting more predictable while all of the antennas are in use (Vieira et al., 2014). It improves system stability and predictability by decreasing fluctuations in channel quality (Müller et al., 2014). The channel vector of an arbitrary user approaches a massive MIMO BS with M antennas is provided by $g \sim CN(0, I_M)$, asymptotic channel hardening can be estimated as (Björnson et al., 2017)

$$\frac{||g||^2}{\Sigma\{||g||^2\}} \rightarrow 1 \tag{2.12}$$

When the BS evaluated the received signal, a squared norm appeared; this is significant since it helps to determine the communication performance. $||g||^2$ is considered to be close to its average value due to asymptotic channel hardening, the fluctuations are insignificant. The idea of spatial diversity from traditional small-scale MIMO systems is extended to the situation when the BS has a large number of antennas. According to channel hardening, for a given channel realization, the average channel quality $\Sigma||g||^2$ approaches the channel quality $||g||^2$.

2.3.4 Duplexing Protocol

There are two techniques of duplex protocol approaches used in massive MIMO systems; TDD and Frequency division duplex (FDD) are these methods. Each BS must estimate the channel vectors of its serving users in each channel coherence block in order to process the uplink and downlink signals.A time-frequency block with a continuous fading channel is called a coherence block. Massive MIMO assumes that the BSs have access to all statistical channel state data. Channel estimations should be performed at each BS in order to obtain the instantaneous Channel state information (CSI). Channel estimate uses pilot transmission (Björnson et al., 2017; Marzetta et al., 2016). During the pilot transmission phase, each transmitter (user) sends a sequence to the receiver (the BS) from a predetermined set of pilot signal sequences. In order to determine the transmitter's channel, the receiver evaluates the signal with the "true" signal from the set (Jose et al., 2011; Marzetta et al., 2016).

Generally, the number of orthogonal pilot sequences needed for the pilot transmission of several transmitters in massive MIMO systems is equal to the number of transmitting antennas. It is also important to keep the pilot signals as short as feasible in order to make the best use of a coherence block's resources for data transfer. In a massive MIMO system, the downlink and uplink pilot transmissions require different numbers of pilot symbols to estimate the channel.ă Assuming that K single-antenna users occur, the system requires an approximate number of K pilot signal sequences in the uplink to estimate the uplink channels. On the other hand, M pilot signals are required for pilot transmission in the downlink if the BS has M antennas. For massive MIMO systems, $M \gg K$ is common (Björnson et al., 2017). TDD operation is independent of CSI feedback since both uplink and downlink propagation channels are reciprocal. The only difficulty is receiving RF chains and adjusting the BS broadcast (X. Gao et al., 2012). The coherence block's time-frequency separation for the FDD and TDD protocols is shown in Figure 2.4.

TDD is the time-domain separation of uplink and downlink broadcasts while using all available bandwidth; channel reciprocity is maintained when both occur at the same coherent moment. It shows that the same channel is used in both directions. Therefore, if the channel is estimated in one direction (the uplink), it is likewise valid in the other direction (the downlink). Therefore, in TDD massive MIMO systems, it just requires K pilot sequences. Accordingly, the channel estimate is not affected by M Björnson et al., 2017. On the other

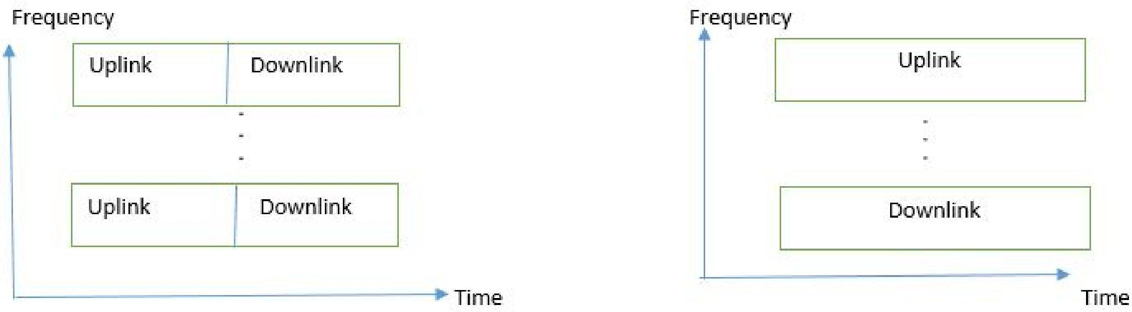

Figure 2.4: Time-frequency coherence block separation for protocols a) TDD and b) FDD (X. Gao et al., 2012)

hand, FDD allows for simultaneous uplink and downlink transmission in different frequency bands. Consequently, because the uplink and downlink frequency bands mismatch, the channel reciprocity is not maintained. So, for each direction's channel estimation must be done separately. For channel estimate in FDD, it thus needs both uplink and downlink pilots. To transmit the estimated channel back to the BS in the uplink, more M signals and M pilot signal sequences in the downlink are necessary. Moreover, uplink channel estimate requires N pilots. Assuming that resources are distributed equally between uplink and downlink, FDD requires $(2M+K)/2$ pilot signals overall (Björnson et al., 2017). There is usually a large 100 MHz difference between the uplink and downlink in FDD. It is evident that TDD Massive MIMO does not scale with M and has a far lower channel estimation overhead than FDD Massive MIMO. TDD is the recommended duplexing option over FDD for massive MIMO systems.

2.4 Multi-User Massive MIMO

Next-generation wireless communication systems (Larsson et al., 2014b; Rashid, 2021; Wu et al., 2018) rely on multi-user massive MIMO technology. With the use of the several antennas at the BS, numerous users can be serviced at once. By utilizing multi-user MIMO technology, multiple users can establish communications with BS within the same frequency band. Through the use of effective signal processing techniques, it is possible to separate the signals designed for various users by spatially multiplexing. Where it is expected that K mobile stations can interact simultaneously with a BS having a significant number, N_{BS}, of antennas and M_{BS} RF chains. To support N_s data streams, each mobile station has M_{MS} RF chains and N_{MS} antennas. Suppose a multi-user MIMO network consisting of K users

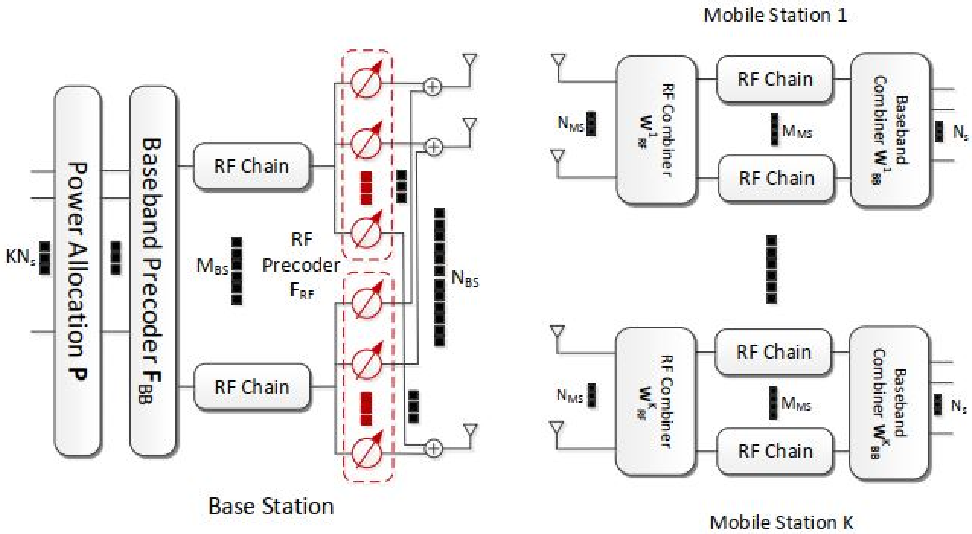

Figure 2.5: System diagram for a hybrid processing structure multiuser massive MIMO system (Wu et al., 2018)

distributed inside each of the L cells, each of which has a BS of its own. Each user has a single-antenna transceiver, and each BS in a cell has M antennas. Assumed to be $M \gg K$ is that the BS has a greater number of antennas than users. The channel gain between every pair at time t is represented by $h_{limk}(t)$.

$$h_{limk}(t) = g_{limk}(t)\sqrt{\beta_{lik}} \tag{2.13}$$

Whereas β_{lik} shows the large-scale fading carried on by the shadowing and geometric attenuation effects,$g_{limk}(t)$ represents the small-scale fading narrow-band channel between the m-th antenna of BS l and the k-th user in cell i. Consider $g_{limk}(t)$ to be a wide-sense stationary complex Gaussian process with zero mean and unit power, and β_{lik} to be a known constant that is independent of the antenna index m. Let $g_{lik}(t) = [g_{li1k}(t), g_{li2k}(t), \ldots, g_{liMk}(t)]$ be considered. The $M \times 1$ small-scale fading channel vector, represented by T, connects the k-th user in cell i to the l-th BS antenna array. The $M \times K$ fading matrix $G_{li}(t) = [g_{li1}(t), \ldots, g_{liK}(t)]$ becomes the result of calculating all $g_{lik}(t)$ vectors for the K users in cell i. The $l-th$ BS and the users in cell i have a total channel gain that is determined by

$$H_{li}(t) = G_{li}(t)D_{li}^{\frac{1}{2}}, \tag{2.14}$$

where $D_{li} = \text{diag}\{\beta_{li1}, \beta_{li2}, \ldots, \beta_{liK}\}$. In the case of favorable propagation, when $M \to \infty$ for a fixed K, the channel vectors of users to the BS (the columns of H_{li}) become mutually orthogonal

$$H_{li}^H(t)H_{li}(t) = D_{li}^{\frac{1}{2}}G_{li}^H(t)G_{li}(t)D_{li}^{\frac{1}{2}}$$

The following assumes a single cell (L = 1) situation for the sake of simplicity.

$$\approx MD_{li}^{\frac{1}{2}}I_K D_{li}^{\frac{1}{2}} = MD_{li} \tag{2.15}$$

2.5 Channel Estimation

In the massive MIMO system, the process of identify the characteristics of the communication channel that exists between the transmitter and the receiver is known as channel estimation. This is significant since it influences system performance. The accuracy of the channel estimate influences how successfully the system transmits and receives data; hence, it is an important factor to consider while developing and running massive MIMO systems.

2.5.1 Channel Estimation in TDD Systems

A method in which uplink and downlink broadcasts occur at separate times within the same frequency band is TDD. This means that the BS and user devices send and receive data alternately. From the beginning, the massive MIMO idea is based on TDD and utilises reciprocity to obtain CSI at the BS. User equipment transmits pilots on the uplink; every antenna has its own RF electronics; and each user equipment to BS channel is estimated. The uplink and downlink channels are reciprocal (Flordelis et al., 2018; Ngo, 2015a). The process for obtaining the CSI is shown in Figure 2.6. Let's assume that the channel stays constant throughout T symbols. Consequently, $2K < T$ is required.

- For the uplink transfer: The BS needs the CSI to determine which signals are being sent by the K users. This is an estimated CSI at the BS. During the uplink, the K users specifically communicate the BS K orthogonal pilot sequences. Once the pilot signals have been received, the BS estimates the channels. This operation requires a minimum channel use of K (Ngo, 2015a).

- For the downlink: To identify the desired signals, every user needs the effective channel gain, while the BS needs CSI to precode the signals that are broadcast. The broadcast symbols can be precoded using the channel calculated at the BS in the uplink due to the channel reciprocity. Each user can utilize the received pilot signals to estimate the effective channel gains, which can be determined by the BS beamforming pilots. This requires that at least K channel use (Ngo, 2015a).

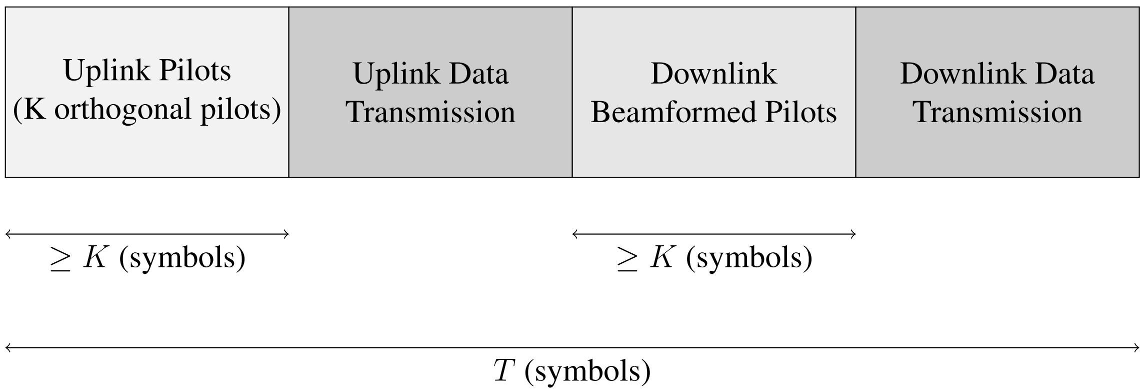

Figure 2.6: Slot structure and channel estimate for TDD systems.

2.5.2 Channel Estimation in FDD Systems

The FDD communication technology uses different frequency bands for uplink and downlink data transmissions. Data transmission from user devices to the network (uplink) and from the network to user devices (downlink) is done using separate frequency bands that are designated by FDD. There are no channels that are reciprocal between the uplink and downlink. For FDD to function, the UEs must provide the BS with CSI feedback. CSI can only be effectively encoded by utilizing side information on the propagation. Channel estimate in FDD systems is shown in Figure 2.7. The following training scheme (Flordelis et al., 2018; Ngo, 2015a) can be used to get the channel knowledge for users and at the BS:

- The BS requires CSI to decode the signals sent by the K users in the uplink transmission scenario. Orthogonal pilot sequences can be sent from the K users to the BS. Following that, the BS will estimate the channels based on the pilot signals received. At least K channel utilization is necessary for this operation in the uplink (Ngo, 2015a).

- Regarding the downlink transmission: The K users receive orthogonal pilot sequences from the M BS antennas. Every user will utilize the pilots they have been given to estimate the channel. It then sends its channel estimates (M channel estimates) to the BS via the uplink in sequence. In this procedure, the downlink requires at least M channels, and the uplink requires M channels (Ngo, 2015a).

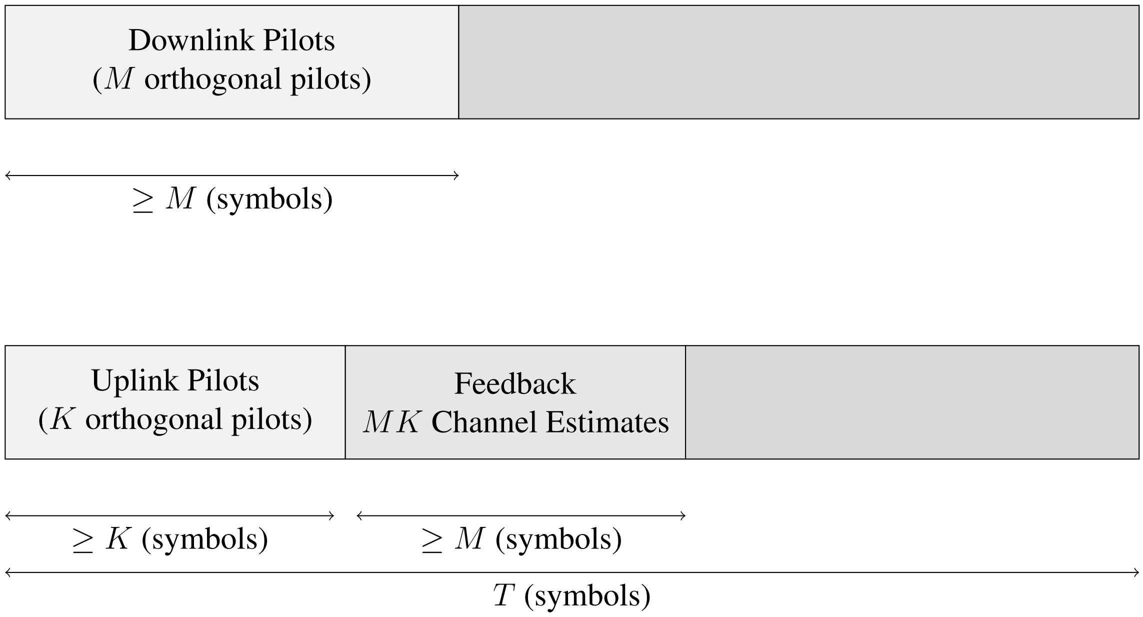

Figure 2.7: Slot structure and channel estimate for TDD systems (Ngo, 2015a).

The entire process of channel estimation requires at least $M + K$ channel uses in the uplink and M channel uses in the downlink. The coherence interval lengths for the uplink and downlink are taken to be equal to T. The constraints are as follows: $M <$ T and $M + K <$ T. Thus, $M + K <$ T is the requirement for FDD systems.

2.6 Channel Models

A channel model is a mathematical representation of how a communication channel that is used to send wireless signals works. It can represent the signal's power loss as it travels over the wireless medium.

2.6.1 Perfect Channel Model

A perfect channel model (Proakis & Salehi, 2008; Rappaport, 2024a; Shannon, 2001) is an idealized communication link in which the transmitted signal is received precisely as it was sent, with no degradation. This means that the signal is free of distortions, losses, and noise. While real-world communication channels are never perfect, this model serves as a theoretical standard against which real-world channels can be measured. It is an idealized medium of communication that enables information to be transmitted without error.

Properties of perfect channel model

- Noiseless: The channel is free of all forms of noise, including thermal noise and interference.
- Distortion-less: Throughout the transmission, the signals shape and form remain unchanged.
- No attenuation: The signal strength remains consistent over the distance traveled.
- No delay: The signal has no delay or latency between the transmitter and the receiver.

Mathematically, it can be expressed by the shannon capacity formula as below.

$$C = B \cdot \log_2(1 + \text{SNR}) \tag{2.16}$$

Where C represents maximum data that can be achieved means channel capacity, B represents bandwidth, and SNR represents signal-to-noise ratio.

2.6.2 Additive White Gaussian Noise (AWGN) Channel Model

AWGN Haykin, 2008; Proakis and Salehi, 2008 is a fundamental noise model used in communication systems to imitate different random processes occurring in nature. The only thing that limits communication in this channel model is the linear summation of white noise. The term additive describes the noise that is introduced when a signal passes through a channel; white describes the introduced noise that affects all frequencies equally, which means the noise has the same spectral power density, and Gaussian describes the introduced noise amplitude following normal distribution. A discrete-time AWGN channel is defined by the input output equation as below.

$$y_k = x_k + n_k \tag{2.17}$$

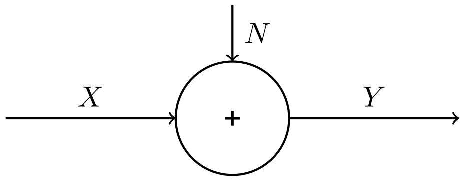

Figure 2.8: AWGN channel

where the noise samples n_k are realizations of iid variables with a zero-mean appropriate complex Gaussian distribution, with a variance of σ^2.

Properties of AWGN

- Power spectral density: The power of noise per unit bandwidth remains constant.
- Gaussian distribution: The noise samples amplitudes have a normal distribution.
- Memoryless: Each sample noise is independent of the noise in the other samples.

2.6.3 Rayleigh fading model

Rayleigh fading (Edition et al., 2002; Goldsmith, 2005) is a statistical model that describes how the propagation environment affects a radio signal. It is assumed that the magnitude of a signal going via a communication channel will vary randomly following the Rayleigh distribution. When the transmitter and receiver cannot see each other clearly, this technique is applied. The transmitter and receiver are considered to be well-separated, with independently distributed channels. It is especially important in cases when there are many things in the surroundings that disperse the signal before it reaches the receiver, such as in urban locations or indoor environments. The sent signal travels several pathways to the receiver, resulting in varying delays, phases, and amplitudes. There is no direct LoS between the transmitter and the receiver.

Properties of Rayleigh Fading

- Amplitude distribution: The envelope of received signal amplitude follows the Rayleigh distribution.
- Phase distribution: The phase of the transmitted signal is distributed equally.
- Power: The received power changes quickly due to constructive and destructive interference from multipath components.

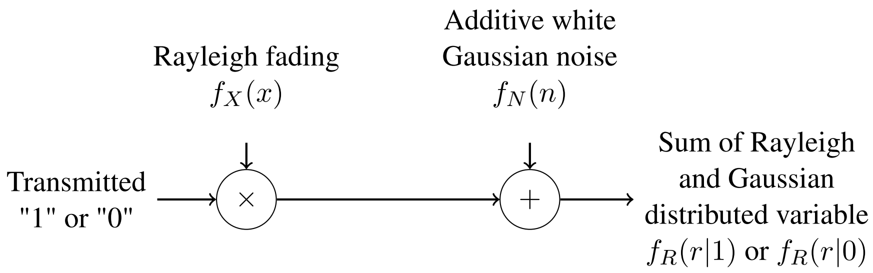

Figure 2.9: Block diagram of Rayleigh fading model (Orten & Svensson, 2002)

where $f_X(x)$ denotes the rayleigh fading distribution, $f_N(n)$ denotes the channel noise distribution, and $f_R(rj1)$ and $f_R(rj0)$ denote the effects of AWGN and rayleigh fading, respectively. The Rayleigh fading channel complex coefficient is given by two Gaussian random variables, each having a zero mean and a 0.5 variance. Every Gaussian random factor has defined real and imaginary components. Its complex form can be written as

$$h_{ij} = c + jd \tag{2.18}$$

Where

$$c \in \mathcal{N}\left(0, \frac{1}{\sqrt{2}}\right) \, and \;\, d \in \mathcal{N}\left(0, \frac{1}{\sqrt{2}}\right)$$

The joint probability density function can be written as

$$f_{c,d}(c,d) = \frac{1}{2\pi\sigma^2}\exp\left(-\frac{c^2+d^2}{2\sigma^2}\right) \tag{2.19}$$

Expressing h_{ij} in a polar form we obtain

$$h_{ij} = r\exp(j\theta) \tag{2.20}$$

where

$$r = \sqrt{c^2+d^2}$$

$$\theta = \arctan\frac{d}{c}$$

Let R and Θ be random variables representing the magnitude and angle in polar coordinates, respectively. The joint PDF $f_{R,\Theta}(r,\theta)$ and the marginal PDF of R, denoted as $P_R(r)$, are given by:

$$f_{R,\Theta}(r,\theta) = \frac{r}{2\pi\sigma^2}\exp\left(-\frac{r^2}{2\sigma^2}\right) \tag{2.21}$$

$$P_R(r) = \frac{r}{\sigma^2} \exp\left(-\frac{r^2}{2\sigma^2}\right) \tag{2.22}$$

where σ^2 is the variance of the underlying Gaussian distribution.

2.6.4 Rician Fading Channel

In the Rician fading scenario, every multipath component is superimposed on a dominating signal. It typically happens when one path is relatively stronger than the other (Kaur et al., 2017; Stüber & Stüber, 2012). The Rician distribution describes the received signal envelope. The ratio of power in the direct LoS path to power in the distributed paths is known as the K-factor, and it serves as a parameter for this distribution. The mathematical

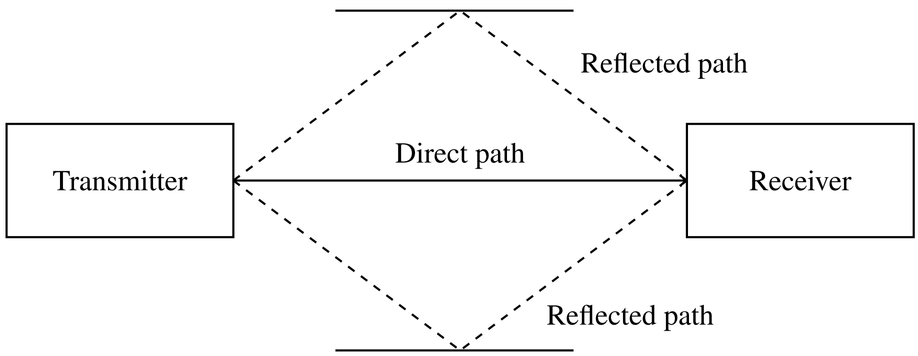

Figure 2.10: The Block schematic for the Rician fading model

description of the Rician fading model is as follow

$$Z = Z_{\text{LOS}} + Z_{\text{NLOS}} \tag{2.23}$$

where Z_{LOS} is a LoS component and Z_{NLOS} is a NLoS component. The amplitude of $|Z|$ can be given by:

$$f_{|Z|}(z) = \frac{z}{\sigma^2} \exp\left(-\frac{z^2 + A^2}{2\sigma^2}\right) I_0\left(\frac{zA}{\sigma^2}\right) \tag{2.24}$$

where I_0 is the modified Bessel function, A is the amplitude of the LoS component, and σ^2 is the variance of the scattered components. The Rician K-factor is expressed as:

$$K = \frac{A^2}{2\sigma^2} \tag{2.25}$$

This K-factor measures the strength of the LoS component relative to the scattered components. When K = 0, the channel becomes a Rayleigh fading channel, indicating a no-LoS path.

2.7 Channel Estimation Techniques in Massive MIMO

Massive MIMO systems require a large number of antennas at the BS in order to accommodate many users at once. An precise channel estimation is necessary for these systems to minimize interferences and achieve high SE. The channel acts as a connection between the user equipment and the BS. Both FDD-based and TDD-based estimation are possible in massive MIMO channels. In FDD-based channel estimation, the number of orthogonal pilots needed must match the number of antennas; but, in TDD-based channel estimation, the number of orthogonal pilots needed is equal to the number of users, which is lower than the number of antennas. This thesis focuses on TDD-based channel estimation. There are three different types of channel estimation in the TDD method. These include blind channel estimation methods, semi-blind channel estimation methods, and pilot-based (non-blind) channel estimation methods (Devasia & Reddy, 2013; Ganesh, Kumari, et al., 2013; Govil, 2018; Parmar & Patel, 2016; Zaier & Bouallègue, 2012).

2.7.1 Pilot-based Channel Estimation method

Pilot-based estimation can be used to estimate the channel by introducing pilot tones to all OFDM symbol sub-carriers with a specific duration or to each Orthogonal frequency division multiplexing (OFDM) symbol. Pilots are known to transmitters and receivers. The receiver can use acceptable received samples and known pilot bits ((Parmar & Patel, 2016)). Block, comb, and lattice are the several types of pilot arrangements that depend on how the pilots are arranged.

Block-Type Pilot Arrangement

An accurate channel estimate and synchronization technique utilized in OFDM systems is block-type pilot configuration. This configuration inserts pilot symbols at regular intervals into all subcarriers of a given OFDM symbol. This offers an in-depth overview of the channel condition over the whole frequency range. When the channel conditions remain mostly stable throughout multiple OFDM symbols, such as slow-varying channels, this approach works very well. Usually, based on the channel coherence time, the interval between pilot symbols is determined. At the expense of higher overhead, it offers errorless and detailed channel information (Li & Stuber, 2006; Nee & Prasad, 2000). Figure 2.11 indicates the block-type pilot configuration.

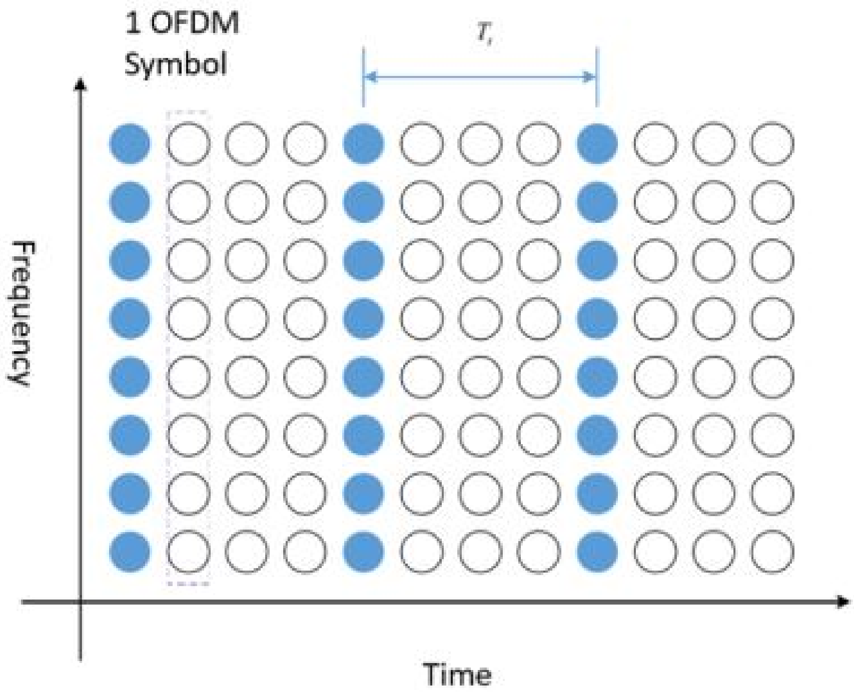

Figure 2.11: Block-type pilot configuration (Liao, 2022)

Comb-Type Pilot Arrangement

Another technique in OFDM systems is the comb-type pilot arrangement, which works especially well for channel estimation in rapidly changing channels. Periodic sampling of the frequency response of the channel becomes possible by this regular spacing. Under this approach, each OFDM symbol has a pilot symbol inserted into a particular subcarrier. Continuous tracking of the channel fluctuations is made possible by the frequent pilot symbols (Li & Stuber, 2006; Nee & Prasad, 2000). The comb-type pilot configuration shown in Figure 2.12.

Lattice-type pilot Arrangement

Lattice-type pilot arrangement (Agarwal, 2011; Manasseh et al., 2010; Vidhya & Kumar, 2012) describes a training sequence or pilot symbol pattern that is systematically arranged in order to estimate channel properties. To reliably transmit data, the impulse response or

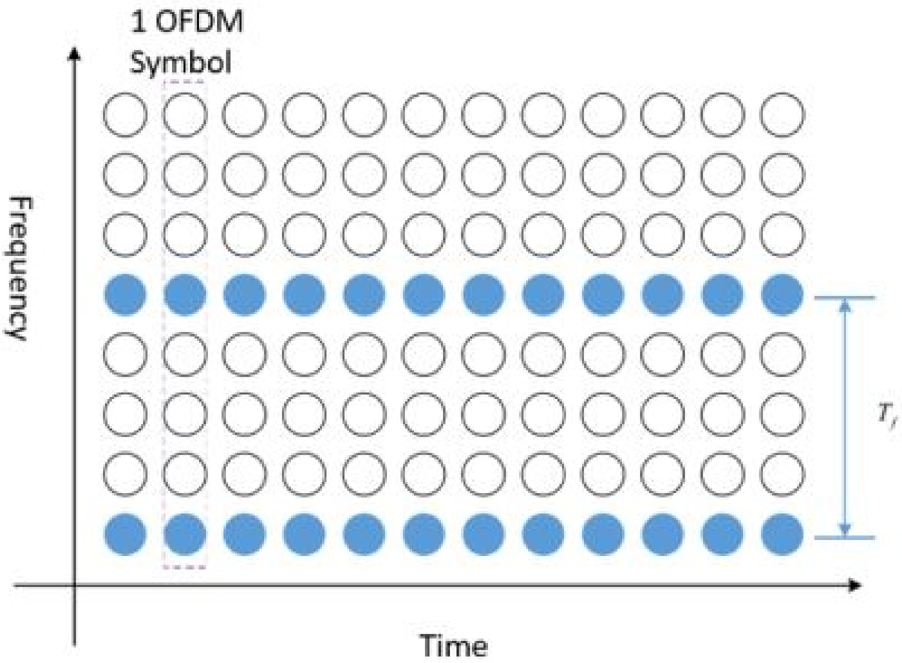

Figure 2.12: Comb-type pilot configuration (Liao, 2022)

frequency response of the channel must be precisely estimated, and this requires certain configurations. Pilots along the frequency and time axes are used to estimate the channel. Two interpolations are performed using the pilots to estimate the channel: one along the frequency axis in the frequency domain and another along the time axis in the time domain. When tracking the frequency-selective and time-varying channel properties, the pilot symbol period (S_t) and pilot subcarrier spacing (S_f) need to be less than the coherence time and bandwidth, respectively. The following difference needs to be met by the pilot symbol arrangement. The lattice-type pilot configuration is shown in Figure 2.13.

$$S_t \leq \frac{1}{f_a} \quad \text{and} \quad S_f \leq \frac{1}{\sigma_{\max}} \tag{2.26}$$

Advantages of Lattice Type Pilot Arrangement

- **Improved accuracy**: It improves channel estimation accuracy because a lattice structure offers a uniform sampling of the channel conditions, it can increase the accuracy of channel estimate.

- **Error reduction**: It helps in reducing interpolation errors by ensuring that the pilot symbols cover the entire signal space more effectively.

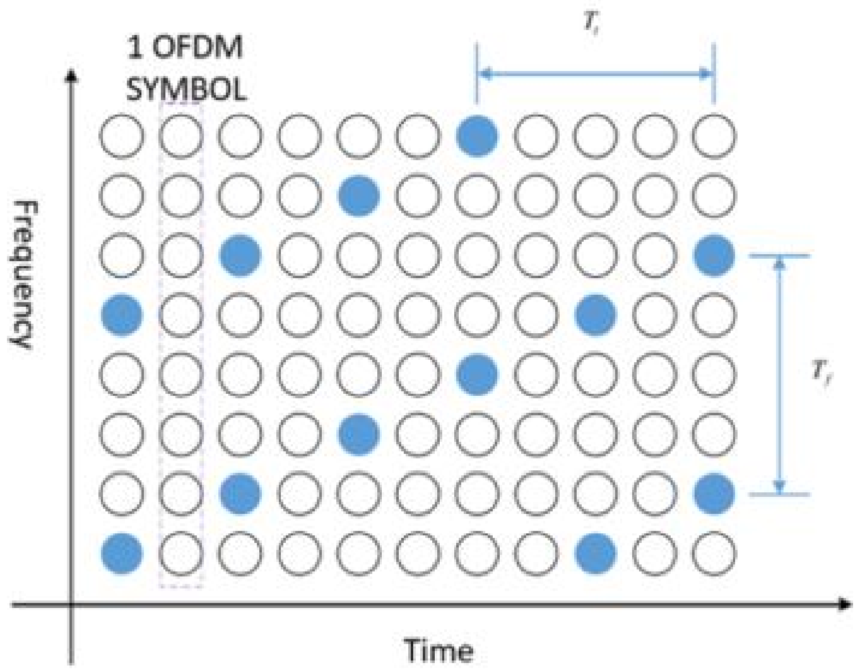

Figure 2.13: Lattice-type pilot configuration (Liao, 2022)

- **Efficient computation**: Channel estimation and interpolation computations are made simpler by the regular grid pattern.

2.7.2 Blind Channel Estimate method

Blind channel estimation techniques use data streams to estimate the channel rather than using pilots. An orthogonal space time-coded system is proposed for the blind channel estimation method, which combines linear prediction and the noisy subspace method. The process of estimating a blind channel involves examining both the statistical data about the channel and the particular features of the broadcast signals. There is no overhead loss and this blind channel estimation is only applicable to channels that vary slowly in time. However, in training-based channel estimation, the training symbols or pilot tones that the receiver identifies are multiplexed into the data stream (Ganesh, Kumari, et al., 2013; Zaier & Bouallègue, 2012).

2.7.3 Semi-blind Channel Estimation method

Semi-blind channel estimation approaches usually have higher SE because they utilize features such as correlative coding and second-order stationary statistics with a small number of practice symbols. The semi-blind channel estimating technique, which takes advantage of pilot carriers and other typical constraints, by including training-based channel estimation and pilot carriers to make channel estimation easier (Ganesh, Kumari, et al., 2013; Govil, 2018).

2.8 Channel Estimation Algorithm

A channel estimate is a quantitative assessment of the present CSI that makes use of specific algorithms and procedures that go through all available data. The reference signals for a transmit/receive antenna pair are selected out of the received grid by the channel estimation extract. At the receiving end, implement a suitable channel estimation technique. The most common algorithms include EW-MMSE, MMSE estimation, and LS estimation. The decision is based on variables including performance, computational complexity, and resource availability.

2.8.1 Least Squares (LS) Channel Estimator Algorithm

The LS algorithm estimates the channel by reducing the squared error between the expected and received signals. It can be sensitive to noise but is easy to deploy. When a receiver estimates the channel through pilot symbols for slow time-varying frequency selective channels, the most popular and fundamental frequency-domain channel estimation algorithm is the LS algorithm. In communication engineering, LS is frequently used for channel estimation and equalization in digital communication systems. It's objective is to reduce the absolute squared magnitude of the variation between the estimated and true values (Liao, 2022; Maria et al., 2017). In the ideal scenario, there is no noise and imperfection in the channel, which would mean it was assumed to be perfectly known channel estimate because the channel state may be known precisely. Minimizing the difference between the received signal Y and the product of the known pilot matrix X and the unknown channel matrix H is the aim of LS estimation. To analyze LS estimation, let X represent for both symbolize the data and pilots transmitted from the user equipment to the BS. The LS estimator minimizes the following function:

$$\hat{H} = \arg\min_{H} \|Y - HX\|_F^2 \tag{2.27}$$

where $\|\cdot\|_F$ is the Frobenius norm. Then Expanding this function becomes

$$\|Y - HX\|_F^2 = \text{Tr}\left((Y - HX)\,(Y - HX)^H\right) \tag{2.28}$$

Set the function to zero and differentiate it with respect to H in order to solve this minimization problem.

$$\frac{\partial}{\partial H}\|Y - HX\|_F^2 = -2YX^H + 2HXX^H \tag{2.29}$$

Setting the derivative to zero:

$$-2YX^H + 2HXX^H = 0 \tag{2.30}$$

Simplify

$$YX^H = HXX^H \tag{2.31}$$

Finally, solving for H, the LS estimator is:

$$\hat{H}_{\text{LS}} = YX^H\left(XX^H\right)^{-1} \tag{2.32}$$

A random matrix with independent and identically distributed (iid) complex Gaussian random variables is used to describe the channel matrix H for a Rayleigh fading channel. $H \sim \mathcal{CN}(0, I_M)$ with abundant scattering and non-LoS component assumed, this indicates that every element of H is a zero-mean, unit-variance complex Gaussian random variable. LS estimator can be (Marzetta, 2010; Mehrpouyan et al., 2012; Ngo et al., 2013)

$$\hat{H}_{\text{LS}} = YX^H\left(XX^H\right)^{-1} \tag{2.33}$$

now substitute the received signal $Y = HX + N$

$$\hat{H}_{\text{LS}} = (HX + N)X^H\left(XX^H\right)^{-1} \tag{2.34}$$

By simplifying this equation

$$\hat{H}_{\text{LS}} = H + NX^H\left(XX^H\right)^{-1} \tag{2.35}$$

The channel matrix H for a Rician fading channel consists of a scattered (non-LoS) component in addition to a LoS component.

$$H = \sqrt{\frac{K_R}{K_R+1}} H_{\text{LoS}} + \sqrt{\frac{1}{K_R+1}} H_{\text{NLoS}} \tag{2.36}$$

where K_R represents the Rician K-factor, H_{LoS} represents the deterministic LoS component, and $H_{\text{NLoS}} \sim \mathcal{CN}(0, I_M)$ represents the Rayleigh-distributed non-LoS component. So, the received signal in Rician fading can be

$$Y = \left(\sqrt{\frac{K_R}{K_R+1}} H_{\text{LoS}} + \sqrt{\frac{1}{K_R+1}} H_{\text{NLoS}} \right) X + N \tag{2.37}$$

The LS estimator can be

$$\hat{H}_{\text{LS}} = Y X^H \left(X X^H \right)^{-1} \tag{2.38}$$

Then substitute the received signal

$$\hat{H}_{\text{LS}} = \left(\sqrt{\frac{K_R}{K_R+1}} H_{\text{LoS}} + \sqrt{\frac{1}{K_R+1}} H_{\text{NLoS}} \right) + N X^H \left(X X^H \right)^{-1} \tag{2.39}$$

After simplification, the Rician fading channel estimation given as

$$\hat{H}_{\text{LS}} = \sqrt{\frac{K_R}{K_R+1}} H_{\text{LoS}} + \sqrt{\frac{1}{K_R+1}} H_{\text{NLoS}} + N X^H \left(X X^H \right)^{-1} \tag{2.40}$$

In practical scenarios, the pilot signal duration and effective channel power are important factors. So LS estimator becomes

$$\hat{h}_k = \frac{1}{\sqrt{\phi_k} \cdot \tau_p} \cdot y^{pilot} \tag{2.41}$$

Where ϕ_k is the effective channel gain or power for user K and τ_p is the pilot signal duration, which influences the SNR.

2.8.2 Minimum Mean Square Error (MMSE) Channel Estimator Algorithm

In order to estimate the channel matrix H, MMSE channel estimation minimizes the mean square error (MSE) between the actual channel H and its estimate $\hat{H}$. The MMSE estimator minimizes the average squared error over all potential channel realizations and noise changes, yielding the best linear unbiased estimate of the channel (Goldsmith, 2005; Marzetta, 2010; Moqbel et al., 2017; Ngo et al., 2013; Tse & Viswanath, 2005). Consider a massive MIMO system that has K single-antenna users and M antennas at the BS. At the BS, the received signal Y is provided by

$$Y = XH + N \tag{2.42}$$

where: X is the pilot matrix, which is known at both the transmitter and the receiver; H is the channel matrix that can be estimated; and N is the noise, where $N \sim \mathcal{CN}(0, \sigma_n^2 I)$. The channel coefficient in a Rayleigh fading environment can be represented as complex Gaussian random variables with a zero mean. $H \sim \mathcal{CN}(0, R_h)$ where $R_h = E[HH^H]$ is the channel covariance matrix, which describes the spatial correlation. The MMSE estimator minimizes the MSE between the estimated channel $\hat{H}$ and the true channel H, and is given by:

$$\hat{H}_{\text{MMSE}} = E[H|Y] \tag{2.43}$$

For joint Gaussian variables, the MMSE estimator can be:

$$\hat{H}_{\text{MMSE}} = R_{hy} R_y^{-1} Y \tag{2.44}$$

Where $R_{hy} = E[HY^H] = R_h X^H$ is the cross-covariance between the received signal and the channel, and $R_y = E[YY^H] = XR_hX^H + \sigma_n^2 I_M$ is the covariance of the received signal. When it substituted into these MMSE estimators,

$$\hat{H}_{\text{MMSE}} = R_h X^H \left(X R_h X^H + \sigma_n^2 I_M \right)^{-1} Y \tag{2.45}$$

Equation 2.45 is the MMSE channel estimate in case of Rayleigh fading.

In a Rician fading channel, the channel matrix H consists of a random NLOS component in addition to a deterministic LOS component. The Rician channel model expressed as:

$$H = \sqrt{\frac{K_r}{K_r+1}} H_{\text{LOS}} + \sqrt{\frac{1}{K_r+1}} H_{\text{NLOS}} \tag{2.46}$$

Where K_r is the Rician factor, which shows the ratio between the LoS component and the NLoS component power, H_{LoS} is the deterministic LOS component, and $H_{\text{NLOS}} \sim \mathcal{CN}(0, R_h)$ is the random NL0S component, with R_h as its covariance matrix given as; $R_h = \frac{1}{K_r+1} R_{NLOS}$. In the Rician channel, the MMSE estimator takes into account both the LoS and the NLoS components. Mathematically, it can be expressed as:

$$\hat{H}_{\text{MMSE}} = E[H|Y] = E[H_{\text{LOS}}|Y] + E[H_{\text{NLOS}}|Y] \tag{2.47}$$

Since H_{LOS} is deterministic, $E[H_{\text{LOS}}|Y] = H_{\text{LOS}}$. Similar to the Rayleigh fading scenario, the NLOS component H_{NLOS} is estimated using the same MMSE estimator:

$$\hat{H}_{\text{NLOS}} = R_h X^H \left(X R_h X^H + \sigma_n^2 I_M \right)^{-1} Y \tag{2.48}$$

Then, the total MMSE estimate for the Rician fading channel can be given as;

$$\hat{H}_{\text{MMSE}} = H_{\text{LOS}} + R_h X^H \left(X R_h X^H + \sigma_n^2 I_M \right)^{-1} Y \tag{2.49}$$

In practical scenarios, MMSE becomes

$$\hat{H}_{\text{MMSE}} = \hat{h} + \sqrt{p_k} R_k \Psi_k \left(y_k^{\text{pilot}} - \hat{y}_k^{\text{pilot}} \right) \tag{2.50}$$

The covariance matrix that characterizes the spatial correlation of the NLoS components is R_k, and $\hat{h}$ is the LoS component. The Ψ_k is $\tau_p \text{Cov}\{y_k^{\text{pilot}}\}^{-1}$ and $\hat{y}_k^{\text{pilot}}$ is $\sum_{k=1}^{K} \hat{h}_k \sqrt{p_k}$.

2.8.3 Element-wise MMSE Channel Estimator Algorithm

EW-MMSE channel estimation is an essential method for estimating the channel conditions between an enormous number of antennas at the BS and user equipment (Choi, 2010; Larsson et al., 2014a; Marzetta, 2010). Let's look at a massive MIMO system that has K single-antenna users and M antennas at the BS. The received signal $\mathbf{y} \in C^M$ can be written as follows:

$$y = xh + n \tag{2.51}$$

Where h is the channel vector, and $n \sim \mathcal{CN}(0, \sigma_n^2 I)$ is the AWGN vector. With R as the covariance matrix, the channel matrix h in the Rayleigh fading model has a complex Gaussian distribution of $h \sim \mathcal{CN}(0, R)$. The EW-MMSE estimator for Rayleigh fading model is given by:

$$\hat{h} = R(R + \sigma_n^2 I)^{-1} y \tag{2.52}$$

Where $R_y = R + \sigma_n^2 I$ is the received signal covariance matrix y.
In the Rician fading model, the channel vector h can be expressed as a combination of a LoS component and a Rayleigh-distributed scattering component.

$$h = \sqrt{\frac{K}{K+1}} h_{\text{LOS}} + \sqrt{\frac{1}{K+1}} h_{\text{scatt}} \tag{2.53}$$

Where K is the Rician factor, h_{LOS} is the deterministic LOS component, and $h_{\text{scatt}} \sim \mathcal{CN}(0, R)$ is the scattering component. The EW-MMSE estimate for the Rician fading channel expressed as;

$$\hat{h} = h_{\text{LOS}} + R_{\text{scatt}}(R_{\text{scatt}} + \sigma_n^2 I)^{-1}(y - h_{\text{LOS}}) \tag{2.54}$$

2.9 Challenges of channel estimation

A variety of difficulties arise when estimating channels in communication systems because wireless channels are essentially imprecise and dynamic. The following are some major challenges with channel estimation:

1. **Time-Varying Nature**: Time-based variations in wireless channels occur due to various variables, including fading, motion, and environmental changes. It is difficult to estimate channel parameters accurately under such dynamic situations (Rappaport et al., 2013).

2. **Frequency selectivity**: Various frequency components of the transmitted signal encounter varying attenuation and phase shifts in the wireless channel; this causes frequency-selective fading. It is challenging to quantify the channel response with accuracy at different frequencies (Proakis & Salehi, 2007).

3. **Noise and Interference**: The received signal is distorted by noise and other signals, making it difficult to choose between the required signal and undesirable components (Haykin, 2002).

4. **Pilot overhead**: The portion of available bandwidth or resources used for pilot signal transmission is referred to as pilot overhead. In order to achieve coherent demodulation and decoding of the transmitted data symbols, the receiver uses pilot signals to estimate the characteristics of the channel, such as channel frequency response or channel impulse response (Proakis & Salehi, 2007).

5. **Multiple path transmission**: Multiple transmitted signal versions with various delays and attenuation arrive at the receiver as a result of multipath propagation. In order to retrieve the original signal, it is hard to estimate the channel impulse response (Goldsmith et al., 2003b).

6. **Complexity of computation**: Certain channel estimating algorithms can be computationally challenging, requiring a large amount of processing power. These algorithms are especially prevalent in complex systems like massive MIMO and OFDM (Haykin, 2002).

2.10 Pilot Contamination

Users send pilot sequences to estimate channel conditions during the massive MIMO training phase. The goal is to ensure that all pilot communications occur at the same time and frequency, free from other pilot interference (Jose et al., 2011; Mehrotra & Chaubey, 2017; Ngo, 2015a). The effect of pilot contamination is the main essential limitation of massive MIMO. Orthogonal pilot sequences cannot be assigned to all users in all cells due to the channel coherence interval constraint in multicell systems. Reusing orthogonal pilot sequences from one cell to another is necessary. Therefore, pilots transmitted by users in other cells will contaminate the channel estimate in that cell. Pilot contamination is the effect that reduces the system performance (Jose et al., 2011). Pilot signals are utilized to obtain CSI. But the pilots have been contaminated by a number of factors. Poor estimate approaches, multi-cell interference from insufficient channel coherence, and intercell interference from inaccurate channel estimation due to hardware degradation can all affect the pilot signals (Elijah et al., 2015). The following are some possible causes of pilot contamination:

- **Non-orthogonal pilot training**: Assuming mutual orthogonality among the pilots, intracellular interference in a multi-cell system with all L cells sharing the same frequency is considered insignificant. A frequency reuse factor of 1 causes pilot contamination from nearby cells that is introduced into the system because it interferes with the pilot signals through intercellular interference. Every BS correlates the incoming pilot signals with its own orthogonal pilot signals, while each terminal in the other cells increases to the pilot contamination.

- **Hardware impairment**: The radio frequency chain hardware components are vulnerable to problems such as quantization errors, phase noise, amplifier non-linearity, and quadrature imbalance. The impairment has been shown to have an effect on the performance of the massive MIMO system and on the realibility of the channel estimation, which causes pilot contamination. The non-ideal behavior of each component has been modeled in order to create a compensation algorithm, which helps to overcome the difficulty posed by these limitations. On the other hand, modeling of the total residual receiver impairments is thought to improve system performance more than modeling of the individual components.

- **Inter-cell coordinated pilot assignment**: An algorithm has been presented to study this approach using slow-rate, inter-cell coordinated pilot assignment. Compiling coordinated pilot assignments requires that every cross-channel covariance matrix be accessible at every base station. The expected channel estimate error when a certain set of terminals reuses a pilot sequence is evaluated using this data in a closed-form formula. The terminal that minimizes this mistake is assigned pilots in each cell iteratively by a greedy method.

2.11 Pilot Decontamination

One of the most important technological platforms for the 5G of cellular systems is massive MIMO. However, pilot contamination affects massive MIMO systems and degrades the system performance. The reason for this contamination is that the pilot sequences that appear in a cell that is similar to its neighbors are non-orthogonal (Salh et al., 2020). In massive

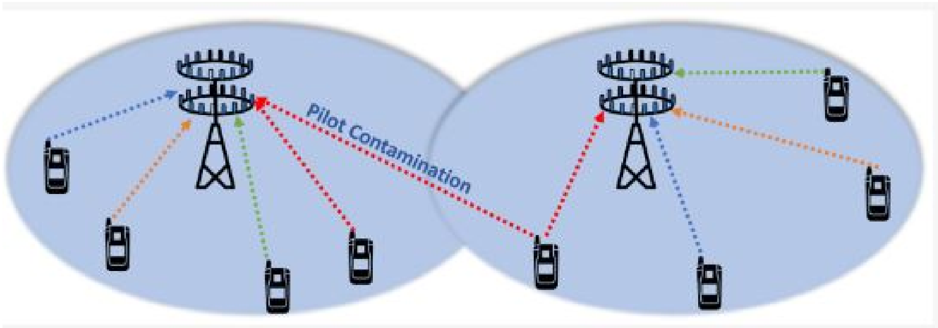

Figure 2.14: Effect of pilot contamination on Massive MIMO (Chataut & Akl, 2020)

MIMO, pilot decontamination is crucial for increasing channel estimate accuracy, particularly when several users share similar pilot signals across cells, which can cause interference and decreased CSI. This problem more affects TDD systems because channel estimates are based on uplink and downlink reciprocity.

2.11.1 Random Pilot Reuse

The assignment and reusing of pilots between cells is made random in the random pilot reuse technique. Pilots are dynamically assigned in a random fashion rather than being strictly allocated in a defined reuse pattern, which can greatly reduce the deterministic overlap of pilot sequences among neighboring cells. A pilot sequence from a predetermined set is assigned at random to every user in the system. Instead of having concentrated interference in certain locations, this randomization serves to disperse the disturbance more evenly throughout the network. This minimizes the likelihood that two users in neighboring cells may share the same pilot during each coherence interval (Cheng et al., 2016; Dey & Pattanayak, 2024; Salh et al., 2020).

2.11.2 Soft Pilot Reuse

Pilots are allocated in soft pilot reuse according to the spatial correlation of users. Low spatial correlation users can share the same pilots, whereas high spatial correlation users, that means, those who are near to one another are allocated different pilots. Through careful pilot assignment management, it decreases interference between users who share similar pilots. This is accomplished by taking into account both AoA data and large-scale fading coefficients of users. In this pilot decontamination technique, users in the cell are usually divided into two groups; the first category is cell-center users, in which users have strong signal strength and are situated close to the BS. They can exchange pilots with users in nearby cells with less contamination and are less affected by interference from nearby cells. The other one is the cell-edge user; these users are located close to the edge of the cell, where there is more interference from nearby cells. These users are assigned orthogonal pilot sequences or pilots that are utilized less frequently in order to reduce pilot contamination (Björnson et al., 2016; D. Gao et al., 2016; Omid et al., 2021; Saeed et al., 2024).

2.11.3 Weighted Graphed Coloring Pilot Assignment

Graph coloring is a strategy that involves allocating vertices (nodes/users) different colors so that neighboring vertices have different colors while using the fewest colors feasible. By reducing the amount of colors (pilots) utilized and increasing the gap between vertices according to predetermined criteria, like interference graphs, this strategy increases the effective use of limited pilot signal resources in pilot contamination situations (Saeed et al., 2024). In a weighted graph, the edges are given weights that represent the level of user interference. Greater interference is suggested by higher values. Each vertex in a graph represents a user, while the edges linking vertices indicate possible interference. The weights of the edge are based on spatial correlation between users and large-scale fading coefficients. Then assign pilots (colors) to users (vertices) in a way that minimizes the overall interference the sum of the weights of the edges that connect users with the same pilot is the objective. So, graph coloring techniques consider weights of the edge to achieve pilot decontamination (Baranidharan et al., 2021; Dao & Kim, 2018; Zhu et al., 2016).

2.12 Precoding in Massive MIMO

Precoding technology is a fundamental concept in massive MIMO systems. It shifts the complexity system from the side of the received terminals to the side of the BS by using strong signal processing at the transmitter side (Albreem et al., 2021). So, in massive MIMO, precoding is essential to maximize wireless communication by reducing interference, increasing signal quality, and improving SE. Massive MIMO systems, which have several antennas in the BS, require precoding to optimize signal transmission over several antennas. It is especially crucial in channel estimation since it guarantees that signals efficiently reach their intended users and aids in managing interference (Bashu et al., 2024). ă In this thesis, I focus ă ă

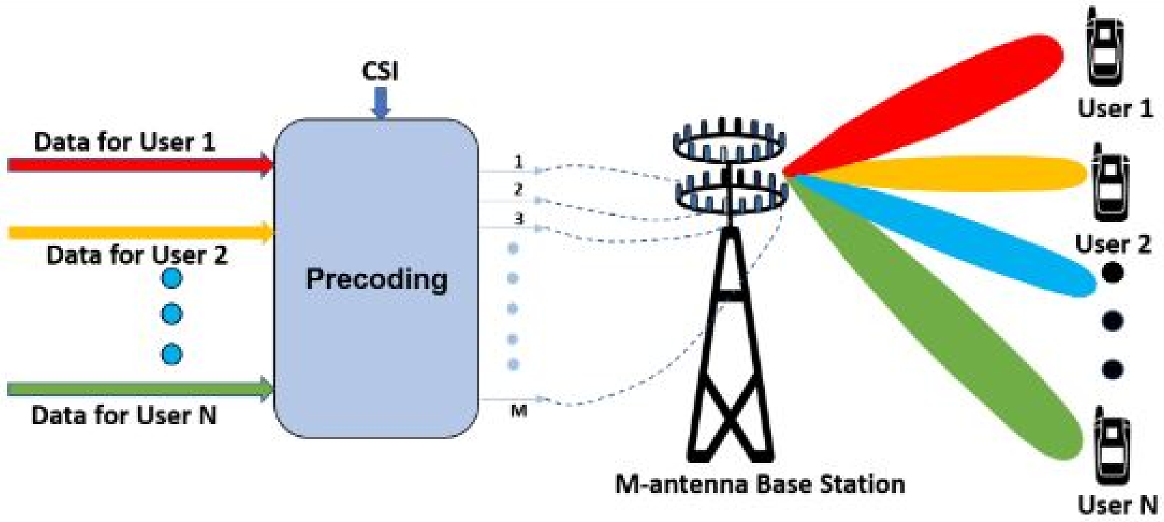

ă

Figure 2.15: Precoding in Massive MIMO System model with M-transmitted antennas and N-received antennas (Chataut & Akl, 2020)

ă

only on linear precoding. The process of linear precoding involves adjusting the transmitted signals linearly using the CSI. The objective is to improve the SNR and minimize multi-user interference by the use of linear matrix operations. Therefore, in the downlink transmission, where $M > N$, the transmitted signal for the N users can be written as follows (Albreem et al., 2021; Fatema et al., 2017):

$$x = \sqrt{\rho}Pa, \quad x \in C^{M\times 1} \tag{2.55}$$

where $\sqrt{\rho}$ is the transmitted average power, P is a $M \times N$ linear precoding matrix, and a is a NŒ1 transmitted vector prior to the precoding operation. H is associated with the precoding matrix P. The vector at the received terminal $y \in C^{N\times 1}$ can be given as

$$\begin{aligned} y &= H^T x + n \\ &= \sqrt{\rho}\ H^T Pa + n \end{aligned} \tag{2.56}$$

2.12.1 Maximum Ratio Transmission

Maximum ratio transmission (MRT) Precoding combines signals from many antennas in a coherent manner to enhance the SNR at the receiver. In MRT, a scaled version of the signal is transmitted by each antenna, maximizing the total signal at the receiver in the channel direction. MRT precoding matrix can be expressed as (Albreem et al., 2021; Fatema et al., 2017)

$$P_{\text{MRT}} = \sqrt{\gamma}\left(H^*\right) \tag{2.57}$$

where γ is a power factor scaling and H^* is the complex conjugate of H matrix. The received signal in MRT can be expressed as:

$$y_{\text{MRT}} = \sqrt{\gamma}\sqrt{\rho}H^T H^* a + n, \quad y \in C^{N\times 1} \tag{2.58}$$

$$= \sqrt{\gamma\rho}H^T H^* a + n, \quad y \in C^{N\times 1} \tag{2.59}$$

ă When the number of transmitted antennas is significantly greater than the number of received antennas and the number of transmitted antennas extends to infinity, the MRT algorithm approaches the sum capacity of a massive MIMO system. As the number of BS antennas increases, the channel vectors in H approach mutual orthogonality. The optimal solution is thus reached when the term $H^T H^*$ approaches a diagonal matrix.

2.12.2 Zero-Forcing Precoding

Zero-forcing (ZF) Precoding is a linear precoding method that inverts the channel matrix in massive MIMO systems to reduce inter-user interference. It is important in order to manage multiple antennas used in massive MIMO systems and enable effective detection and channel estimates. A ZF method nulls the other directions where other users are located while directing the signal beam toward the intended user, hence reducing the interference generated by other users. The nulls in ZF performed by multiplying the ZF precoding matrix with the Gram matrix (Albreem et al., 2021; Fatema et al., 2017).

$$P_{\text{ZF}} = \sqrt{\gamma}H^*\left(C^{-1}\right) \tag{2.60}$$

Where $C = H^T H^*$ is a Gram matrix with non-diagonal components that show the channelsămutual correlations and diagonal components that show power imbalance through the channel. Then P_{ZF} is:

$$P_{\text{ZF}} = \sqrt{\gamma}H^*\left(H^T {H^*}^{-1}\right) \tag{2.61}$$

Then the received signal in ZF is:

$$y_{ZF} = \sqrt{\rho\gamma}H^T H^*\left(H^T H^*\right)^{-1} a + n, \quad y \in C^{N\times 1} \tag{2.62}$$

As the number of transmit antennas increases to infinity in massive MIMO systems, it's C becomes an identity matrix that allows for the simplification of matrix inversion operations.

2.12.3 Regularized Zero-Forcing Precoding

In order to address the problems of the ZF algorithm, the Regularized zero-forcing (RZF) algorithm introduces a regularization into the channel matrix inversion operation. This regularization strengthens the system, particularly in situations with high noise or inaccurate CSI with matching noise amplification and interference suppression ă(Bobrov et al., 2021; Fatema et al., 2017). The precoding matrix of RZF equalization is given by (Fatema et al., 2017)

$$P_{RZF} = \sqrt{\gamma} H^* \left(H^T H^* + X + \lambda I_K\right)^{-1} \tag{2.63}$$

Where X is the conjugate transpose (Hermitian) of the channel matrix, I is the identity matrix, λ is a regularization factor, and γ is a power normalization factor. When the channel matrix is inadequately conditioned, λ is essential because it stops the inverse operation from amplifying noise significantly. RZF interpolates smoothly between MRT when λ approaches to ∞ and ZF when λ approaches to 0 at X = 0. The received signal given by

$$y_{\text{RZF}} = \sqrt{\rho\gamma} H^T H^* \left(H^T H^* + X + \lambda I_K\right)^{-1} a + n \tag{2.64}$$

2.13 Review of Related Works

This section will discuss some significant articles that have been written on the topic of channel estimation techniques in massive MIMO systems with pilot contamination effect, which is the main target of this thesis. Below is a brief summary of some of the studies that have been done on the topic of channel estimate methods with pilot contamination and related to this study.

The paper (Björnson et al., 2015) develops a thorough theoretical framework for examining SE in massive MIMO systems. It suggests mathematical techniques to assess how SE is impacted by the quantity of antennas, users, and pilots. The SE expressions that take into account variables like power control, pilot reuse schemes, and random user locations are derived as part of the process. The results under finite and asymptotic conditions are validated using simulation approaches. Additionally, the study investigates the effects of the different processing schemes Maximum ratio (MR), ZF, and RZF, on the suppression of intra and inter-cell interference. The results of the simulation show that massive MIMO systems can increase SE, especially when pilot and user allocation is implemented carefully. In the case of strong inter-cell interference, ZF and RZF processing algorithms can perform better than MR, although MR is still competitive at lower interference levels. When the number of antennas greatly exceeds the number of users, the SE shows diminishing returns and saturates with increasing (SNR). The study also demonstrates that there is a trade-off between maintaining orthogonality among pilot sequences and optimizing user numbers, highlighting the importance of system-specific configurations in attaining maximized SE.

Analytical expressions for SE and energy effeciency are derived under both perfect and imperfect CSI. The study (Rayi & Prasad, 2017) focuses on mitigating pilot contamination and inter-cell interference, two critical factors limiting SE in massive MIMO. The impact of BS antennas, user equipment, and pilot reuse factors on efficiency of the system is also examined, providing insights into optimal configurations. This paper explores the SE and energy efficiency of massive MIMO systems, with an emphasis on optimizing these metrics under linear processing schemes, such as MRC, ZF, and MMSE algorithms. The findings show that ZF and MRC have lower SE values, whereas MMSE has the largest SE and reaches maximum result with large BS antennas. In order to achieve maximum SE and energy efficiency, the results show the significance of processing scheme selection, pilot reuse optimization, and BS antenna scalability. The study indicates that MMSE offers the highest overall performance, especially in difficult CSI and interference situations, underscoring its applicability for 5G networks.

The effect of pilot contamination on SE in massive MIMO systems running under TDD is investigated in this work (Asiedu & Ahmed, 2018). Using LS channel estimation, the work obtains closed-form lower bounds on feasible rates for the MRC and ZF linear detectors. Three different pilot allocation situations are examined: non-orthogonal sequences, orthogonal pilot sequences, and pilot sequences that are repeated across cells. According to the data, ZF performs best at higher SINR levels, whereas MRC is more beneficial at lower SINR values. The results show that while recycling pilots becomes advantageous with more users or in situations with increased interference, orthogonal pilots perform better in low-interference environments but at a larger resource cost. The methodology makes use of a system model with multi-cell massive MIMO topologies, and resulting analytical expressions are validated by Monte Carlo simulations. In order to assess SE across different BS antenna and user equipment configurations, the study takes into consideration practical factors such as channel path loss, user dispersion, and pilot contamination. SE is computed using attainable SINR for various pilot allocation schemes, and both the uplink and downlink scenarios are examined. These findings show that while more antennas improve SE, pilot contamination is not eliminated. Orthogonal pilots minimize interference and provide greater SE, particularly for systems with fewer users and a sufficient coherence block length. On the other hand, pilot reuse techniques work better in low-mobility situations or with lots of people. The study finds that in order to maximize SE in massive MIMO systems, it is essential to optimize pilot allocation and detector selection based on system parameters.

In order to minimize the crucial problem of pilot contamination, the (de Figueiredo et al., 2018) presents a channel estimator aimed at massive MIMO TDD systems functioning in flat Rayleigh fading conditions. The approach consists of substituting an machine learning estimator for the interference and noise power terms in the ideal MMSE channel estimate. This method greatly simplifies implementation by doing away with the requirement for prior knowledge of inter-cell large-scale fading coefficients. An approximate analytical MSE expression is derived to examine the performance of the suggested estimator, which offers better mathematical tractability and gets around numerical problems seen in previous approaches while being consistent with simulation findings. It shows that, particularly in situations with low SNR or a high number of antennas, the suggested channel estimator achieves mean square error performance that is comparable to the ideal MMSE estimator. Simulation findings show that the suggested estimate outperforms the LS estimator and asymptotically approaches the MMSE performance as the number of base station antennas rises. Additionally, the work emphasizes robustness under random large-scale fading coefficients and various levels of cross-cell interference. The authors examine and assess the influence of pilot contamination on the achievable rates and SE; however, they do not suggest any solutions to address the issue.

In ă(Mai et al., 2020) work, the downlink SE of cell-free massive MIMO systems is examined, with particular attention to configurations in which both users and access points have multiple antennas. Two transmission techniques are suggested for CSI acquisition: one with downlink pilots and one without. It uses the MMSE-SIC detection scheme to obtain analytical equations for SE under both protocols and investigate the impact of non-orthogonal pilots and multiple antennas. In order to mitigate the computing cost, the study modifies the coefficients of the first protocol's max-min fairness power control for the second protocol. Enhancing SE and ensuring equity among system users are the goals of these techniques. The outcomes show that using the suggested approaches significantly improves performance. According to numerical simulations, the second procedure has a greater training overhead but, in some cases, provides superior channel estimation quality and SE. These results show the benefits of integrating intelligent power regulation and multi-antenna configurations in cell-free massive MIMO systems to increase scalability and dependability.

In order to address the difficulties associated with channel estimation in large-scale MIMO systems, this study (Bacci et al., 2024) aims to minimize computational complexity while preserving accuracy and robustness in the face of inaccurate channel statistics. Utilizing the circulate approximations for ULAs, the suggested techniques provide advantages. Spatial correlation matrix computation is made simpler by these methods, which reduce complexity for MMSE estimators. The methods are made to work effectively in dynamic contexts, especially at low-to-medium SNRs, where traditional methods frequently fail. By use of numerical simulations, the authors verify these methods and show that they perform similarly to MMSE and uplink SE. The method focuses on taking advantage of the built-in structures of spatial correlation matrices. The Kronecker product greatly reduces processing complexity for UPAs by separating the horizontal and vertical components. The Discrete fourier transform (DFT) may be applied to ULAs with ease due to a circulant matrix approximation, which yields O(NlogN) complexity scaling. Under low-to-medium SNRs, the suggested techniques also perform better than MMSE, demonstrating increased resilience without requiring adjustments to regularization parameters. These results demonstrate the methodologies' applicability and open opportunities for effective channel estimation in the next generation of massive MIMO systems.

The difficulties of channel estimation in massive MIMO systems are examined in (Amadid et al., 2020) work, especially when pilot contamination is present. Three methods of LS estimation, MMSE, and ML are evaluated in this study. LS estimator is computationally straightforward, but when pilot contamination occurs, its performance significantly degrades. Although it makes unrealistic assumptions, including having perfect knowledge of large-scale fading coefficients, MMSE indicates greater performance. Using the MSE as the main performance parameter, the study evaluates the estimators under different intercell interference levels, antenna numbers, and uplink transmit power. The results show that ML outperforms LS estimator by a significant amount and achieves MSE performance that is comparable to the MMSE, especially in high SNR and high interference scenarios. The paper doesn't specifically provide an approach to multi-cell massive MIMO systems pilot contamination. The performance of three channel estimate methods (LS, MMSE, and ML) is instead compared in the presence of pilot contamination caused by pilot reuse between cells.

2.14 Research Gap and Thesis Contribution

The high spectral and energy efficiency potential of massive MIMO systems depends on accurate channel estimation. Pilot contamination is still a major problem, particularly in multiuser situations where inter-user and inter-cell interference results from local cells using the same pilot sequences. A significant LoS component in Rician fading makes this interference worse and makes precise channel estimation much more difficult. The approaches, including coordinated pilot scheduling and blind estimation techniques, provide some mitigation, but they frequently fall short in achieving a balance between scalability, computational efficiency, and practical adaptability.

An important research gap in this area is highlighted by a lack of reliable methods for handling pilot contamination in multi-user scenarios under Rician fading conditions. In order to minimize the issue of pilot contamination in multi-user massive MIMO incase of Rician fading scenarios, this thesis suggests combining weighted graph coloring with soft pilot reuse for pilot decontamination. The suggested method uses weighted graph coloring to dynamically optimize pilot allocation based on interference levels and user geographical distribution, while utilizing soft pilot reuse to minimize interference by minimizing pilot reuse among closely interfering users. When these techniques are combined together, it mitigates pilot contamination, even in the challenging Rician fading scenario.

3. MATERIALS AND METHODS

3.1 Pilot Based Channel Estimation

Pilot symbols are added to the information from the transmitter in order to gain the channel information, and the receiver uses the pilot symbols it has received to retrieve the channel information. Selecting the appropriate pilot location and spacing between them is essentially the challenge of pilot pattern design. A suitable insert method might be determined based on the predicted speed from the terminal and the known communication environment (Wang, 2011). In OFDM systems, channel estimation and synchronization are accomplished by the use of pilot symbols. The receiver can precisely identify and use pilot signals for channel estimation and synchronization since they have a predetermined and recognized structure. Periodically, either in all subcarriers of a particular OFDM symbol or in a subcarrier of every OFDM symbol, pilots are added into the OFDM frame (Li & Stuber, 2006; Rappaport, 2024b).

The two most crucial pilot parameters are the maximum multipath time delay, which establishes the minimum coherent bandwidth, and the maximum doppler shift (f_m), which establishes the minimum coherent time. The Nyquist theorem determines the lowest number of pilot symbols that can be provided. Time domain Nt and frequency domain Nf should satisfy the interval according to the Nyquist theorem (Wang, 2011).

$$f_m \cdot T \cdot N_t \leq \frac{1}{2}, \quad \tau_{\max} \cdot \Delta f \cdot N_t \leq \frac{1}{2} \tag{3.1}$$

Where Δf is the sub-carrier bandwidth, T is the signal period, and $\tau_{\max}$ is the maximum multipath time delay. In cases of practical application, oversampling with 2 times of the minimum is used. Then,

$$f_m \cdot T \cdot N_t \approx \frac{1}{4}, \quad \tau_{\max} \cdot \Delta f \cdot N_t \approx \frac{1}{4} \tag{3.2}$$

3.2 System Model

Consider (Balevi et al., 2020) a cellular network that has several BSs and users with single antennas. As seen in Figure 3.1, BSs serve U users with $U \ll M$ and have M antennas. Assume that a TDD frame structure is used to transmit OFDM symbols with N_f subcarriers. Users within the same cell submit orthogonal pilot sequences of length N_p in order to compute reciprocal uplink and downlink channels. The frequency domain signal received at the target BS can be represented as $Y \in C^{M \times N_f \times N_p}$ can expressed as:

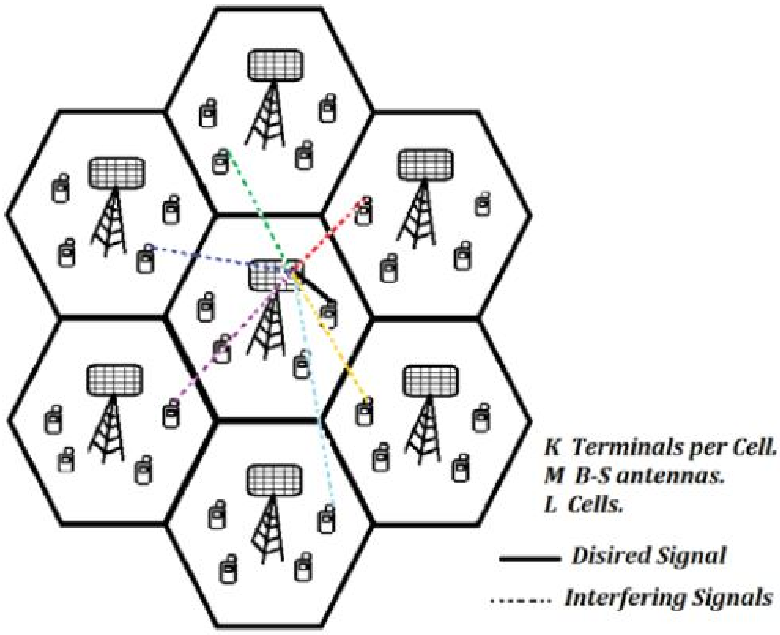

Figure 3.1: Massive MIMO system model (Amadid et al., 2020)

$$Y = \sum_{u \in S_u} \sqrt{\rho_u} H_u \otimes X_u^H + \sum_{v \in S_v} \sqrt{\rho_v} H_v \otimes X_v^H + Z \tag{3.3}$$

Where S_u is the number of users connected to the BS, while ρ_u indicates the transmit power, $H_u \in C^{M \times N_f}$ is the channel between the BS and its u_{th} user, $X_u \in C^{N_p \times 1}$ is the pilot sequence serves for channel estimation, such that $X_u^H X_u = N_P$ and $\otimes$ refers to the Kronecker product. The second term S_v refers to the users linked to the interferer cells, whereas H_v represents the channel between the BS and the interferer users. $Z \in C^{M \times N_{fp}}$ represents the Gaussian noise vector, and its elements are zero-mean Gaussian random variables with variance ^{2} which means it is iid.

Users at other BS can utilize the same pilot sequences as the u_{th} user in the target cell. Due to limited time-frequency resources, orthogonal pilots cannot be allocated to all users in all cells. This interference results pilot contamination. To get a u^{th} user signal at the BS use,

$$Y_u = Y(I_{Nf} \otimes X_u) \tag{3.4}$$

Where $Y_u \in C^{M \times N_f}$. Due to Kronecker product

$$\left(H_u \otimes X_u^H\right)\left(I_{N_f} \otimes X_u\right) = \left(H_u I_{N_f}\right) \otimes \left(X_u^H X_u\right) = N_p H_u \tag{3.5}$$

So, u^{th} the user signal at the BS can be expressed as

$$Y_u = \sqrt{\rho_u N_p} H_u + \sum_{v \in S_v} \sqrt{\rho_v} \tilde{H}_v + Z_u \tag{3.6}$$

Where $\tilde{H}_v = H_v \otimes \left(X_v^H X_u\right)$ and $Z_u = Z(I_{Nf} \otimes X_u)$.

3.3 Uplink Data Transmission

An essential phase in wireless communication systems is the generation of pilot signals for channel estimation. Pilot signals are predetermined sequences that are known to the transmitter and receiver. They are often referred to as training sequences. In order to accurately recover data, these signals assist the receiver in estimating the channel parameters. In time domain slots, known positions for the pilot signals are included in the transmitted data stream. This known signal is used by the receiver to determine the impulse response of the channel.

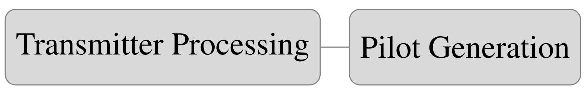

To generate pilot, it has to pass through the following steps (Proakis & Salehi, 2008; Rappaport, 2024b; Tse & Viswanath, 2005).

Step 1: Sequence Choice: In order to reduce interference and increase the accuracy of channel estimation, the pilot sequence should be formed with appropriate autocorrelation features. Gold sequences, Barker codes, and Zadoff-Chu sequences are examples of common sequences.

Gold sequences: Gold sequences are a significant type of periodic sequence that contains larger sets of sequences that have high periodic cross-correlations. A set of Gold sequences with period N = 2n-1 is made up of N+2 sequences for which it has good cross-correlation properties. A set of Gold sequences can be created by carefully choosing maximum length sequences. In communications and cryptography, gold sequences are a kind of pseudo-random binary sequence that are very useful in CDMA systems (Golomb & Gong, 2005; Henríquez et al., 2002). In order to generate a gold sequence, two m-sequences (maximum length sequences) of the same length that were produced by different polynomials must be exclusive OR (XOR). The m-sequence, which possesses favorable autocorrelation features, is a periodic binary sequence produced by a Linear feedback shift register (LFSR). Between two separate Gold sequences, there is minimal cross-correlation. By having this feature, the interference between signals encoded with various sequences is reduced. The cross-correlation function $C_{a,b}(\tau)$ at a lag τ is given by equation 3.7. where N is a sequence of length, a_i and b_i are elements of sequences, and τ is the lag. There are only three possible cross-correlation values: 1, t(n+1), and t(n1), where $t(n) = 2^{n/2}$ where n is the shift register length used for the generation of Gold sequences. where N is a sequence of length, a_i and b_i are elements of sequences, and τ is the lag. There are only three possible cross-correlation values: 1, t(n+1), and t(n1) where $t(n) = 2^{n/2}$ where n is the shift register length used for the generation of Gold sequences.

$$C_{a,b}(\tau) = \sum_{i=0}^{N-1} a_i \cdot b_{i+\tau} \tag{3.7}$$

Barker codes: Digital communication systems frequently use subsets of Pseudonoise (PN) sequences called barker codes for frame synchronization. Barker codes have low correlation side lobes and a maximum length of 13. Barker codes are a particular kind of binary sequence that are particularly helpful in radar and sonar systems because of its unique autocorrelation characteristics (Hossain et al., 2012). Mathematically, for a Barker sequence of length n, the autocorrelation function $R(\tau)$ at a lag τ is defined as equation 3.8. Where b_i is the i^{th} element of the Barker sequence. So, the values of $R(\tau)$ for $\tau \neq 0$ are minimized.

$$R(\tau) = \sum_{i=0}^{n-1} b_i \cdot b_{i+\tau} \tag{3.8}$$

Zadoff-Chu Sequences: A type of complex-valued sequences with superior correlation qualities are known as Zadoff-Chu sequences. These sequences are commonly used for channel estimation and synchronization in telecommunications, especially in LTE systems. A Zadoff-Chu sequence $z(n)$ of length N is defined as

$$z(n) = e^{-j\frac{\pi n(n+1)}{N}} \tag{3.9}$$

where $n = 0, 1, 2, \ldots, N-1$, n is relatively prime to N, and j is the imaginary unit.

Step 2: Pilot Insertion: Pilot signals should be inserted into designated time slots. For instance, in LTE, some subframes are set aside for pilot signals.

Step 3: Pilot Transmission: Send data symbols and the pilot sequences together. Establish synchronization so that the pilot symbol positions are known by the receiver. The system is operating in TDD mode as shown in Figure 3.2; the channel responses remain the same over a block of τ_c samples. Additionally, it assumes that any pair of coherent blocks has independent channel realizations. Coherence blocks are made up of several subcarriers and time samples that allow the channel response to be basically described as flat-fading and constant. Every coherence block includes $\tau_c = B_c \times T_c$ if the coherence bandwidth is B_c and the coherence time is T_c (Björnson et al., 2017). There is no statistical difference between

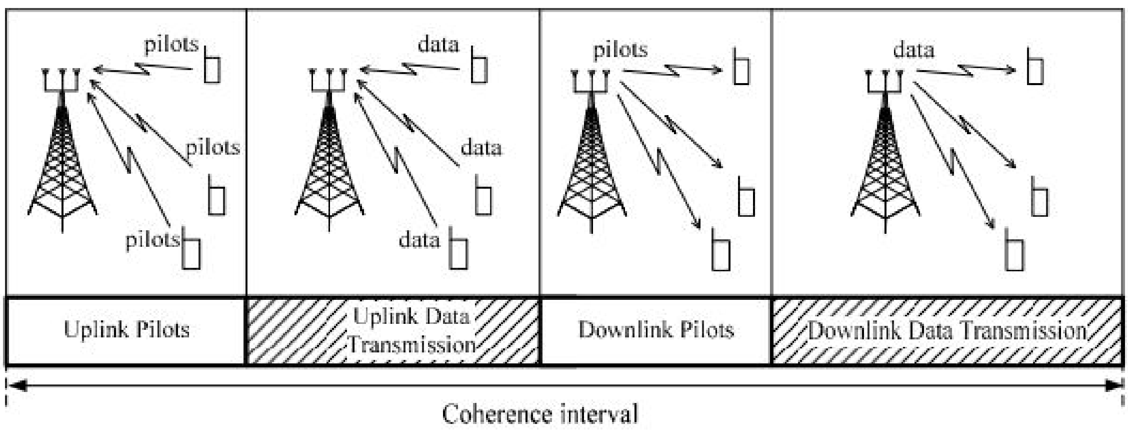

Figure 3.2: TDD Massive MIMO transmission scheme

the random channel responses in one coherence block and in any other coherence block, as shown in Figure 3.3.

As shown on Figure 3.4, τ_p samples are used for uplink pilot signals, τ_u samples are used for uplink data transmission, and τ_d samples are used for downlink data transfer. Uplink pilot signals take advantage of channel reciprocity in the TDD protocol to estimate both uplink and downlink channels. So, $\tau_p + \tau_u + \tau_d = \tau_c$ is required. While the number of pilots per coherent block is a design parameter, the percentage of uplink and downlink data can be chosen based on the characteristics of network traffic (Björnson et al., 2017; Chen et al.,

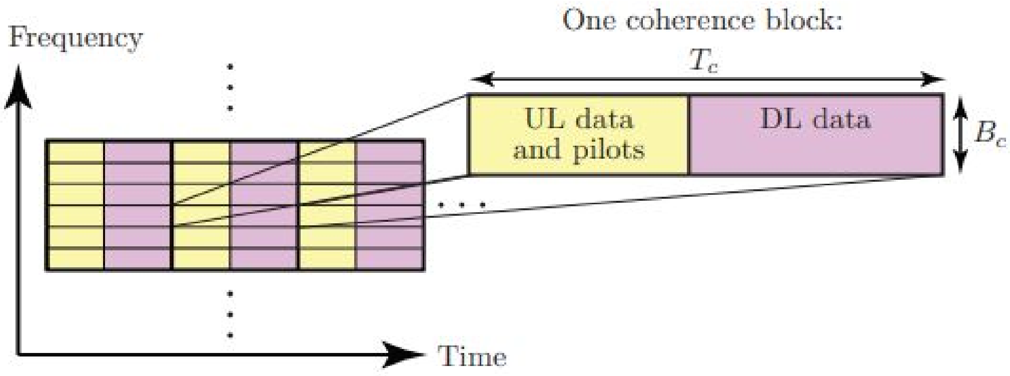

Figure 3.3: TDD multi-carrier modulation technique of a basic Massive MIMO system (Björnson et al., 2017)

2022). Pilots, which are used for channel estimation, are allocated to the user equipment

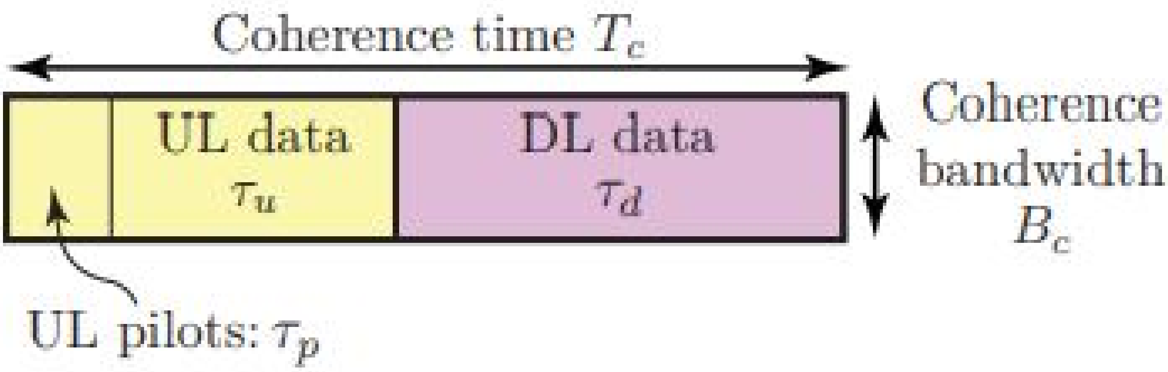

Figure 3.4: Samples for for downlink data, uplink data, and uplink pilots (Björnson et al., 2017)

once they have network access. Assuming τ_p is a constant independent of K, let us assume that there are τ_p mutually orthogonal τ_p-length pilot signals. The time and frequency domain natural channel variations limit the pilot resources. Therefore, in practical terms, τ_p < K, allowing the reuse of pilots between user equipment. When it denotes the index of the pilot assigned to user equipment K by $t_k \in 1, ..., \tau_p$. Then, use $S_k = \{i : t_k = t_i\} \subset \{1, \dots, K\}$ to determine the subset of user equipment sharing pilot t_k, which includes user equipment K. When pilot t_k is transmitted by the user equipment in S_k, the received signal is (Chen et al., 2022)

$$y_{t_k}^{\text{pilot}} = \sum_{i \in S_k} \sqrt{\tau_p p_i} h_{il} + n_{t_k,l} \tag{3.10}$$

where $n_{lk,l}$ is noise and p_i is the transmit power of user equipment i. Each K user transmits a signal to the BS during the uplink transmission. The signal transmitted by the k-th user is denoted by s_k, where $E\{|s_k|^2\} = 1$. The sum of all signals transmitted from all K users equals the $M \times 1$ received signal vector at the BS since K users share the same resource (Ngo, 2015b):

$$y_{ul} = \sqrt{p} \sum_{k=1}^{K} h_k s_k + n \tag{3.11}$$

$$= \sqrt{p} H s \tag{3.12}$$

Where H is channel matrix and s is signal vector. Let n $\in \mathcal{C}^M$ be the additive white Gaussian noise vector $s = [s_1, \ldots, s_K]^T$ and p_1 be the average SNR. Let us assume that the components of n are independent of H and are iid. The CSI and the received signal vector y will allow the BS to identify the signals sent by the K users coherently.

$$C_{\text{u1,sum}} = \log_2(\det\left(I_K + p_u H H^H\right)) \tag{3.13}$$

The sequential interference cancellation (SIC) method can be used to obtain the indicated sum capacity. When a user appears via SIC, its signal is deducted from the received signal before the next user is identified.

3.4 Downlink Data Transmission

In a downlink transmission, every K user receives a signal from the BS. Let $x \in \mathcal{C}^M$, where the signal vector broadcast from the BS antenna array is $E\{||x||^2\} = 1$. Then at the k-th user, the received signal can be;

$$y_{dl,k} = \sqrt{p_k} h_k^T x + z_k \tag{3.14}$$

when the additive noise is at the k-th user, and the average SNR is represented by p_k. With zero mean and unit variance, assume that z_k has a Gaussian distribution. Considered as a whole, the K user's received signal vector can be given as:

$$y_{dl} = \sqrt{p_d} H^T x + z \tag{3.15}$$

where $y_{dl} = [y_1, y_2, \ldots, y_K]^T$ and $z = [z_1, z_2, \ldots, z_K]^T$. The channel model is the broadcast channel whose sum-capacity is given by

$$C_{\text{sum}} = \max_{\substack{q_k, \\ \sum_{k=1}^{K} q_k \leq 1}} \log_2 \det \left(I_M + p_d H^* D_q H^T \right) \tag{3.16}$$

where q_k is the k^{th} diagonal a part of the diagonal matrix Dq. SE for downlink of user equipment k is given as (Chen et al., 2022)

$$SE_k^{(dl)} = \frac{\tau_d}{\tau_c} \log_2 \left(1 + SINR_k^{(dl)} \right) \tag{3.17}$$

when effective SINR given by

$$SINR_k^{(dl)} = \frac{\rho_k \left| E\{h_k^H w_k\} \right|^2}{\sum_{i=1}^{K} \rho_i E\{|h_k^H w_i|^2\} - \rho_k |h_k^H w_k|^2 + \sigma_{dl}^2} \tag{3.18}$$

The downlink SE is dependent on each UE's precoding vectors, which are wi: i = 1,..., K.

3.4.1 Channel Model of the system

Rician channels are commonly used to describe propagation channels, which typically have multiple propagation paths. One of these paths is the direct path, and the others are known as the NLoS component, which is where the signals propagate across various objects like buildings or trees that cause signal degradation. Rician fading is frequently used to statistically describe the fading phenomena that result from the interaction between these paths. The primary assumption is that there are two components to the complex-valued channel coefficient between user equipment K and access point L in the complex baseband (Carrera et al., 2020; Chen et al., 2022).

$$h_{kl} = \hat{h}_{kl} e^{j\varphi_{kl}} + g_{kl} \tag{3.19}$$

Where h_{kl} is the channel coefficient for the k-transmitter and l-receiver, $\hat{h}_{kl}$ is the deterministic or estimated component of the channel coefficient, g_{kl} is the fading component of the channel coefficient, and $e^{j\varphi_{kl}}$ is a phase shift associated with the deterministic channel component The size of the LoS component between user equipment k and access point l is represented by $\hat{h}_{kl}0$, and the corresponding phase shift is represented by $\varphi_{kl} \in$ [0, 2] and g_{kl}, is the NLoS component that includes all of the dispersed pathways, which is a Gaussian distribution model. It suggests $g_{kl} \sim (0, \beta_{kl)}$, where the variance is $\beta_{kl}0$. The phase shift doesn't affect communication performance when the receiver is expected to know the channel perfectly because it can compensate. As a result, it can be cancelled in the case of Rician fading channel performance analyses. (Chen et al., 2022).

3.4.2 Decontamination Scheme

Cell classification is crucial for controlling interference and allocating resources as efficiently as possible, particularly in conditions with a high user density. Cells are classified into center and edge regions; users in the center are closer to the BS; they take advantage of better signal quality, while users in the edge, who are closer to the boundaries, experience more interference from nearby cells (Zheng et al., 2024). Cell classification helps to reduce pilot contamination.

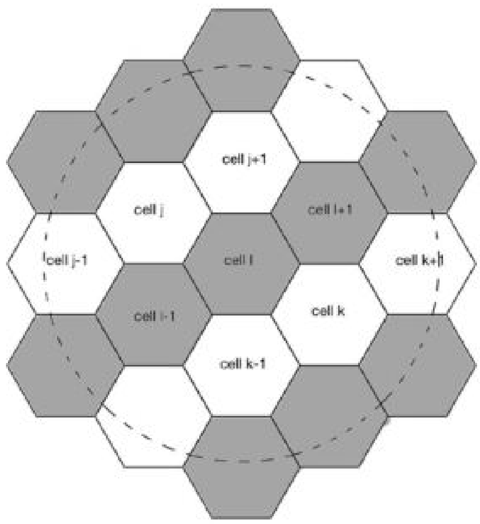

Figure 3.5: Classification of cells (Zhou et al., 2020)

The total number of available users is calculated by applying the soft pilot reuse scheme to the specified users. Based on this, it calculates the overall number of pilot resources that are accessible to users who are present at the center and edge of the cell. Pilots are allocated and added to the specified pilot set using a weighted graph-based approach, which selects users with the highest weight. Following the selection of every other user, a weighted graph estimate is generated using the sum of the weighted edges connecting users and the users with the lowest level of pilot contamination (Pranesh & Ramanathan, 2022). Users still have strong pilot contamination, particularly between two nearby cells, such as cell l and cell l+1 or cell l-1. Pilot contamination is always associated with the fading coefficient on the large scale $\omega^2_{(a,k)}a$. Depending on their locations, users' $\omega^2_{(a,k)}a$ can vary from one cell to another. A higher $\omega^2_{(a,k)}a$ indicates that the user may be more likely to have a pilot contamination with users from other cells; therefore, we can split users in the same cell into two groups and assign them different types of pilots to reduce pilot contamination. The centered users, who have fewer pilot contamination, will use the same pilot resource in every cell, while edge users, who have larger pilot contamination, will be given orthogonal pilots with other neighboring edged cells (Zhou et al., 2020). To identify the boundary between the center and edge users, then consider a threshold Ω.

$$\Omega = \frac{\theta}{K}\sum_{k=1}^{K}\omega^2_{(a,k)}a \tag{3.20}$$

However, θ is threshold parameter it can be changed based on the actual condition of users; in this thesis, it considered as 1

$$\Omega = \frac{1}{K}\sum_{k=1}^{K}\omega^2_{(a,k)} = \frac{K+1}{2}\times\omega^2_{(a,k)} \tag{3.21}$$

When K_{ed} is edge user pilot and K_{ce} is center user, the total orthogonal pilot can be

$$K_{\text{all}} = K_{\text{ce}} + K_{\text{ed}} \tag{3.22}$$

the number of K_{ed} is $K_{\text{ed}} = \sum_{l=1}^{L} K_C$, where K_C is edge users in each cell.

3.5 Performance Metrics

3.5.1 Signal to Interference and Noise Ratio in Massive MIMO

The signal to interference and noise ratio (SINR) for a specific user in a multi-user MIMO system evaluates the quality of the targeted signal in relation to noise and other user interference. It can be described as Castaneda et al., 2016; Raeesi et al., 2018

$$\text{SINR} = \frac{\text{Desired signal power}}{\text{Interference power} + \text{Noise power}} \tag{3.23}$$

For the signal received at the BS for a specific user u in cell, the c desired signal power is $h_{c,u}^H w_{c,u} s_{c,u}$ where $h_{c,u}^H w_{c,u}$ is the channel gain. The signal for user u in cell c is $s_{c,u}$, with normalized power to 1. The desired signal power is $E\left[\left|h_{c,u}^H w_{c,u}\right|^2\right]$. Users utilizing the same frequency in other cells (i.e., cells $j \neq c$) interact with user u in cell c. The cell j interference signal to the user u can be expressed as interference from cell, $j = h_{j,u}^H w_{j,u} s_{j,u}$ where ($h_{j,u}^H w_{j,u}$ is the channel gain for interference from cell $j, and s_{j,u}$ is the signal transmitted from the interfering cell j with normalized power to 1. The sum of each cell's interference together is the total interference power, $jeqc$ which is given by $\sum_{j\neq c} E\left[\left|h_{j,u}^H w_{j,u}\right|^2\right]$. The noise power is σ^2 which is AWGN. Then, SINR can be

$$\text{SINR}_{c,u} = \frac{E[|h_{c,u}^H w_{c,u}|^2]}{\sum_{j\neq c} E[|h_{j,u}^H w_{j,u}|^2] + \sigma^2} \tag{3.24}$$

By balancing the intended signal power with noise and interference, this formula determines the SINR for user u in cell c. Usually, the beamforming vector $w_{c,u}$ is made to optimize SINR.

3.5.2 Spectral Efficiency with Maximum Ratio Combining

The signal $y_j \in C^{M_j}$ at BS j that is received during the transmission of data is (Björnson et al., 2015; Özdogan et al., 2019)

$$y_j = \sum_{k=1}^{K_j} h_{jk}^j s_{jk} + \sum_{\substack{l=1 \\ l\neq j}}^{L} \sum_{i=1}^{K_i} h_{li}^j s_{li} + n_j \tag{3.25}$$

The lower bound of the SE with the effective SINR for k user equipment ergodic uplink capacity in cell j is given by (Özdogan et al., 2019)

$$SE_{jk}^{\text{ul}} = \frac{\tau_{\text{u}}}{\tau_c} \log_2\left(1 + SINR_{jk}^{\text{ul}}\right) \text{ [bit/s/Hz]} \tag{3.26}$$

Where $SINR$ is given by

$$SINR_{jk}^{ul} = \frac{p_{jk}\left|E\{v_{jk}^H h_{jk}^j\}\right|^2}{\sum_{l=1}^{L}\sum_{i=1}^{K_l} p_{li}E\{|v_{jk}^H h_{li}|^2\} - p_{jk}\left|E\{v_{jk}^H h_{jk}\}\right|^2 + \sigma_u^2 E\{\|v_{jk}\|^2\}} \tag{3.27}$$

This $SINR$ is effective $SINR$. Then SE with Maximum ratio combining (MRC) using equation 3.27 is

$$SE_{jk}^{\text{ul}} = \frac{\tau_{\text{u}}}{\tau_c}\log_2\left(1 + \frac{p_{jk}\left|E\{v_{jk}^H h_{jk}^j\}\right|^2}{\sum_{l=1}^{L}\sum_{i=1}^{K_l} p_{li}E\{|v_{jk}^H h_{li}|^2\} - p_{jk}\left|E\{v_{jk}^H h_{jk}\}\right|^2 + \sigma_u^2 E\{\|v_{jk}\|^2\}}\right) \tag{3.28}$$

3.5.3 Spectral Efficiency with LS estimator

A closed-form formula for the SE is provided as follows if the LS estimator in (Özdogan et al., 2019) is applied. For equation 3.27 on the LS estimator, if MR combines with $v_{jk} = \frac{1}{\sqrt{p_{jk}\tau_p}} y_{jjk}^p$ is applied

$$E\left\{v_{jk}^H h_{jk}^j\right\} = \text{tr}\left(R_{jk}^j\right) + \sum_{(l,i)\in\mathcal{P}_{jk}} \frac{\sqrt{p_{li}}}{\sqrt{p_{jk}}}\left(\hat{h}_{li}^j\right)^H h_{jk}^j \tag{3.29}$$

$$E\left\{\left\|v_{jk}^H\right\|^2\right\} = \frac{1}{p_{jk}\tau_p}\text{tr}\left(\left(\Psi_{jk}^j\right)^{-1}\right) + \frac{1}{p_{jk}\tau_p^2}\left\|y_{jjk}^p\right\|^2 \tag{3.30}$$

Then effective $SINR$ can be given as

$$\text{SINR}_k^{\text{UL,LS}} = \frac{p_j k \,\|\,\text{tr}(R_k) + \sum_{i=1}^{K}\frac{\sqrt{p_i}}{\sqrt{p_k}}\hat{h}_i^H \hat{h}_k\|^2}{\sum_{i=1}^{K} p_i\chi_i - p_k\|\,\text{tr}(R_k) + \sum_{i=1}^{K}\frac{\sqrt{p_i}}{\sqrt{p_k}}\hat{h}_i^H\hat{h}_k\|^2 + \sigma_{\text{UL}}^2\left(\frac{\text{tr}(\Psi_k^{-1})}{p_k\tau_p} + \frac{\|y_k^p\|^2}{p_k\tau_p^2}\right)} \tag{3.31}$$

using equation 3.31, SE for LS estimator can be

$$SE_{jk}^{\text{ul}} = \frac{\tau_{\text{u}}}{\tau_c}\log_2\left(1 + \frac{p_j k \,\|\,\text{tr}(R_k) + \sum_{i=1}^{K}\frac{\sqrt{p_i}}{\sqrt{p_k}}\hat{h}_i^H \hat{h}_k\|^2}{\sum_{i=1}^{K} p_i\chi_i - p_k\|\,\text{tr}(R_k) + \sum_{i=1}^{K}\frac{\sqrt{p_i}}{\sqrt{p_k}}\hat{h}_i^H\hat{h}_k\|^2 + \sigma_{\text{UL}}^2\left(\frac{\text{tr}(\Psi_k^{-1})}{p_k\tau_p} + \frac{\|y_k^p\|^2}{p_k\tau_p^2}\right)}\right) \tag{3.32}$$

3.5.4 Spectral Efficiency with MMSE estimator

A closed-form representation of the SE may be obtained by using the MMSE estimator as follows if MR combining with $v_{jkk} = \hat{h}^{j}_{jk}$ is applied using the MMSE estimator (Björnson et al., 2015; Özdogan et al., 2019).

$$E\left\{\left|v^{H}_{jk}h^{j}_{jk}\right|\right\} = p_{jk}\tau_p \mathrm{tr}\left(R^{j}_{jk}\Psi^{j}_{jk}R^{j}_{jk}\right) + \|\hat{h}^{j}_{jk}\|^2 \tag{3.33}$$

$$E\left\{\|y_{jk}\|^2\right\} = p_{jk}\tau_p \mathrm{tr}\left(R^{j}_{jk}\Psi^{j}_{jk}R^{j}_{jk}\right) + \|\hat{h}^{j}_{jk}\|^2 \tag{3.34}$$

Then MMSE estimator SINR can be given as

$$\mathrm{SINR}^{\mathrm{UL,MMSE}}_{k} = \frac{p^2_{jk}\tau_p \mathrm{tr}\left(R^{j}_{jk}\Psi^{j}_{jk}R^{i}_{jk}\right) + p_{jk}\|\hat{h}^{j}_{jk}\|^2}{\sum\limits_{l=1}^{L}\sum\limits_{i=1}^{K_1} p_{il}s^{ul}_{il} + \sum\limits_{(l,i)\in\mathcal{P}_{jk}}\left(p_{il}\Gamma_{ul,li} - p_{jk}vjk^{ul}\right) + \sigma^2_{ul}}. \tag{3.35}$$

where $v^{ul}_{jk} = \frac{\|\hat{h}^{j}_{jk}\|^2}{p_{jk}\tau_p \mathrm{tr}\left(R^{j}_{jk}\Psi^{j}_{jk}R^{j}_{jk}\right) + \|\hat{h}^{j}_{jk}\|^2}$ is LoS-related interference, s is non-coherent interference, and $\Gamma_{ul,li}$ is coherent interference. Then SE for MMSE estimator can be

$$SE^{\mathrm{ul}}_{jk} = \frac{\tau_{\mathrm{u}}}{\tau_c}\log_2\left(1 + \frac{p^2_{jk}\tau_p \mathrm{tr}\left(R^{j}_{jk}\Psi^{j}_{jk}R^{i}_{jk}\right) + p_{jk}\|\hat{h}^{j}_{jk}\|^2}{\sum\limits_{l=1}^{L}\sum\limits_{i=1}^{K_1} p_{il}s^{ul}_{il} + \sum\limits_{(l,i)\in\mathcal{P}_{jk}}\left(p_{il}\Gamma_{ul,li} - p_{jk}vjk^{ul}\right) + \sigma^2_{ul}}\right) \tag{3.36}$$

3.5.5 Computational time

Computational time is the amount of time needed by algorithms to process pilot signals that are received and estimate Channel State Information (CSI) while operating in real-time. Massive MIMO systems often manage a high number of antennas, which results in significant data processing requirements, making this time crucial Khichar et al., 2024. The computational time evaluation in this thesis was carried out on an HP laptop that had an Intel(R) Core(TM) i5-6200U processor running at a base clock speed of 2.30 GHz with a turbo boost up to 2.40 GHz. Operating on a 64-bit operating system with an x64-based processor architecture, the system has 8 GB of installed RAM (7.89 GB usable). The mid-range computational capability offered by this setup makes it appropriate for moderate data processing tasks, such as simulation testing and algorithmic evaluations.

3.6 Simulation Environment

The system is simulated using MATtrix LABoratry (MATLAB) R2023a. For each simulation, 1000 channel realizations are used to generate an accurate and smooth result. Considering the high data rates needed by urban environments, this research focuses on 5G systems. Considering the urban macrocell has a coverage of less than 2 km and this thesis has a coverage of 200 m, assume that the cell in this thesis is an urban macrocell as shown in Figure 3.6. User equipment 4 is the nearest to the BS, and user equipment 5 is the farthest from the BS.

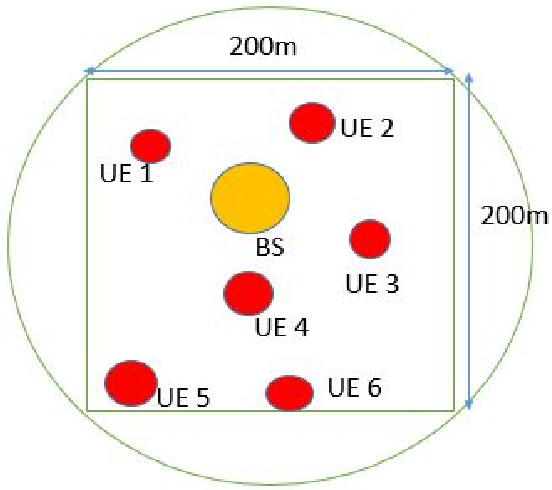

Figure 3.6: Single cells with six user equipment (UE) users

A coherence block is made up of many subcarriers and time samples that allow the channel response to be roughly described as flat-fading and constant. Consider a single-cell Massive MIMO system that serves K single-antenna user equipment with a single BS equipped with M antennas per cell. The channel responses are constant during a coherence block of τ_c samples when the system is operating in TDD mode. Furthermore, let us assume that any pair of coherent blocks has independent channel realizations. Each coherence block includes τ_c = $B_c \times T_c$ if the coherence bandwidth is B_c and the coherence time is T_c (Björnson et al., 2017). Now let us choose the frequency of the system, in order to support high data rates, which are necessary for urban density, the high-frequency offers broader bandwidths. More efficient beamforming is supported by this frequency, improving spatial resolution and directing signals toward particular users. Additionally, it can lessen interference, which is important in places where there are a lot of users, and it is one of the selected potential 5G frequencies. Based on the above reason, I chose 28 GHz frequency for this thesis. Now it is possible to calculate T_c and B_c based on the frequency chosen.

$$T_c = \frac{\lambda}{8 \times v} \tag{3.37}$$

Where λ is wavelength and v is speed of user equipment. From this chosen frequency, it's λ can be calculated using $C = \lambda \times f$. C is the speed of light, which is 3×10^8 m/s, and f is frequency. Then, using the above formula, λ become 10.71 mm. In this thesis, the user equipment speed is chosen as the average speed of human walking. As stated on (Hu et al., 2023) the average walking speed of a normal person is 1.51 m/s. Now using equation 3.37, T_c becomes 0.89 ms. Based on (Debaenst et al., 2020) coherence bandwidth can be calculated as

Table 3.1: Value of different parameters used in the simulation

Parameters	**Values**
Number of users (K)	15
Range of BS antenna (M)	Ranges from 10 to 90
Number of cells	16
SINR	0.2dB
Radius of a cell	1000 m
Minimum distance between a user	100 m
Communication bandwidth	20×10^6 Hz
Total uplink transmit power per UE	0.1 W
Noise figure at the BS	7
Length of coherence block	379KHz
Power control parameter	10 dB

$$B_c = \frac{1}{2\pi \times ds} \tag{3.38}$$

where ds is delay spread. As stated on (Xing & Rappaport, 2021) the delay spread for 5G systems in urban macrocells at 28 GHz is 420 ns. So, using equation 3.38, coherence bandwidth (B_c) is 379 kHz. Then the length of the coherence block is $\tau_c = B_c \times T_c$ approximately 336. Consider a 20 MHz channel for communication. Each coherence block has $\tau_c = 336$ samples, and the same $\tau_p = 15$ pilots are assigned at random throughout the cell.

3.7 Flow chart of the methodology

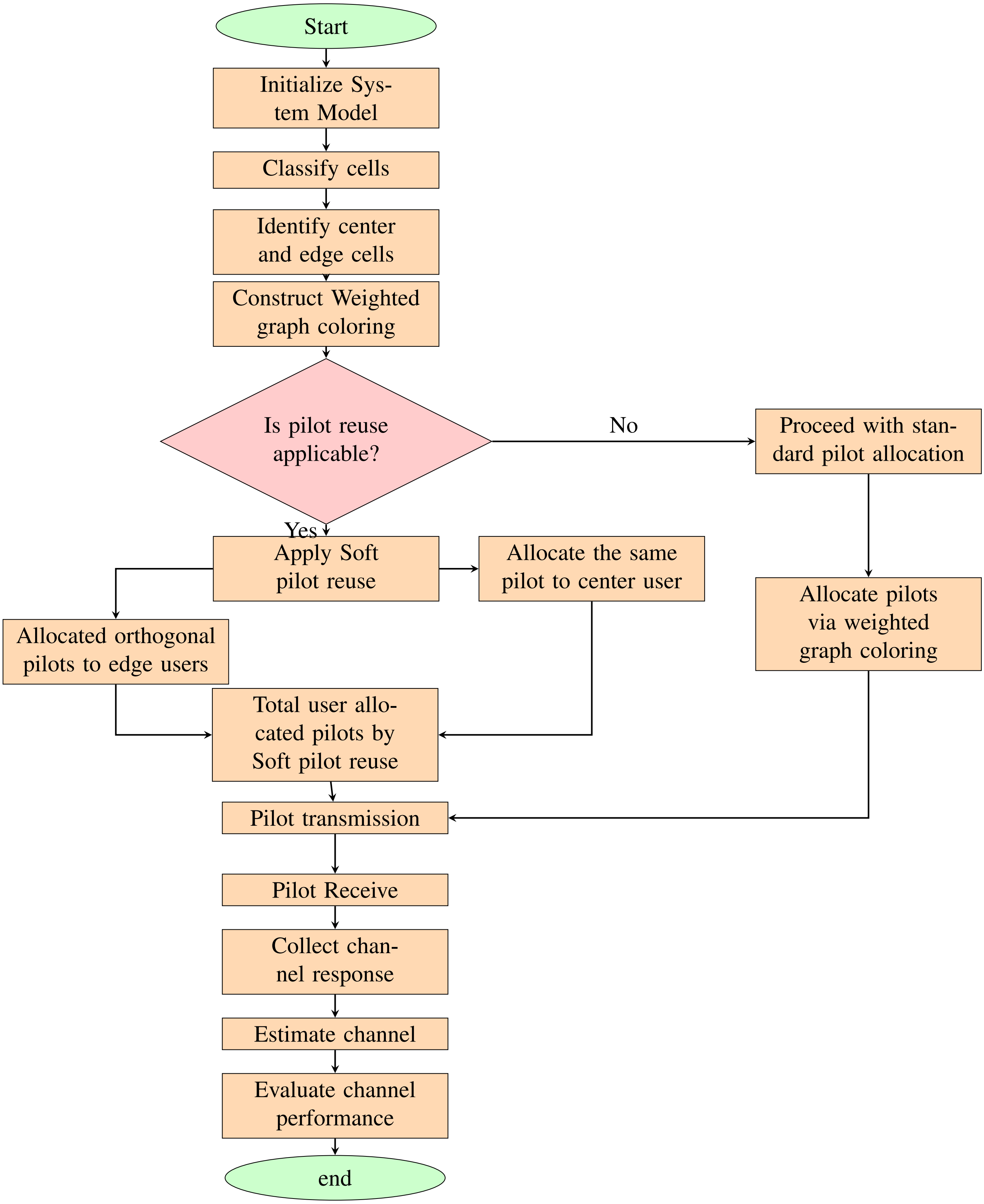

Figure 3.7: Flowchart of the methodology

4. RESULT AND DISCUSSION

4.1 Introduction

This chapter mainly presents the simulation result of the massive MIMO channel estimation with and without pilot decontamination for 5G wireless communication in Rician fading models. The frequency chosen for this thesis is 28 GHz due to its support for high data rates, which are necessary for urban density since it offers broader bandwidths, and it is one of the selected potential 5G frequency. In a massive MIMO system, the BS is equipped with many

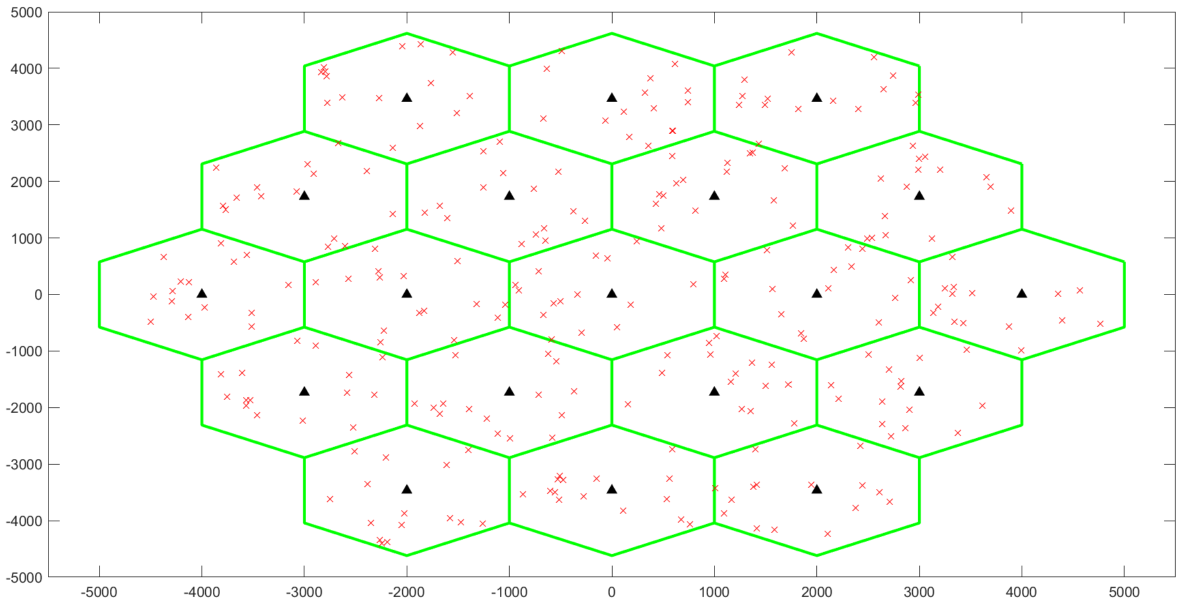

Figure 4.1: Cell topology of the system with 15 users and 16 BS. The red star represents users, and the black triangle represent Bs.

antennas, usually much more than the number of users. As a result, the BS may serve more users simultaneously on the same time-frequency resource by increasing system performance and SE. Figure 4.1 shows the users are arranged in the hexagonal cells at random. This hexagonal layout optimizes the use of available space while reducing overlapping coverage. Signal reception and channel quality are impacted by the distribution of user locations.

4.2 Channel estimation without pilot decontamination

This section shows the simulation result of a massive MIMO cellular network in order to validate and analyze the SE without pilot decontamination in both uplink and downlink systems. The system consists of a single cell that is 200 m by 200 m in size. Each cell contains

K = 15 user equipments, which are distributed independently and at random within the cell at a distance greater than 35 m from the BS. Every user equipment has been assigned to the BS that offers the highest channel gain among all the possible pairings of user equipment and BS in the system. Each user's equipment position is used to determine the large-scale fading and nominal angle between the user equipment and BS. Every BS has a Uniform linear array (ULA) antenna with an antenna spacing of 0.8.

4.2.1 Uplink SE as a function of number of BS antenna

The simulation result in Figure 4.2 illustrates the average overall SE in [b/s/Hz/cell] as a function of the massive MIMO BS uplink antenna number (M). The system model considers 15 users (K = 15) sending data to a BS equipped with up to 90 antennas (M = 90). The SE increases as the number of antennas grows; however, the rate of increase varies depending on the fading type and the channel estimation technique. The number of BS antennas varies from 10 to 90. The simulation considers the Rician and Rayleigh fading models; compared to Rayleigh fading, Rician fading always results in higher SE. This is a result of Rician fading's LoS component, which enhances signal strength and channel estimate.

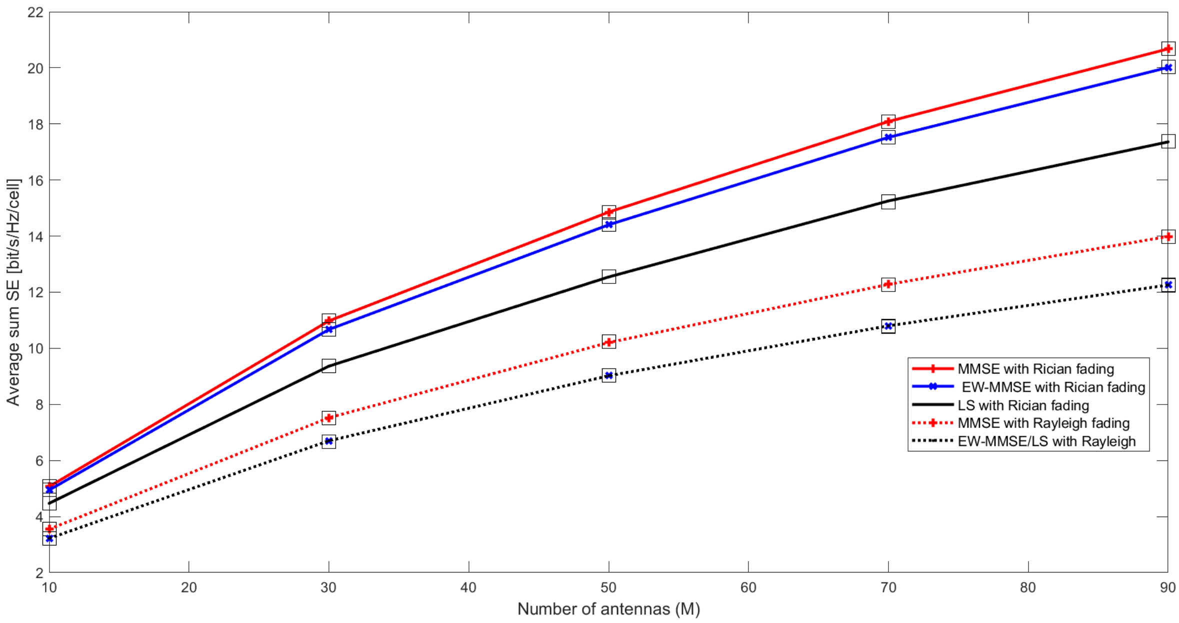

Figure 4.2: Average uplink SE as a function of the BS antennas

The simulation result compares MMSE, LS, and EW-MMSE in both Rician and Rayleigh fading. MMSE performs best across all values of M, proving that it is efficient at minimizing error and optimizing SE when fading is involved. It is better in the Rician fading scenario than in Rayleigh fading. In Rician fading, it's SE is 5.6 b/s/Hz/cell at M = 10 and 20.9 b/s/Hz/cell at M = 90, whereas in Rayleigh fading, it's about 4.8 b/s/Hz/cell and 14 b/s/Hz/cell, respectively. EW-MMSE performs slightly less effectively than MMSE, but it still exceeds LS significantly. It's SE is about 5.5 b/s/Hz/cell at M = 10 and 20 b/s/cell/Hz at M = 90 in Rican fading and around 4.7 b/s/Hz/cell at M = 10 and 11.9 b/s/Hz/cell at M = 90 in Rayleigh fading. The LS estimate is the least effective of the techniques, showing its weakness in challenging fading conditions.

4.2.2 Downlink SE as a function of antenna number

The simulation result depicted in Figure 4.3 illustrates the average overall SE in [b/s/Hz/cell] as a function of the downlink massive MIMO BS antenna number (M). The system model considers 15 users (K = 15) sending data to a BS configured with up to 90 antennas (M = 90). Like in uplink massive MIMO, SE increases as the number of BS antennas increases. Across

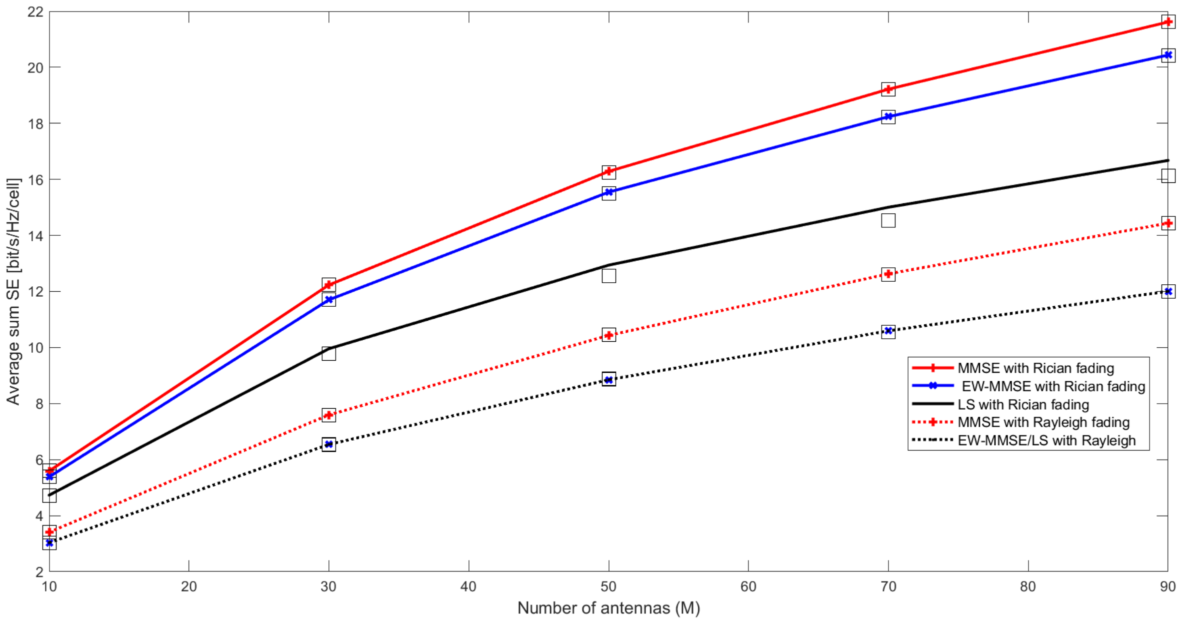

Figure 4.3: Average downlink of SE as a function of the BS antennas

all estimate techniques, the SE improves as the number of antennas M rises. This benefit results from the additional array gain and spatial diversity that more antennas at the BS give, which improves the capacity to differentiate and efficiently serve many users. Like in the uplink case, when compared to Rayleigh fading, Rician fading consistently yields greater SE because it has a LoS component, which creates a more dependable and stable channel. From these channel estimate methods, the MMSE with Rician fading SE is around 5.8 b/s/Hz/cell at M = 10 and 21.8 b/s/Hz/cell at M = 90, and the EW-MMSE with Rician fading methods achieve a SE of about 5.7 b/s/Hz/cell at M = 10 and 20.4 b/s/Hz/cell at M = 90; they perform better. The LS with Rician fading SE is about 4.9 b/s/Hz/cell at M = 10 and 16.9 b/s/Hz/cell at M = 90. The MMSE with Rayleigh fading techniques is in the middle of the performance range, with SE of about 3.8 b/s/Hz/cell at M = 10 and 14.2 b/s/Hz/cell at M = 90. While the

EW-MMSE/LS with Rayleigh fading method is performing the worst.

In general, downlink SE is higher than uplink SE due to the BS having greater transmission power available in the downlink than individual users do in the uplink. SE is enhanced by the increased signal strength. In addition to this, during the downlink, the BS is more efficient to control and handle interference between users. There may be greater inter-user interference in the uplink since each user transmits separately.

4.2.3 Cumulative Distribution Function (CDF) versus SE of user equipment

Figure 4.4 shows the SE per user equipment in bits per second per Hertz (b/s/Hz) that varies between 0 and 5 b/s/Hz versus the CDF, which has a range of 0-1. A CDF indicates the possibility that a SE per user equipment will take a value that is less than or equal to a specific value. Three different channel estimating methods, MMSE, LS, and EW-MMSE, are

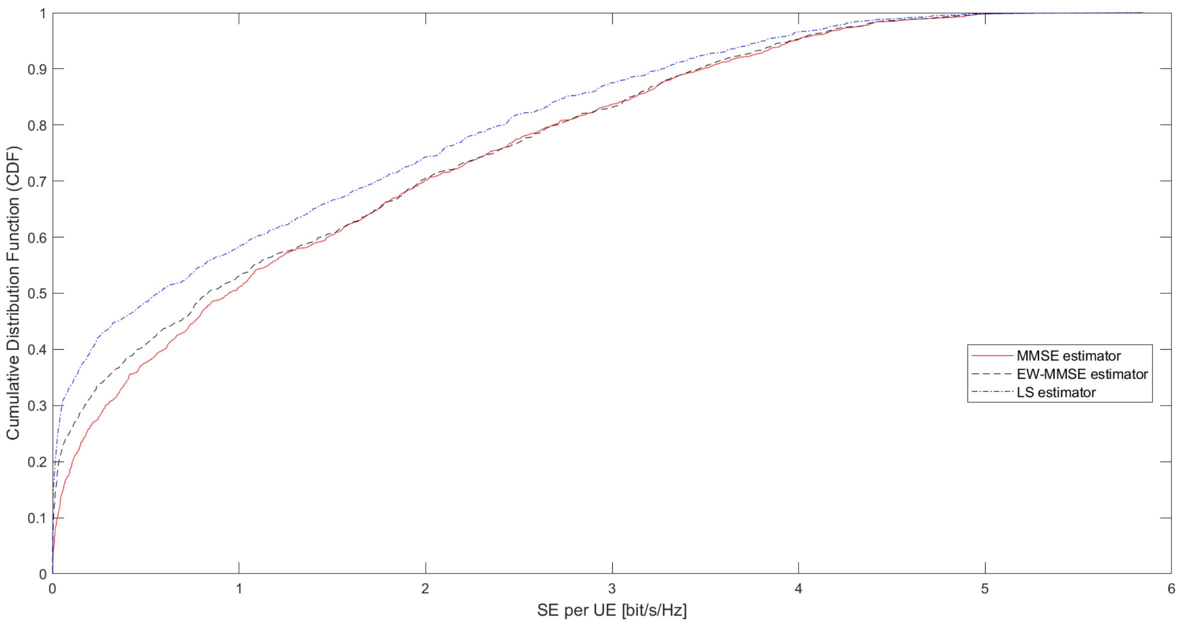

Figure 4.4: CDF of uplink SE per user equipment

compared in the simulation. The possibility of fulfilling high SE values for each method is indicated by the shape of the CDF curve. Out of all the estimators simulated, MMSE offers the best SE, suggesting that this approach produces the most accurate channel condition estimation. Compared to the other approaches, the MMSE CDF is moved to the right, indicating that a larger percentage of users have better SE. MMSE offers the highest SE per user equipment at 0.5, followed by EW-MMSE and LS. This suggests that at least 50% of system users obtain higher SE using MMSE as compared with other estimation methods. The left-shifted CDF curve in relation to the MMSE curve indicates EW-MMSE that has a little lower SE than the MMSE estimator. This implies that while EW-MMSE is more effective, some SE performance is lost as a result of simplifications. In comparison to MMSE and EW-MMSE, the leftmost CDF is LS, which indicates a lower SE per user equipment. This implies that LS is insufficient in optimizing SE for uplink users while being computationally simpler.

4.2.4 Uplink SE as a function of BS antenna number with spatially uncorrelated Rician fading

Figure 4.5 indicates the average uplink sum SE under various channel estimate algorithms in a massive MIMO system with spatially uncorralled Rician fading as a function of the number of BS antennas. For all three methods, the average uplink SE gets higher as the number

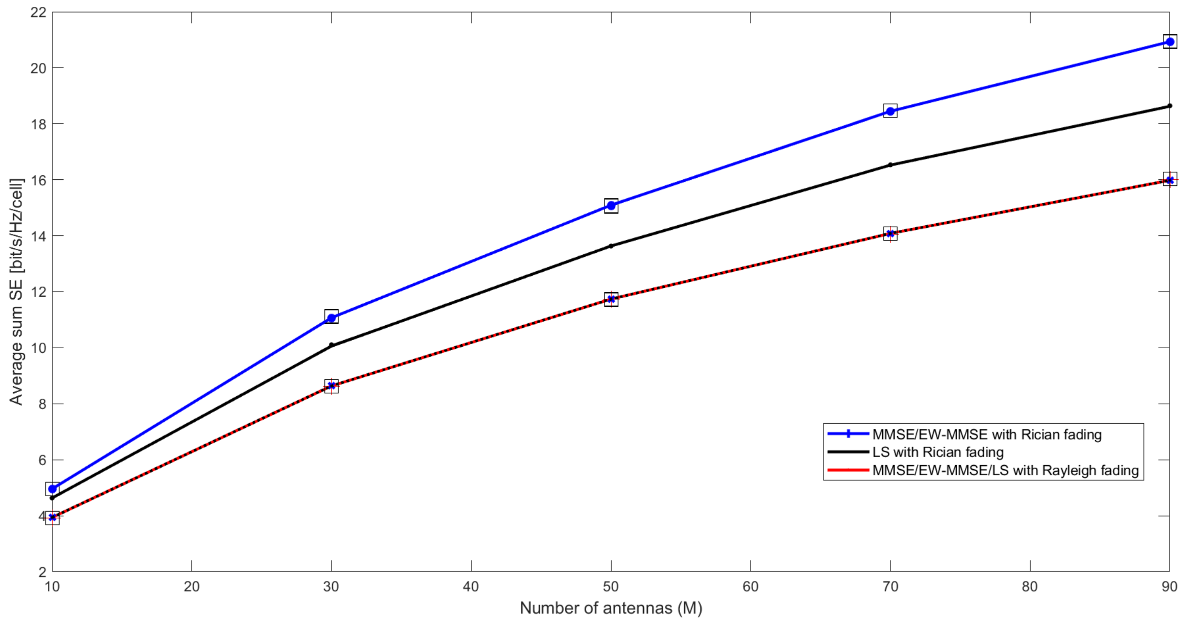

Figure 4.5: Average uplink SE as a function of BS antennas with spatially uncorrelated Rician fading

of BS antennas (M) increases. When fading is spatially uncorrelated, it means that separate antenna elements or users experience fading independently, which means that fluctuations in fading at one antenna are not associated with those at other antennas. Because the fading at one antenna does not predict the fading at another, this feature makes channel modeling easier. Out of the three scenarios, MMSE/EW-MMSE with Rician Fading has the highest SE of around 5.5 b/s/Hz/cell at M = 10 and 21.5 b/s/Hz/cell at M = 90. It shows that the SE much improves as the number of antennas increases. Better performance is achieved by utilizing the LoS component of Rician fading, which can be seen from the MMSE/EW-MMSE channel estimate technique. Rician fading with LS has a poorer spectral efficiency than Rician-fading MMSE/EW-MMSE. Despite its simplicity, LS estimation is not as effective as MMSE, particularly in channels with both scattered links and LoS it's SE is about 5.1

b/s/Hz/cell at M = 10 and 18.3 b/s/Hz/cell at M = 90. MMSE/EW-MMSE/LS Rayleigh fading shows, out of the three techniques, it exhibits the lowest SE with value of 4.0 b/s/Hz/cell at M = 10 and 16.0 b/s/Hz/cell at M = 90. Since Rayleigh fading lacks a LoS link, it presents a more difficult channel estimation environment, resulting in lower SE.

4.3 Pilot decontamination scheme

Pilot contamination is a major problem in wireless communication systems, especially in massive MIMO systems. It occurs when users reuse non-orthogonal pilot sequences, which causes interference and reduces system performance. In this section, pilot mitigation mechanisms such as random pilot decontamination, soft pilot reuse, weighted graph coloring pilot decontamination, and the combination of soft pilot reuse and weighted graph coloring simulation results are shown.

4.3.1 Average user capacity as a function of transmit power

The simulation result in Figure 4.6 indicates the average user uplink capacity in a massive MIMO system under various pilot allocation and decontamination schemes as the transmit power varies (in dB). The transmission power levels are between 2 and 20 dB. This vari-

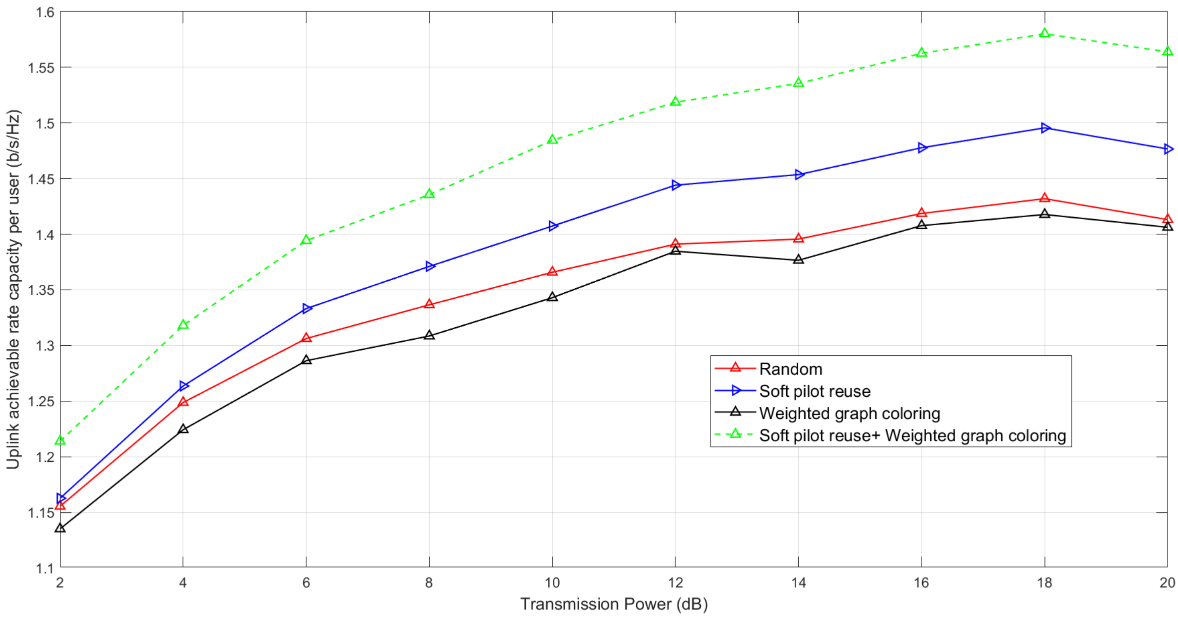

Figure 4.6: Average user uplink capacity as a function of transmit power

able shows the average data rate per unit of bandwidth that each user can get, expressed in bits per second per Hz (bps/Hz), as well as the strength at which signals are transferred from the users to the BS. Better data throughput performance is indicated by higher capacity values. Across all transmit power levels, the combination of soft pilot reuse and weighted graph coloring pilot decontamination approach continuously achieves the maximum average user uplink capacity. This suggests that integrating these strategies optimizes capacity and successfully reduces pilot contamination in massive MIMO channel estimation. Compared to random allocation, the soft pilot reuse technique performs better but not as well as the combined strategy. In random pilot allocation, users are randomly allocated pilots without taking inter-user interference effect. Usually, this approach has pilot contamination, which reduces uplink capacity, particularly in situations where the number of users in this system is 15 in each cell.

4.3.2 Average achievable rate per user in relation to the number of BS antennas

Figure 4.7 shows the average uplink capacity (bits/Hz) for various pilot decontamination techniques as a function of the number of antennas in a massive MIMO BS (M) system. The uplink achievable rates improved for all approaches as the number of antennas at the

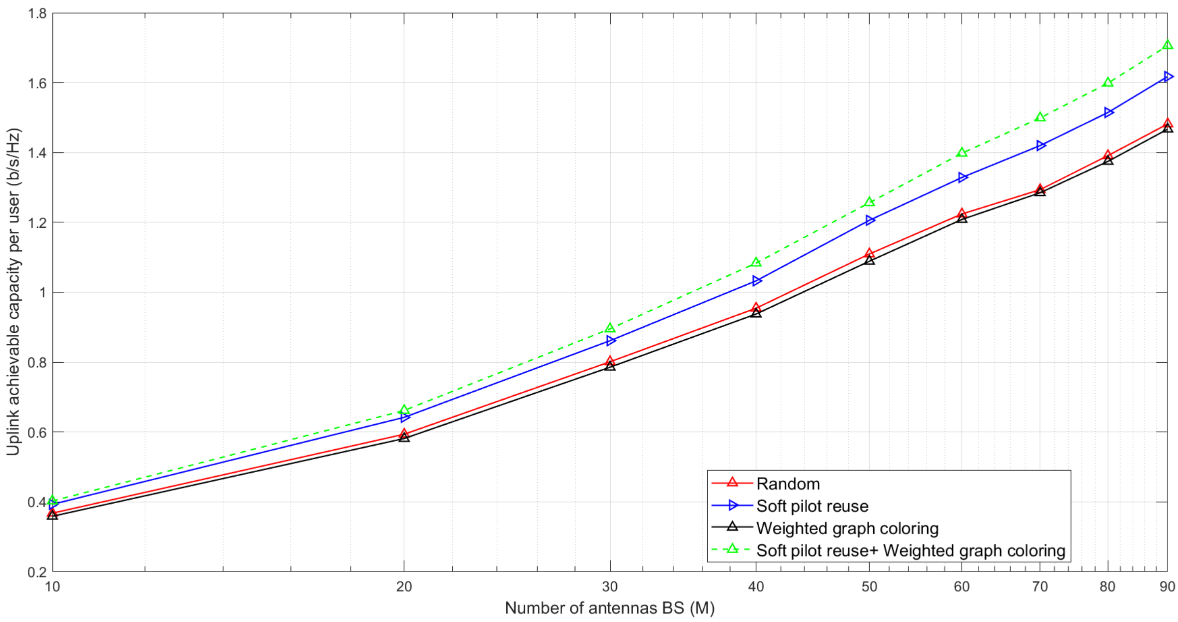

Figure 4.7: Average achievable rate per user versus the number of BS antennas

antenna BS rises because of improved spatial diversity and interference reduction. But when it comes to utilizing the full benefits associated with larger antenna arrays, techniques like weighted graph coloring pilot decontamination and soft pilot reuse become less effective separately. When weighted graph coloring combined with soft pilot reuse, it performs better than the others due to the fact that they can integrate interference-aware pilot assignment with geographic separation. This technique is beneficial in minimizing contamination and maximizing resource use since it provides the greatest uplink rates over a range of antenna configurations.

4.3.3 CDF of the achievable uplink rate of users as a function of SINR

The CDF of the possible user uplink rate versus the SINR in a massive MIMO system under various pilot allocation and decontamination procedures is shown in Figure 4.8. The CDF

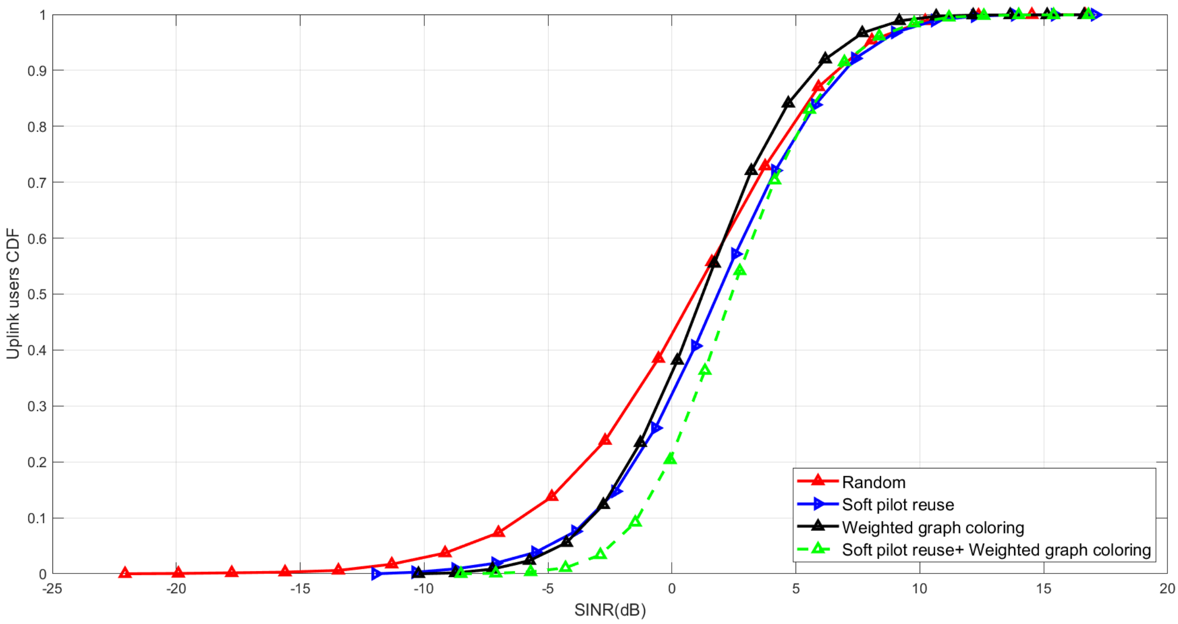

Figure 4.8: CDF of the achievable uplink rate of users versus SINR

curves increase more quickly as the SINR increases, suggesting that more users attain greater rates. SINR is a crucial wireless communication study because it shows how well a signal is performing in relation to interference and noise. CDF shows the possibility that a given value is less than or equal to the feasible rate for users. A higher number of CDF indicates higher performance. The simulation shows that significant variations between the pilot allocation strategies become noticeable as SINR approaches specific thresholds (about 0 dB and more). The best SINR performance is obtained when soft pilot reuse and weighted graph coloring are combined, followed by weighted graph coloring, soft pilot reuse, and random pilot allocation.

In this thesis, the combination of soft pilot reuse and weighted graph coloring pilot decontamination is used to mitigate the pilot contamination based on the simulation from Figures 4.6 to 4.8, which greatly lowers pilot contamination by improving the user interface and system performance.

4.4 Channel estimation with pilot decontamination

Through the combination of weighted graph coloring to maintain effective pilot assignment and soft pilot reuse to control interference distribution, this technique greatly increases the accuracy of channel estimates. Thus, the SE of massive MIMO networks is improved by a system that achieves the appropriate balance between interference mitigation and pilot reuse efficiency. In this section, the simulation result in Section 4.2 is improved by adding pilot mitigation that combines both soft pilot reuse and weighted graph coloring pilot decontamination.

4.4.1 Average uplink SE as a function of antenna number with pilot mitigation

The simulation result in Figure 4.9 illustrates how the combination of weighted graph coloring and soft pilot reuse can greatly improve channel estimation for massive MIMO systems by minimizing the effect of pilot contamination. It uses a combination of weighted graph

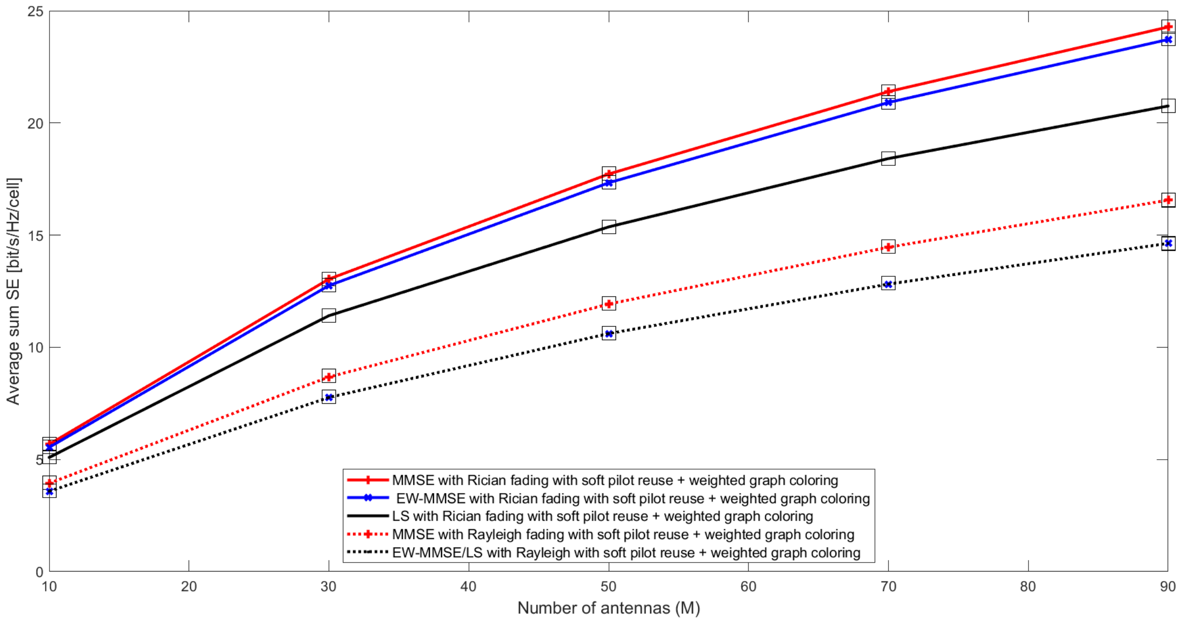

Figure 4.9: Average uplink sum of SE as a function of BS antennas with pilot decontamination

coloring pilot decontamination and soft pilot reuse to mitigate the pilot contamination effect in order to show the improvement of the average sum of SE as a function of the number of BS antennas (M) in a massive MIMO system shown in the simulation of Figure 4.2.

MMSE with Rician Fading performs effectively for all antenna numbers. This suggests that MMSE channel estimation efficiently eliminates the influence of pilot contamination and utilizes the LoS component in Rician fading when soft pilot reuse and weighted graph coloring pilot decontamination are combined. The SE at M = 10 is about 5.9 bits/s/Hz/cell and 24.7 bits/s/Hz/cell at M = 90. EW-MMSE with Rician fading performs SE of around 5.8 bits/s/Hz/cell at M = 10 and 24.1 bits/s/Hz/cell when M = 90; that is somewhat worse than MMSE, but because of its improved channel estimating capacity, it still exceeds LS with Rician fading estimation, where SE at M = 10 is around 5.4 bits/Hz/s/cell and 20.8 bits/s/Hz/cell at M = 90. MMSE with Rayleigh fading is poorer performance than the Rician fading situations; it is about 4.9 bits/s/Hz/cell at M = 10 and 16.5 bits/s/Hz/cell at M = 90, but better performance than EW-MMSE/LS with Rayleigh fading. This indicates the effect of a LoS component is absent. Rayleigh fading in EW-MMSE/LS has the lowest SE, indicating that the SE degrades when LoS is absent and lower level estimate methods are used.

4.4.2 Average downlink SE as a function of antenna number with pilot decontamination

Figure 4.10 analyzes the average sum SE of a massive MIMO system for downlink channel estimation by combining weighted graph coloring for pilot decontamination with soft pilot reuse. The results show how different estimating techniques and fading work differently.

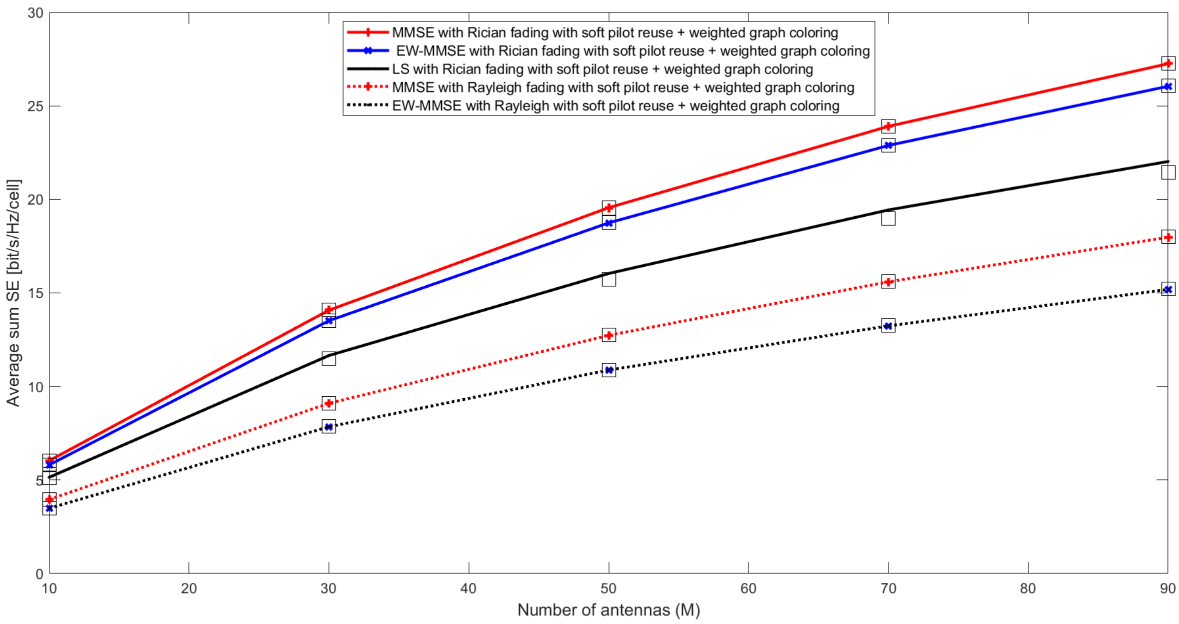

Figure 4.10: Average downlink sum of SE as a function of BS antennas with pilot decontamination

The advantages of having a robust LoS component along with efficient pilot contamination mitigation are shown by the better performance of MMSE estimation with Rician fading over all other approaches. The SE is around 6.0 bits/s/Hz/cell at M = 10, and it becomes 27.5 bits/s/Hz/cell when M becomes 90. Although EW-MMSE with Rician fading also performs well. It's SE is approximately 5.9 bits/s/Hz/cell at M = 10, and it increased to around 26.3 bits/s/Hz/cell when M = 90. Due to being sensitive to noise and pilot contamination, LS estimation, though simpler, exhibits lower SE. The SE in LS Rician fading is about 5.5 bits/s/Hz/cell at M = 10 and 22.1 bits/s/Hz/cell when M becomes 90. The SE is typically smaller in the Rayleigh fading scenario, where there are simply scattered multipath signals and no LoS component. It's MMSE SE at M = 10 is around 4.9 bits/s/Hz/cell and 17.5 bits/s/Hz/cell at M = 90.

4.4.3 Cumulative Distribution Function versus SE of UE with pilot decontamination

Figure 4.11 illustrates the CDF of the SE per user equipment for various channel estimate techniques in a massive MIMO system that uses weighted graph coloring for pilot decontamination in the downlink together with soft pilot reuse. Out of the three methods, the

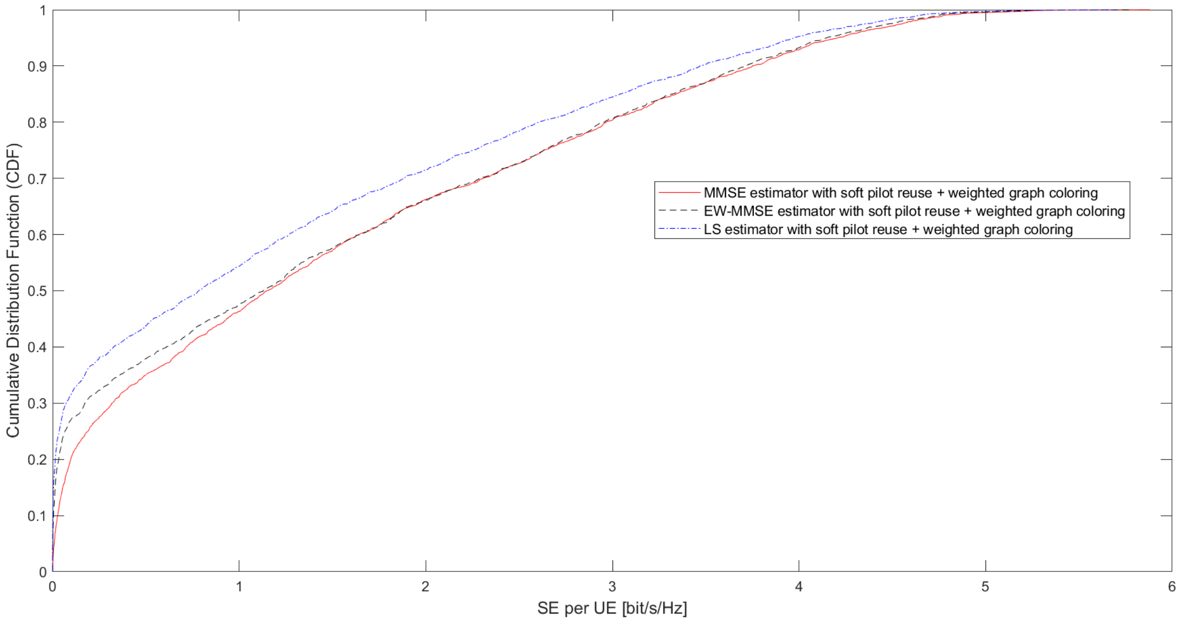

Figure 4.11: CDF of uplink SE per UE with pilot decontamination

MMSE estimator performs the best. For the majority of UEs, it obtains the greatest SE values, demonstrating its effectiveness in reducing pilot contamination and precise channel estimation. It outperforms the other estimators by providing a SE of approximately 1.18 bits/s/Hz/cell at a CDF value of 0.5. It has the capacity to reduce the MSE in channel estimation, especially when combined with weighted graph coloring and soft pilot reuse pilot decontamination. Together with pilot decontamination, these methods increase SE, minimize interference, and improve channel estimate accuracy. When compared to the MMSE estimator, the SE values from the EW-MMSE estimate and the LS estimator are gradually lower. The LS estimator obtains the lowest SE of approximately 0.76 bits/s/Hz at a 0.5 CDF value, whereas the EW-MMSE estimator produces a SE of approximately 1.15 bits/s/Hz. The LS estimator is less appropriate for massive MIMO systems due to its poorer performance, which emphasizes its incapacity to adequately reduce interference and pilot contamination.

4.4.4 Average uplink SE as a function of antenna number with spatially uncorrelated Rician fading with pilot decontamination

The simulation result in Figure 4.12 shows the average uplink SE as a function of antenna number (M) in a massive MIMO system with spatially uncorrelated Rician fading. Using the soft pilot reuse scheme and weighted graph coloring, the system integrates pilot decontamination. The highest SE values are obtained for all antenna numbers when using MMSE/EW-

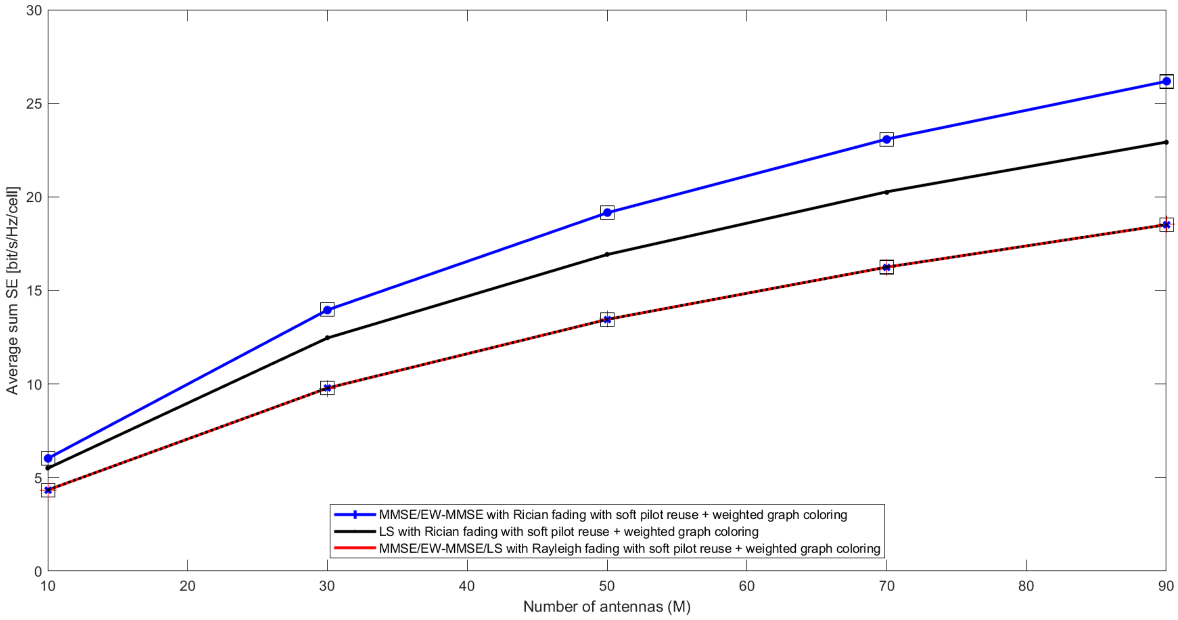

Figure 4.12: Average uplink sum of SE as a function of BS antennas with spatially uncorrelated Rician fading with pilot decontamination

MMSE channel estimation with Rician fading. The average SE is roughly 5.6 bits/s/Hz/cell when M = 10, and it increases dramatically to 25.3 bits/s/Hz/cell when M = 90. With the use of the enhanced channel estimate in the presence of a significant LoS component in Rician fading, this shows how the MMSE/EW-MMSE estimator scales with the number of antennas. While LS estimation with Rician fading outperforms Rayleigh fading, it falls short of MMSE/EW-MMSE estimation. The SE is about 5.3 bits/s/Hz/cell at M = 10 and rises to about 22.1 bits/s/Hz/cell at M = 90. This difference from the MMSE demonstrates the LS estimator's inferior channel estimating capacity, which prevents it from fully utilizing the advantages of the Rician fading environment. Because there is no LoS component in Rayleigh fading, which results in increased channel uncertainty, this configuration exhibits the lowest SE values of any scenario. For M = 10, the SE begins at about 4.8 bits/s/Hz/cell, and for M = 90, it reaches about 17.5 bits/s/Hz/cell. This significant performance gap emphasizes how important Rician fading is for enhancing SE and channel estimation.

4.5 Comparison of the channel estimation simulation result with and without pilot decontamination

Table 4.1: Average uplink SE in b/s/Hz/cell for different techniques

Techniques	**Channel estimation without pilot decontamination**		**Channel estimation with pilot decontamination**	
	M = 10	**M = 90**	**M = 10**	**M = 90**
MMSE with Rician	5.6	20.9	5.9	24.7
EW-MMSE with Rician	5.5	20.0	5.8	24.1
LS with Rician	5.2	17.6	5.4	20.8
MMSE with Rayleigh	4.8	14.0	4.9	16.5
EW-MMSE with Rayleigh	4.7	11.9	4.8	14.8

Table 4.1 shows the average uplink SE of massive MIMO channel estimation for two fading models (Rician and Rayleigh) under various channel estimate methods with and without pilot decontamination. For M = 90, MMSE with Rician fading gives the maximum SE (20.9 b/s/Hz/cell) without pilot mitigation, closely followed by EW-MMSE (20.0 b/s/Hz/cell). Even with a lower SE (17.6 b/s/Hz/cell for M = 90), the MMSE offers the best performance for the Rayleigh fading. The SE values of all methods are improved with pilot decontamination, particularly for larger antenna arrays (M = 90). The biggest SE boost occurs in MMSE with Rician fading, raising it to 24.7 b/s/Hz/cell; EW-MMSE also improves to 24.1 bits/s/Hz/cell. Compared to alternative techniques, MMSE obtains 16.5 bits/s/Hz/cell for Rayleigh fading. This indicates the importance of pilot decontamination in improving channel estimation performance.

Table 4.2 shows that the maximum SE, 20.9 bits/s/Hz/cell for M = 90, is achieved by MMSE with Rician fading in a with pilot contamination. EW-MMSE with Rician fading comes in next, with 20.0 bits/s/Hz/cell. SE values are lower for smaller antenna arrays (M = 10), with an MMSE of 5.6 bits/s/Hz/cell. Performance in Rayleigh fading channels is often poorer; for M=90, MMSE achieves 14.2 bits/s/Hz/cell, while EW-MMSE and LS perform marginally worse. All methods observed an improvement in SE values after pilot mitigation, particularly for large antenna arrays (M = 90). In EW-MMSE obtains 26.3 bits/s/Hz/cell, suggesting a significant performance gain; MMSE with Rician fading achieves 27.5 bits/s/Hz/cell. Similarly, MMSE improves to 17.5 bits/s/Hz/cell with Rayleigh fading.

Table 4.2: Average downlink SE in bits/s/Hz/cell for different techniques

Techniques	Channel estimation without pilot decontamination		Channel estimation with pilot decontamination	
	M = 10	**M = 90**	**M = 10**	**M = 90**
MMSE with Rician	5.8	21.8	6.0	27.5
EW-MMSE with Rician	5.7	20.4	5.9	26.3
LS with Rician	4.9	16.9	5.5	22.1
MMSE with Rayleigh	3.8	14.2	4.9	17.5
EW-MMSE with Rayleigh	3.7	12.1	4.8	15.0

Table 4.3 makes it clear that, in every situation, pilot decontamination increases the accuracy of the channel estimate. With Rician fading, MMSE/EW-MMSE improves from 5.5 bits/s/Hz/cell to 5.6 bits/s/Hz/cell when M = 10 and from 21.5 bits/s/Hz/cell to 25.3 bits/s/Hz/cell when M = 90. MMSE/EW-MMSE with Rayleigh also improved from 4.0 bits/s/Hz/cell to 4.8 bits/s/Hz/cell when M = 10 and from 16.0 bits/s/Hz/cell to 17.5 bits/s/Hz/cell when M = 90. In massive MIMO systems, the uplink typically requires more computing

Table 4.3: Average uplink SE with spatially uncorrelated Rician fading in bits/s/Hz/cell for different techniques

Techniques	Channel estimation without pilot decontamination		Channel estimation with pilot decontamination	
	M = 10	**M = 90**	**M = 10**	**M = 90**
MMSE/EW-MMSE with Rician	5.5	21.5	5.6	25.3
LS with Rician	5.1	18.3	5.3	22.1
MMSE/EW-MMSE with Rayleigh	4.0	16.0	4.8	17.5

time for channel estimation than the downlink. This is due to the fact that each user equipment sends pilot signals that must be processed by the BS in order to estimate the channel matrix for each user in the uplink. When several user equipment uses the same pilot sequence, the BS must strive to differentiate and separate these pilot signals in order to control pilot contamination in the absence of pilot decontamination, as shown in Table 4.4.

Table 4.4: Comparison of computational time in seconds

Comparison	Computational time for Channel estimation without pilot decontamination	Computational time for Channel estimation with pilot decontamination
Average uplink sum of SE	10,9644.17	10,396.59
Average downlink sum of SE	9,106.02	8,794.75
Cumulative Distribution Function (CDF)	2,128.14	2,022.87
Average uplink SE with Spatially Uncorrelated Rician Fading	7,826.91	7,626.27

4.6 Comparison of the proposed result with other work

Table 4.5 shows the comparison of different articles published related to massive MIMO channel estimation. They compared based on the channel estimation scheme, number of users, number of BS antennas, and achieved SE in bits/s/Hz/cell. The proposed research improves overall system performance and offers an efficient approach for addressing issues in multi-user wireless systems. To increase channel estimate accuracy and get improved SE, this thesis mitigates the effect of pilot contamination using the combination of soft pilot reuse and weighted graph coloring pilot decontamination.

Table 4.5: Comparison of the proposed result with other work

References	Year	Channel estimation scheme	Number of users (K)	Number of BS antennas (M)	SE (bits/s/Hz/cell)
(Björnson et al., 2015)	2015	It develops a system model with arbitrary pilot reuse factors, power control, and random user locations. It then derives new SE expressions for uplink and downlink under a variety of processing strategies, including as MR, ZF, and an RZF method	10	1000	70
(Rayi & Prasad, 2017)	2017	Analyze SE and energy efficiency under different scenarios while taking into consideration variables such as pilot reuse factors, the number of BS antennae, and ideal user terminals. Channel estimation is done using linear processing algorithms including ZF, MRC, and MMSE, and system performance is evaluated for both perfect and imperfect CSI	10	1500	180
(Asiedu & Ahmed, 2018)	2018	Uses LS channel estimation to examine pilot contamination in TDD massive MIMO systems. Closed-form SE limitations are derived for ZF and MRC detectors under reuse-based, non-orthogonal, and orthogonal pilot allocation strategies	20	500	75
(Özdogan et al., 2019)	2019	Provides a multi-cell massive MIMO model that combines LoS and NLoS components with Ricians fading. For both uplink and downlink, closed-form SE expressions are obtained using MMSE, EW-MMSE, and LS estimators with MR combining and precoding	10	100	20
(Mai et al., 2020)	2020	It uses two protocols, one with and one without downlink pilots, as well as MMSE-SIC identification and power control modification to assess downlink SE of cell-free massive MIMO systems with multiple antenna users	5	50	18
(Bacci et al., 2024)	2024	It uses circulant approximation for linear arrays and Kronecker decomposition for planar arrays to simplify calculations in reduced-complexity channel estimation techniques for large-scale MIMO systems. These techniques greatly reduce computing cost, improve robustness under faulty channel statistics, and accomplish accuracy of the channel	10	200	20.3
Proposed Research	2024	This thesis mitigates the effect of pilot contamination using the combination of soft pilot reuse and weighted graph coloring pilot decontamination to increase channel estimate accuracy and improve SE (for uplink)	15	90	24.7

5. CONCLUSION AND RECOMMENDATION

5.1 Conclusion

Massive MIMO systems are used to achieve performance improvements in wireless communication, particularly in the 5G system. A vital component of communication systems, particularly in wireless communication, is the estimation of channels. The accuracy of the channel estimate is affected by pilot contamination in situations where pilot signals are repeated by several users or cells. System performance may be affected by this phenomenon by introducing interference and inaccurately determining the CSI. This thesis investigates methods for estimating channels in massive MIMO systems when Rayleigh and Rician fading are present in 5G wireless communication. Soft pilot reuse is combined with the weighted graph coloring to overcome pilot contamination. By reducing the effects of pilot contamination, this method improves the accuracy of the channel estimate for both Rayleigh and Rician fading. It focuses on the effectiveness of common estimating techniques such as LS, EW-MMSE, and MMSE.

The simulation result shows that the better method for channel estimation in both uplink and downlink situations is MMSE with Rician fading. In the uplink system, spectral effeciency (SE) of the channel estimate using MMSE is improved from 20.9 bits/s/Hz/cell to 24.7 bits/s/Hz/cell with pilot decontamination at M = 90. For downlink, it improved from 21.8 bits/s/Hz/cell to 27.5 bits/s/Hz/cell. In Rayleigh fading, for the uplink system using MMSE, SE improved from 14.0 bits/s/Hz to 16.5 bits/s/Hz/cell at M = 90 with pilot decontamination, whereas in the downlink it improved from 14.2 bits/s/Hz/cell to 17.5 bits/s/Hz/cell. With spatially uncorrelated Rician fading, MMSE/EW-MMSE improved from 21.5 bits/s/Hz/cell to 25.3 bits/s/Hz/cell when M = 90. MMSE/EW-MMSE with Rayleigh also improved from 16.0 bits/s/Hz/cell to 17.5 bits/s/Hz/cell when M = 90. The results show that the addition of decontamination techniques increases the accuracy of channel estimates, hence improving system performance for massive MIMO networks.

In general, this thesis emphasizes how crucial it is to use pilot decontamination procedures and suitable massive MIMO channel estimate approaches in order to handle the particular difficulties associated with Rician and Rayleigh fading environments. MMSE and EW-MMSE are useful for utilizing channel characteristics, while soft pilot reuse combined with weighted graph coloring is a reliable way to mitigate the effect of pilot contamination in both Rician and Rayleigh fading.

5.2 Recommendation

This thesis offers an in-depth investigation of channel estimation methods for massive MIMO systems in environments with Rician and Rayleigh fading, providing insightful information about their capabilities and drawbacks. Future research could build on these results by investigating advanced machine learning-based estimation techniques to improve the accuracy of channel estimates in challenging fading scenarios. Also, it could be beneficial to extend this thesis to more advanced pilot decontamination methods and optimize pilot allocation procedures for dynamic and heterogeneous network environments. Furthermore, more reliable and scalable wireless solutions may be made possible by combining the approaches used in this thesis with higher-order MIMO systems and advanced technologies like reconfigurable intelligent surfaces and mmwave communications.

Bibliography

Agarwal, A. A. (2011). *Pilot based channel estimation 3gpp lte downlink* [Doctoral dissertation, University of Texas at Arlington].

Albreem, M. A., Al Habbash, A. H., Abu-Hudrouss, A. M., & Ikki, S. S. (2021). Overview of precoding techniques for massive mimo. *IEEE Access*, *9*, 60764–60801.

Amadid, J., Boulouird, M., & HASSANI, M. M. (2020). Channel estimation with pilot contamination in mutli-cell massive mimo systems. *2020 IEEE 2nd International Conference on Electronics, Control, Optimization and Computer Science (ICECOCS)*, 1–4.

Asiedu, E. O., & Ahmed, R. (2018). Spectral efficiency analysis and achievable rates in massive mimo systems with ls channel estimation. *Proceedings of the 6th ACM/ACIS International Conference on Applied Computing and Information Technology*, 43–48.

Bacci, G., DAmico, A. A., & Sanguinetti, L. (2024). Mmse channel estimation in large-scale mimo: Improved robustness with reduced complexity. *IEEE Transactions on Wireless Communications*.

Balevi, E., Doshi, A., & Andrews, J. G. (2020). Massive mimo channel estimation with an untrained deep neural network. *IEEE Transactions on Wireless Communications*, *19*, 2079–2090.

Baranidharan, V., Karthikeyan, S., Hariharan, R., Mugunthan, T., & Vhivek, S. (2021). Pilot decontamination algorithm with iterative weighted graph coloring scheme for multi-cell mimo system in 5g applications. *International Conference on Communication, Computing and Electronics Systems: Proceedings of ICCCES 2020*, 501–513.

Bashu, T. B., Feisso, S., & Tulu, M. M. (2024). Performance evaluation of precoding schemes for multi user massive mimo system over nakagami-m fading channel. *Wireless Personal Communications*, 1–12.

Benzaghta, M., & Rabie, K. M. (2021). Massive mimo systems for 5g: A systematic mapping study on antenna design challenges and channel estimation open issues. *IET Communications*, *15*(13), 1677–1690.

Björnson, E., Hoydis, J., Sanguinetti, L., et al. (2017). Massive mimo networks: Spectral, energy, and hardware efficiency. *Foundations and Trendső in Signal Processing*, *11*(3-4), 154–655.

Björnson, E., Larsson, E. G., & Debbah, M. (2015). Massive mimo for maximal spectral efficiency: How many users and pilots should be allocated? *IEEE Transactions on Wireless Communications*, *15*(2), 1293–1308.

Björnson, E., Larsson, E. G., & Marzetta, T. L. (2016). Massive mimo: Ten myths and one critical question. *IEEE Communications Magazine*, *54*(2), 114–123.

Björnson, E., Sanguinetti, L., Hoydis, J., & Debbah, M. (2014). Designing multi-user mimo for energy efficiency: When is massive mimo the answer? *2014 IEEE wireless communications and networking conference (WCNC)*, 242–247.

Bobrov, E., Chinyaev, B., Kuznetsov, V., Lu, H., Minenkov, D., Troshin, S., Yudakov, D., & Zaev, D. (2021). Adaptive regularized zero-forcing beamforming in massive mimo with multi-antenna users. *arXiv preprint arXiv:2107.00853*.

Borges, D., Montezuma, P., Dinis, R., & Beko, M. (2021). Massive mimo techniques for 5g and beyondopportunities and challenges. *Electronics*, *10*(14), 1667.

Busari, S. A., Huq, K. M. S., Mumtaz, S., Dai, L., & Rodriguez, J. (2017). Millimeter-wave massive mimo communication for future wireless systems: A survey. *IEEE Communications Surveys & Tutorials*, *20*(2), 836–869.

Caire, G., & Shamai, S. (2003). On the achievable throughput of a multiantenna gaussian broadcast channel. *IEEE Transactions on Information Theory*, *49*(7), 1691–1706.

Carrera, D. F., Vargas-Rosales, C., Azpilicueta, L., & Galaviz-Aguilar, J. A. (2020). Comparative study of channel estimators for massive mimo 5g nr systems. *IET Communications*, *14*(7), 1175–1184.

Castaneda, E., Silva, A., Gameiro, A., & Kountouris, M. (2016). An overview on resource allocation techniques for multi-user mimo systems. *IEEE Communications Surveys & Tutorials*, *19*(1), 239–284.

Chataut, R., & Akl, R. (2020). Massive mimo systems for 5g and beyond networksoverview, recent trends, challenges, and future research direction. *Sensors*, *20*(10), 2753. https://doi.org/10.3390/s20102753

Chen, S., Zhang, J., Zhang, J., Björnson, E., & Ai, B. (2022). A survey on user-centric cell-free massive mimo systems. *Digital Communications and Networks*, *8*(5), 695–719.

Cheng, Q., Fang, G., Nguyen, D., & Dutkiewicz, E. (2016). Novel pilot decontamination methods for massive mimo systems under practical scenarios. *2016 16th International Symposium on Communications and Information Technologies (ISCIT)*, 77–81.

Choi, J. (2010). *Optimal combining and detection: Statistical signal processing for communications*. Cambridge University Press.

Dao, H. T., & Kim, S. (2018). Vertex graph-coloring-based pilot assignment with location-based channel estimation for massive mimo systems. *IEEE Access*, *6*, 4599–4607.

Debaenst, W., Feys, A., Cuiñas, I., Garcia Sanchez, M., & Verhaevert, J. (2020). Rms delay spread vs. coherence bandwidth from 5g indoor radio channel measurements at 3.5 ghz band. *Sensors*, *20*(3), 750.

de Figueiredo, F. A., Cardoso, F. A., Moerman, I., & Fraidenraich, G. (2018). Channel estimation for massive mimo tdd systems assuming pilot contamination and flat fading. *EURASIP Journal on wireless Communications and Networking*, *2018*, 1–10.

Devasia, A., & Reddy, R. (2013). Semi blind channel estimation: An efficient channel estimation scheme for mimo-ofdm system. *Australian Journal of Basic and Applied Sciences*, *7*(7), 531–538.

Dey, A., & Pattanayak, P. (2024). Pilot allocation technique for massive mimo systems based on clustering. *Sdhan*, *49*(4), 275.

Edition, F., Papoulis, A., & Pillai, S. U. (2002). *Probability, random variables, and stochastic processes*. McGraw-Hill Europe: New York, NY, USA.

Elijah, O., Leow, C. Y., Tharek, A. R., Nunoo, S., & Iliya, S. Z. (2015). Mitigating pilot contamination in massive mimo system5g: An overview. *2015 10th Asian Control Conference (ASCC)*, 1–6.

Fatema, N., Hua, G., Xiang, Y., Peng, D., & Natgunanathan, I. (2017). Massive mimo linear precoding: A survey. *IEEE systems journal*, *12*(4), 3920–3931.

Fernandes, F., Ashikhmin, A., & Marzetta, T. L. (2013). Inter-cell interference in noncooperative tdd large scale antenna systems. *IEEE Journal on Selected Areas in Communications*, *31*(2), 192–201.

Flordelis, J., Rusek, F., Tufvesson, F., Larsson, E. G., & Edfors, O. (2018). Massive mimo performancetdd versus fdd: What do measurements say? *IEEE Transactions on Wireless Communications*, *17*(4), 2247–2261.

Ganesh, R., Kumari, J. J., et al. (2013). A survey on channel estimation techniques in mimo-ofdm mobile communication systems. *International journal of scientific & engineering research*, *4*(5), 1850–1855.

Gao, D., Zhu, X., & Huang, Y. (2016). Multiple division soft pilot reuse in massive mimo cellular networks. *2016 6th International Conference on Information Communication and Management (ICICM)*, 187–192.

Gao, X., Tufvesson, F., Edfors, O., & Rusek, F. (2012). Channel behavior for very-large mimo systems-initial characterization. *COST IC1004, 2012*.

Gesbert, D., Kountouris, M., Heath, R., Chae, C., & Salzer, T. (2008). From single user to multiuser communications: Shifiting the mimo paradigm. *IEEE Signal Processing Magazine*.

Goldsmith, A. (2005). *Wireless communications*. Cambridge university press.

Goldsmith, A., Jafar, S. A., Jindal, N., & Vishwanath, S. (2003a). Capacity limits of mimo channels. *IEEE Journal on selected areas in Communications*, *21*(5), 684–702.

Goldsmith, A., Jafar, S. A., Jindal, N., & Vishwanath, S. (2003b). Capacity limits of mimo channels. *IEEE Journal on selected areas in Communications*, *21*(5), 684–702.

Golomb, S. W., & Gong, G. (2005). *Signal design for good correlation: For wireless communication, cryptography, and radar*. Cambridge University Press.

Govil, R. (2018). Different types of channel estimation techniques used in mimo-ofdm for effective communication systems. *Int J Eng Res Technol (IJERT)*, *7*(07), 271–275.

Haykin, S. (2002). Adaptive filter theory. *Prentice Hall google schola*, *2*, 67–94.

Haykin, S. (2008). *Communication systems*. John Wiley & Sons.

Heath Jr, R. W., & Lozano, A. (2018). *Foundations of mimo communication*. Cambridge University Press.

Henríquez, F. R., Cortés, N. C., & Rocha-Pérez, J. (2002). Generation of gold-sequences with applications to spread spectrum systems. *IEEE communications letters*, *4*(8).

Hossain, A., Islam, S., & Ali, S. (2012). Performance analysis of barker code based on their correlation property in multiuser environment. *International Journal of Information Sciences and Techniques (IJIST) Vol*, *2*.

Hoydis, J., Ten Brink, S., & Debbah, M. (2013). Massive mimo in the ul/dl of cellular networks: How many antennas do we need? *IEEE Journal on selected Areas in Communications*, *31*(2), 160–171.

Hu, Z., Ren, L., Wei, G., Qian, Z., Liang, W., Chen, W., Lu, X., Ren, L., & Wang, K. (2023). Energy flow and functional behavior of individual muscles at different speeds during human walking. *IEEE Transactions on Neural Systems and Rehabilitation Engineering*, *31*, 294–303. https://doi.org/10.1109/TNSRE.2022.3221986

Jose, J., Ashikhmin, A., Marzetta, T. L., & Vishwanath, S. (2011). Pilot contamination and precoding in multi-cell tdd systems. *IEEE Transactions on Wireless Communications*, *10*(8), 2640–2651.

Kaur, T., Singh, J., & Sharma, A. (2017). Simulative analysis of rayleigh and rician fading channel model and its mitigation. *2017 8th International Conference on Computing, Communication and Networking Technologies (ICCCNT)*, 1–6.

Khichar, S., Santipach, W., Wuttisittikulkij, L., Parnianifard, A., & Chaudhary, S. (2024). Efficient channel estimation in ofdm systems using a fast super-resolution cnn model. *Journal of Sensor and Actuator Networks*, *13*(5), 55.

Larsson, E. G., Edfors, O., Tufvesson, F., & Marzetta, T. L. (2014a). Massive mimo for next generation wireless systems. *IEEE communications magazine*, *52*(2), 186–195.

Larsson, E. G., Edfors, O., Tufvesson, F., & Marzetta, T. L. (2014b). Massive mimo for next generation wireless systems. *IEEE communications magazine*, *52*(2), 186–195.

Li, Y. G., & Stuber, G. L. (2006). *Orthogonal frequency division multiplexing for wireless communications*. Springer Science & Business Media.

Liao, M. (2022). *Channel estimation for massive mimo systems* [Doctoral dissertation, University of York].

Lu, L., Li, G. Y., Swindlehurst, A. L., Ashikhmin, A., & Zhang, R. (2014). An overview of massive mimo: Benefits and challenges. *IEEE journal of selected topics in signal processing*, *8*(5), 742–758.

Mai, T. C., Ngo, H. Q., & Duong, T. Q. (2020). Downlink spectral efficiency of cell-free massive mimo systems with multi-antenna users. *IEEE Transactions on Communications*, *68*(8), 4803–4815.

Manasseh, E., Ohno, S., & Nakamoto, M. (2010). Pilot symbol design for channel estimation in mimo-ofdm systems with null subcarriers. *2010 18th European Signal Processing Conference*, 1612–1616.

Maria, S. L., et al. (2017). *Pilot contamination reduction in massive mimo systems* [Doctoral dissertation, Universitat Politècnica de Catalunya. Escola Tècnica Superior d'Enginyeria].

Marzetta, T. L. (2010). Noncooperative cellular wireless with unlimited numbers of base station antennas. *IEEE transactions on wireless communications*, *9*(11), 3590–3600.

Marzetta, T. L., & Hochwald, B. M. (2006). Fast transfer of channel state information in wireless systems. *IEEE Transactions on Signal Processing*, *54*(4), 1268–1278.

Marzetta, T. L., Larsson, E. G., & Yang, H. (2016). *Fundamentals of massive mimo*. Cambridge University Press.

Masood, K. F. (2022). Low-rank channel estimation for millimeter wave and terahertz hybrid mimo systems.

Masood, K. F., Tong, J., Xi, J., Yuan, J., Guo, Q., & Yu, Y. (2023). Low-rank matrix sensing-based channel estimation for mmwave and thz hybrid mimo systems. *IEEE Journal of Selected Topics in Signal Processing*.

Mehrotra, N., & Chaubey, A. K. (2017). Pilot contamination effect in massive mimo and analysis of mitigation techniques. *International Journal of New Technology and Research*, *3*(2), 263359.

Mehrpouyan, H., Nasir, A. A., Blostein, S. D., Eriksson, T., Karagiannidis, G. K., & Svensson, T. (2012). Joint estimation of channel and oscillator phase noise in mimo systems. *IEEE Transactions on Signal Processing*, *60*(9), 4790–4807. https://doi.org/10.1109/TSP.2012.2202652

Moqbel, M. A. M., Wangdong, W., & Ali, A.-m. Z. (2017). Mimo channel estimation using the ls and mmse algorithm. *IOSR J. Electron. Commun. Eng*, *12*(1), 13–22.

Müller, R. R., Cottatellucci, L., & Vehkaperä, M. (2014). Blind pilot decontamination. *IEEE Journal of Selected Topics in Signal Processing*, *8*(5), 773–786.

Naqvi, S., Hassan, S., & Mulk, Z. (2017). Encoding and detection in mmwave massive mimo. In *Mmwave massive mimo* (pp. 63–78). Elsevier.

Nee, R. v., & Prasad, R. (2000). *Ofdm for wireless multimedia communications*. Artech House, Inc.

Ngo, H. Q. (2015a). *Massive mimo: Fundamentals and system designs* (Vol. 1642). Linköping University Electronic Press.

Ngo, H. Q. (2015b). *Massive mimo: Fundamentals and system designs* (Vol. 1642). Linköping University Electronic Press.

Ngo, H. Q., Larsson, E. G., & Marzetta, T. L. (2013). Energy and spectral efficiency of very large multiuser mimo systems. *IEEE Transactions on Communications*, *61*(4), 1436–1449.

Ngo, H. Q., Larsson, E. G., & Marzetta, T. L. (2014). Aspects of favorable propagation in massive mimo. *2014 22nd European Signal Processing Conference (EUSIPCO)*, 76–80.

Omid, Y., Hosseini, S. M., Shahabi, S. M., Shikh-Bahaei, M., & Nallanathan, A. (2021). Aoa-based pilot assignment in massive mimo systems using deep reinforcement learning. *IEEE Communications Letters*, *25*(9), 2948–2952.

Orten, P., & Svensson, A. (2002). Sequential decoding of convolutional codes for rayleigh fading channels. *Wireless Personal Communications*, *20*, 61–74.

Özdogan, Ö., Björnson, E., & Larsson, E. G. (2019). Massive mimo with spatially correlated rician fading channels. *IEEE Transactions on Communications*, *67*(5), 3234–3250.

Parmar, K. A., & Patel, S. M. (2016). A survey on channel estimation algorithms for lte downlink systems. *Int J Innov Res Comput Commun Eng*, *4*(2), 1251–1258.

Pranesh, M., & Ramanathan, R. (2022). Investigation of pilot decontamination algorithm in multicell massive mimo systems. *2022 7th International Conference on Communication and Electronics Systems (ICCES)*, 525–529.

Proakis, J. G., & Salehi, M. (2007). Digital communications, 5th expanded ed.

Proakis, J. G., & Salehi, M. (2008). *Digital communications*. McGraw-hill.

Raeesi, O., Gokceoglu, A., Zou, Y., Björnson, E., & Valkama, M. (2018). Performance analysis of multi-user massive mimo downlink under channel non-reciprocity and imperfect csi. *IEEE Transactions on Communications*, *66*(6), 2456–2471.

Rappaport, T. S. (2024a). *Wireless communications: Principles and practice*. Cambridge University Press.

Rappaport, T. S. (2024b). *Wireless communications: Principles and practice*. Cambridge University Press.

Rappaport, T. S., Sun, S., Mayzus, R., Zhao, H., Azar, Y., Wang, K., Wong, G. N., Schulz, J. K., Samimi, M., & Gutierrez, F. (2013). Millimeter wave mobile communications for 5g cellular: It will work! *IEEE access*, *1*, 335–349.

Rashid, M. (2021). *Channel estimation in multi-user massive mimo systems by expectation propagation based algorithms*. Louisiana State University; Agricultural & Mechanical College.

Rayi, P., & Prasad, M. (2017). Enhancement of spectral and energy efficiency in massive mimo systems with linear schemes. *2017 Fourth International Conference on Signal Processing, Communication and Networking (ICSCN)*, 1–6.

Saatlou, O., Ahmad, M. O., & Swamy, M. N. S. (2019). Spectral efficiency maximization of a single cell massive mu-mimo down-link tdd system by appropriate resource allocation. *IEEE Access*, *7*, 182758–182771. https://doi.org/10.1109/ACCESS.2019.2959711

Saeed, M. K., Khokhar, A., & Ahmed, S. (2024). Pilot contamination in massive mimo systems: Challenges and future prospects. *arXiv preprint arXiv:2404.19238*.

Salh, A., Audah, L., Shah, N. S. M., & Hamzah, S. A. (2020). Mitigating pilot contamination for channel estimation in multi-cell massive mimo systems. *Wireless Personal Communications*, *112*, 1643–1658.

Shannon, C. E. (2001). A mathematical theory of communication. *ACM SIGMOBILE mobile computing and communications review*, *5*(1), 3–55.

Stüber, G. L., & Stüber, G. L. (2012). Digital modulation and power spectrum. *Principles of Mobile Communication*, 189–269.

Tse, D., & Viswanath, P. (2005). *Fundamentals of wireless communication*. Cambridge university press.

Van Chien, T., & Björnson, E. (2017). Massive mimo communications. *5G mobile communications*, 77–116.

Vidhya, K., & Kumar, R. S. (2012). Channel estimation techniques for ofdm systems. *International Conference on Pattern Recognition, Informatics and Medical Engineering (PRIME-2012)*, 135–139.

Vieira, J., Malkowsky, S., Nieman, K., Miers, Z., Kundargi, N., Liu, L., Wong, I., Öwall, V., Edfors, O., & Tufvesson, F. (2014). A flexible 100-antenna testbed for massive mimo. *2014 IEEE Globecom Workshops (GC Wkshps)*, 287–293.

Wang, F. (2011). *Pilot-based channel estimation in ofdm system* [Master's thesis, University of Toledo].

Wu, X., Beaulieu, N. C., & Liu, D. (2017). On favorable propagation in massive mimo systems and different antenna configurations. *IEEE Access*, *5*, 5578–5593.

Wu, X., Liu, D., & Yin, F. (2018). Hybrid beamforming for multi-user massive mimo systems. *IEEE Transactions on Communications*, *66*(9), 3879–3891.

Xing, Y., & Rappaport, T. S. (2021). Millimeter wave and terahertz urban microcell propagation measurements and models. *IEEE Communications Letters*, *25*(12), 3755–3759. https://doi.org/10.1109/LCOMM.2021.3117900

Zaier, A., & Bouallègue, R. (2012). Blind channel estimation enhancement for mimo-ofdm systems under high mobility conditions. *arXiv preprint arXiv:1203.4434*.

Zheng, J., Zhang, J., Du, H., Niyato, D., Ai, B., Debbah, M., & Letaief, K. B. (2024). Mobile cell-free massive mimo: Challenges, solutions, and future directions. *IEEE Wireless Communications*.

Zhou, Y., et al. (2020). A novel way for pilot decontamination in massive mimo multi-cell systems. *The Frontiers of Society, Science and Technology*, *2*(12).

Zhu, X., Dai, L., Wang, Z., & Wang, X. (2016). Weighted-graph-coloring-based pilot decontamination for multicell massive mimo systems. *IEEE Transactions on Vehicular Technology*, *66*(3), 2829–2834.